ANTI-TUBERCULAR ACTIVITIES OF *SACCHARUM OFFICINARUM, CURCUMA LONGA* EXTRACTS AND SYNTHESIZED NANOPARTICLES AGAINST SOME *MYCOBACTERIUM* SPECIES

BY

OKURUMEH, Eguono Ogheneyore
M.Tech/SLS/2018/9049

DEPARTMENT OF MICROBIOLOGY
SCHOOL OF LIFE SCIENCES
FEDERAL UNIVERSITY OF TECHNOLOGY MINNA, NIGER STATE

AUGUST, 2023

TABLE OF CONTENT

LIST OF TABLES

LIST OF FIGURES

LIST OF PLATES

CHAPTER ONE

1.0 INTRODUCTION

1.1 Background of the study

Infectious diseases represent a critical issue for health and are the major cause of morbidity and mortality worldwide. Tuberculosis (TB) is one of the major human diseases primarily caused by *Mycobacterium tuberculosis* with other members of the *Mycobacterium* complex (*M. bovis*, *M. africanum*, *M. canetti*, and *M. microti).* The Mycobacterial cell envelope is critical for cell function because many crucial processes are located in this structure. Important functions of the cell wall include the protection of the bacterial cell from hostile environments, general antimicrobial resistance, and the transport of nutrients. A key component of the cell wall is mycolic acid which is not differentiated by Grams staining; hence these organisms are referred to as acid-fast (Maiolini *et al.*, 2020).

Worldwide, an estimated 10.6 million people fell ill with tuberculosis and 1.2 million people died globally, it was also recorded that there was an additional 1.6 million death from it (World Health Organization, 2023). In 2019, an estimated 10.0 million people became ill with Tuberculosis and almost 1.5 million patients suffered death. Patients do not exhibit any symptom of disease except when impairment of immunity arises due to malnutrition, diabetes, malignancy, and AIDS. However, about 10 % of healthy individuals may develop active tuberculosis in their lifetime due to genetic factors (Assam *et al*., 2020). At the end of 2022, US$ 13 billion will be needed for TB prevention, diagnosis, treatment, and care to achieve the global target agreed upon at the UN high level-meeting on TB in 2018 (World Health Organization, 2022).

Tuberculosis occurs in every part of the world but developing countries have the highest tuberculosis burden (India, China, Indonesia, the Philippines, Pakistan, Nigeria, Bangladesh,

and South Africa) in 2020 which account for two-thirds of the total new TB cases (WHO, 2022). Ninety-five percent of tuberculosis cases occur in developing countries, where few resources are available to ensure proper treatment and where human immunodeficiency virus (HIV) infection may be common. It is estimated that between 19 and 43 % of the world's population is infected with *Mycobacterium tuberculosis*, the bacterium that causes tuberculosis infection (Zignol *et al*., 2020).

Tuberculosis spreads from one person to another through tiny droplets released into the air via coughing, spitting, and sneezing. Since their first discovery in the 1950s, TB infected patients have since been relying on the current anti-TB drugs, which are divided into three main groups: First-line anti-TB drugs (isoniazid, rifampicin, pyrazinamide, ethambutol, and streptomycin), second-line anti-TB drugs (kanamycin, capreomycin, amikacin, and fluoroquinolones) and third-line anti-TB drugs (clofazimine, linezolid, amoxicillin, and clarithromycin). Despite the high level of efficacy of these anti-TB drugs, their administration is accompanied by several side effects ranging from nausea, vomiting, fever, and headache to psychosis, hyperuricemia, ototoxicity, and hepatotoxicity. The emergence of new strains of multi-drug resistant tuberculosis (MDR-TB) and extensively-drug resistant tuberculosis (XDR-TB) has since exacerbated this global health problem. Therefore, an effort towards discovering a novel anti-TB drug is required (Mazlun *et al.*, 2019).

Mycobacterium tuberculosis resides in the granuloma in a dormant state for decades by utilizing the host lipids, slowing down their replicative genes, and waiting for an opportunity such as a weakened immune system to reactivate and cause active disease (Assam *et al*., 2020). *M. tuberculosis* is an intracellular pathogen with an unusually thick, waxy cell wall and a complex life cycle. The bacteria are transmitted by aerosol droplets and often infect the

lungs and can also infect cells of bones, the genitourinary tract, skin, and joints (Weissberg *et al.,* 2020).

Mycobacterium bovis is a slow growing (16 to 20 hours' generation time) aerobic bacterium. Bovine tuberculosis is an infectious disease caused by the acid-resistant *Mycobacterium bovis* and *Mycobacterium caprae*, which belong to the *Mycobacterium tuberculosis* complex (MTBC). The bacterial strain is Gram-positive, acid-fast and the cell wall contains as high as 60 % lipid, giving the mycobacteria their hydrophobic characteristics, slow growth, resistance to desiccation, disinfectants, acids, and antibiotics (Hadi, 2022). Bovine tuberculosis is a chronic disease that affects mainly cattle but also a wide range of hosts including other domesticated animals, certain wildlife species, and human beings. The geographic spread of *M. bovis* corresponds primarily to the distribution of livestock throughout the world (Mekonnen *et al.*, 2020). In Nigeria, cattle population is estimated at approximately 21 million, most of which are found in the northern part of the country. *Mycobacterium smegmatis* is the microbial species of choice to use in learning more about *Mycobacterium* physiology *in vitro* (Nyambuya *et al*., 2017). *Mycobacterium smegmatis* is an acid–fast bacterial species in the phylum *Actinobacteria* and the genus *Mycobacterium*. *M. smegmatis* is a useful research surrogate for pathogenic Mycobacterial species in laboratory experiments.

Plants are multicellular organisms in the kingdom Plantae that use photosynthesis to make their food, and were once considered daily food. Now, plants are popularly used as a common source of medicinal agents and food additives. Plants synthesize hundreds of chemical compounds for functions including defense against insects, diseases, and herbivorous mammals. The interest in plant derived drugs is mainly due to the current widespread belief that green medicine is safe and more dependable than expensive synthetic drugs, which have

adverse side effects. Therefore, the extraction of bioactive compounds from herbal medicinal plants offers great potential for new drug discoveries (Azizi *et al.,* 2021). As such sugarcane peel and turmeric extracts were selected for their anti-tubercular potentials in the present study.

Sugarcane (*Saccharum officinarum* Linn.) is a well-known crop of the family Poaceae. *Saccharum* is derived from the Greek word '*Sakcharon,*' which means sugar, especially sucrose. The stems vary in colour being green, pinkish, or purple, can reach 5 m (16 ft) in height, and are characterized by their sweet taste due to their high sucrose content. It is known as ireke by Yorubas, arakke by the Hausas, kpansannako by Nupe, and okpete in Igbo. It is grown for its sweet juice which is consumed directly or processed for sugar. Sugarcane juice is highly nutritious with medicinal and pharmacological properties to fight sore throats, colds, influenza and has a low glycemic index that keeps the body healthy. The roots and stems are used to treat urinary and bronchial tract infections, anemia, cough, constipation, and regulate blood pressure (Adjatin *et al*., 2019). Apart from sucrose, sugarcane products have been used for several other purposes. Sugarcane is a principal raw material for the sugar industry as 70 % of the world's sugar comes from it. Besides sugar production, a large population in the world relishes its juice and consumes raw cane (Abbas *et al.,* 2014). Despite all the research that has been done on the leaves and juice of sugarcane, literature is scarce on the importance of the bark.

Turmeric is a spice that is spread throughout the world's tropical and subtropical regions, with a short stem that bears 8-12 leaves. Curcumin (a flavonoid) is found in many constituents present in this plant. Curcumin enhanced the phagocytic activity of macrophages (Ong *et al*., 2020). The plant measures up to 1 meter long, it can be planted throughout the year

preferably in the north and it is an important spice throughout the world. *Curcuma longa* (Turmeric) is a member of the *Zingiberaceae* family. It is known as Ata ile pupa by Yorubas, Gangamau by the Hausas, Turi by Nupe, Iblue by the Urhobos, and Girgir by the Tivs. In terms of medicinal properties, plants have a lot of promise. It is an anti-inflammatory, anti-tubercular, hepatoprotective, blood-purifying, antioxidant, liver tissue detoxifier, and regenerator (Dejene, 2021).

To improve the effectiveness of *Curcuma longa* fractions the need to introduce nanotechnology which is an environmentally friendly and cost effective approach to the synthesis of green silver nanoparticles (AgNPs). Nanotechnology is considered one of the most important fields of study in material science. Nanotechnology can be defined as the formation, development, and exploration of nano-sized materials having a size range of (1-100 nm) that confers their unique physicochemical properties (Majid *et al*., 2020)**.** Nanoparticles synthesized using biological techniques or green technology have diverse natures, with greater stability and appropriate dimensions since they are synthesized using a one-step procedure. Plants provide a better platform for nanoparticle synthesis as they are free from toxic chemicals as well as contain natural capping agents. Silver nanoparticle (AgNP) is a strong antibacterial and also toxic to cells, it can damage bacterial cell walls, inhibits bacterial cell growth, and disrupts cell metabolism because of the interaction between Ag ions with macromolecules in cells, such as proteins and deoxyribonucleic acid (DNA). Nanoparticles synthesized from plants with medicinal properties proves to be beneficial in treating various ailments in a better and easy way (Swetha *et al*., 2020).

1.2 Statement of the Research Problem

Tuberculosis poses a huge global burden and leads to a large number of death due to an infectious agent (*Mycobacterium tuberculosis*). Treatment of tuberculosis is globally known as Directly Observed Treatment Short-course (DOTS) which can lead to immune-impairment, vulnerability towards reactivation, and reinfection. Directly observed short-course is a multidrug and long-term therapy and consists of many antibiotics that cause severe toxicity and side effects ranging from nausea, vomiting, fever, headache, anemia, skin rash, leukopenia, gastrointestinal upset psychosis, hyperuricemia, and hepatotoxicity. Frontline anti-TB drugs such as rifampin cause itching and thrombocytopenia. Isoniazid causes neuropathy, T-cell immune reduction, and mortality (Mazlun *et al.*, 2019, Samreen and Prakash, 2021).

The patient's condition improves significantly after four weeks of treatment with antibiotics causing him/her to discontinue the treatment regimen. Frequent drug shortages, use of drugs inappropriately through incorrect prescription by health care providers, poor quality drugs, and patients stopping treatment prematurely as a result of lack of money and social stigmatization are the challenges faced with TB drugs (Samreen and Prakash, 2021).

The global emergence of multidrug resistant (MDR), extensively drug resistant (XDR), and more recently totally drug resistant (TDR) strains of *Mycobacterium tuberculosis* has become a major problem and cause of drug ineffectiveness (WHO, 2022). Another problem is the failure of *Bacillus Calmette-Guerin* (BCG) vaccination in protection against adult pulmonary TB and the slow progress in new drug development.

1.3 Aim and objectives of the Study

The aim of the study was to evaluate the anti-tubercular activities of *Saccharum officinarum, Curcuma longa* extracts, and synthesized nanoparticles against some *Mycobacterium* species.

The objectives of the study were to:

i. screen for phytochemical components in extracts of *Saccharum officinarum* and *Curcuma longa.*

ii. determine the anti-tubercular activities of the crude extracts and fractions of the medicinal plants and nano synthesized particles.

iii. determine the MIC and MBC of the extracts and fractions of the medicinal plants.

iv. determine the MIC and MBC of the synthesized nanoparticles.

v. characterize the synthesized nanoparticles.

vi. carry out toxicological studies on the most active extract in rats.

1.5 Justification for the Research

Medicinal plants have been discovered and used traditionally in medical practice since prehistoric times. Medicinal plants have been used to treat cough, fever, and itch and plants synthesize hundreds of bioactive compounds which will help balance out the toxicity associated with currently used drugs. It is estimated that a large population of the world especially in developing countries still depends mainly on medicinal plants and they are readily available and inexpensive. Medicinal plants can also be used for all age groups. Data generated from this research will contribute to the knowledge of the anti-tubercular effectiveness of sugarcane peel and turmeric rhizome.

CHAPTER TWO

2.0 LITERATURE REVIEW

2.1 History of Tuberculosis

Right from ancient times to date and throughout different human civilizations, *M. tuberculosis* (causative agent of tuberculosis (TB)) has been widely known and mentioned. The earliest description can be found in Vedas, where TB was described as 'Yakshma' which implies "wasting disease" (Natarajan *et al*., 2020). *Mycobacterium tuberculosis* infection was believed to have existed on the horizon of the earth about 150 million years ago (Marcu *et al*., 2023). Evidence of TB was first observed in bone lesions of a 500 thousand year old skull in Turkey. Similarly, further evidence also revealed the presence of TB in the lesions of the spines of the Mummies in the Egyptian pre-dynastic era and the Peruvian pre-Colombian era (Sanyaolu *et al*., 2019). The ancient Greeks termed the illness 'Phthisis' and later the 'great white plague' infection which is known throughout human history. The bacterium was believed to have originated from East Africa and migrations from East Africa into Europe and Asia coupled with the rapid rise in industrialization in Europe, assisted the propagation and spread of the bacterium in Europe. Tuberculosis continued to ravage the world, particularly Europe, and without a cure for the disease.

A lot of scientists from 1720 until 1882 worked tirelessly in trying to establish and isolate the causative bacterium responsible for tuberculosis not until 1882 when Robert Koch a German scientist cultured and isolated the bacterium in animal serum using methylene staining recommended by Paul Ehrlich and then reproduced the disease by inoculating the bacilli into laboratory animal (Barberis *et al*., 2017). He expounded further on the aetiology of tuberculosis in his presentation “Die Aetiologie der Tuberculose” to the Berlin

physiological society (Barberis *et al*., 2017). On the 24th of March 1882, he presented his findings and later received the Nobel Prize in 1905 for his contribution to medicine. This was the start of an era of unprecedented milestones in the treatment and prevention of this deadly disease. For decades following this discovery, the Pirquet and Mantoux tuberculin skin tests, Selman Waksman streptomycin, Albert Calmette and Camille Guérin (BCG) vaccine, and other anti-tuberculosis drugs were developed (Barberis *et al*., 2017).

2.2 Epidemiology of Tuberculosis

Tuberculosis (TB) in humans is caused by *Mycobacterium tuberculosis*, it majorly causes severe pulmonary dysfunction (pulmonary tuberculosis) as well as other body parts apart from the lungs (known as extrapulmonary tuberculosis). According to the World health organization (WHO), tuberculosis spread easily in settings with little or no adequate ventilation or flow of air (overpopulated settings) and in conditions of abject poverty and malnutrition. Urgent redress needs to be given to the prognosis and diagnosis of TB because according to Allue-Guardia *et al*. (2021), TB kills one person every 21 seconds. Nigeria as of 2018 was ranked as number one in Africa and number six in the world amongst 30 countries highly burdened with TB disease with complications arising from the emergence and spread of resistant TB and a high Human immuno-deficiency virus/ Acquired imunno-deficiency syndrome (HIV/AIDS) (Ezeonu *et al*., 2021).

2.3 Tuberculosis

Tuberculosis is a bacterial disease spread from one person to another principally by airborne transmission. The causal agent is *Mycobacterium tuberculosis* (the tubercle bacillus). Tuberculosis (TB) is an infectious disease that can affect any organ in the body but usually affects the lungs, pulmonary tuberculosis is the most frequent site of involvement while

extrapulmonary tuberculosis is less frequent. Only pulmonary tuberculosis is infectious. It can develop when bacteria spread through droplets in the air. Tuberculosis can be fatal, but in many cases, it is preventable and treatable (Kozińska *et al.,* 2023).

2.3.1 Tuberculosis infection (latent (LTB))

Latent TB is defined by the presence of an *M. tuberculosis*-specific immune response with the absence of radiological evidence of clinical signs or symptoms. A person can have TB bacteria in their body and never develop symptoms. In most people, the immune system can contain bacteria so that they do not replicate and cause disease. In this case, a person will have a TB infection but not an active disease. A person may never experience symptoms and be unaware that they have the infection. There is also no risk of passing on a latent infection to another person. However, a person with latent TB still requires treatment (Medrano *et al.*, 2023)

2.3.2 Tuberculosis disease (active TB)

The body may be unable to contain TB bacteria. This is more common when the immune system

is weakened due to illness or the use of certain medications. When this happens, the bacteria can

replicate and cause symptoms, resulting in active TB. People with active TB can spread the infection. Without medical intervention, TB becomes active in 5–10 % of people with the infection. Patients with active TB disease experience general symptoms, such as fever, fatigue, lack of appetite, and weight loss, and those with the pulmonary disease can have persistent cough and hemoptysis (coughing up blood) in advanced disease. However, some

patients with the active, culture-positive disease may be asymptomatic and are best described as having subclinical (Barry *et al.*, 2019; Esmail *et al.*, 2019).

2.3.3 Mycobacterium tuberculosis

Mycobacterium tuberculosis is an intracellular pathogen with an unusually thick, waxy cell wall and a complex life cycle. The bacteria are transmitted by aerosol droplets and often infect the lungs and can also infect cells of bones, the genitourinary tract, skin, and joints (Ryder, 2021).

The Mycobacterium genus includes a high diversity of species, with differential phenotypic and genotypic traits, as well as epidemiological relevance, including several important human and animal pathogens (Parte, 2018). Mycobacterium species can be included in three groups: (1) mycobacteria that cause tuberculosis (TB), (2) mycobacteria that cause leprosy, and (3) the non-tuberculous mycobacteria (NTM), a wider diverse group of species also referred to in this literature as typical or environmental mycobacteria. *Mycobacterium tuberculosis* belongs to the kingdom: animalia, phylum: actinomycetota, order: corynebacteriales, and family: mycobacteriaceae (Natarajan *et al*., 2020). From a clinical and public health perspective, patients with TB are pragmatically classified as having latent TB infection (LTBI), which is an asymptomatic and non-transmissible state, or active TB disease, which is transmissible (in active pulmonary TB) and for which culture-based or molecular diagnostics can be used. It is estimated that among individuals who are infected with *M. tuberculosis*, around 85–90 % can control the infection but are unable to completely eradicate the *bacillus* from their bodies resulting in a latent tuberculosis infection (LTBI) (Chopra *et al.*, 2023).

2.3.4 Mycobacterium bovis

Mycobacterium bovis is a slow growing (16 to 20 hours' generation time) aerobic bacterium. Bovine tuberculosis is an infectious disease caused by the acid-resistant *Mycobacterium bovis* and *Mycobacterium caprae,* which belong to the *Mycobacterium tuberculosis* complex (MTBC). The bacteria are curved or straight rods. The bacteria strain is Gram-positive, acid-fast and the cell wall contains as high as 60% lipid, giving the mycobacteria their hydrophobic characteristics, slow growth, resistance to desiccation, disinfectants, acids, and antibiotics (Hadi, 2022). Bovine tuberculosis is a chronic disease that affects mainly cattle but also a wide range of hosts including other domesticated animals, certain wildlife species, and human beings. The geographic spread of *M. bovis* corresponds primarily to the distribution of livestock throughout the world (Mekonnen *et al.*, 2020). In Nigeria, the cattle population is estimated at approximately 21 million, most of which are found in the northern part of the country. Consequently, the endemicity of bovine TB in Nigeria has contributed significantly to economic losses in the livestock industry.

Although there is limited epidemiological information on bovine TB in Nigeria, some known risk factors include the lack of a national TB control programme (including poor animal management and weak veterinary services, unrestricted animal movement, and poor meat inspection services), the nature of travelling from one place to another by the Fulani's, who manage over 90% of the cattle population in Nigeria, and illiteracy (Cadmus *et al*., 2019). The disease is transmitted to humans primarily through the consumption of cattle products such as unpasteurized milk or raw meat products that have been contaminated with *Mycobacterium bovis* or the transmission could be due to close contact with infected cattle. Also, the transmission could occur through aerosol inhalation of infective droplets or infected body fluids or tissues in the presence of wounds from infected animals, animal handlers

comprising of livestock farmers, abattoir workers, veterinarians, and their assistants, hunters, wildlife workers as well as other animal handlers are at different risk of contracting *Mycobacterium bovis* infection, depending on the nature of their jobs and their interaction with infected animals (Devi *et al*., 2021).

Mycobacterium bovis is intrinsically resistant to pyrazinamide, a standard first-line anti-TB drug. Without prompt diagnosis and drug susceptibility testing, patients with zoonotic TB may receive less effective treatment. Moreover, some *Mycobacterium bovis* strains exhibit resistance to other first-line anti-TB drugs such as isoniazid and rifamcipin. The resistance to at least two first-line anti-TB drugs results in a multidrug resistance phenomenon, which is an emerging public health threat globally and poses huge challenges to human tuberculosis control and treatment (Singh *et al.,* 2023).

2.3.5 Mycobacterium smegmatis

Mycobacterium smegmatis is the microbial species of choice to use in learning more about *Mycobacterium* physiology *in vitro* (Nyambuya *et al*., 2017). *Mycobacterium smegmatis* is an acid–fast bacterial species in the phylum *Actinobacteria* and the genus *Mycobacterium*. It is 3.0 to 5.0 μm long with a bacillus shape and can be stained by Ziehl–Neelsen method and the auramine-rhodamine fluorescent method. It was first reported in November 1884 by Lustgarten. It is usually known as saprophytic group that rarely causes disorder and is not susceptible to live in mammals. The organism is aerobic. *Mycobacterium smegmatis* is a useful research surrogate for pathogenic Mycobacterial species in laboratory experiments. Although this bacterium is Gram-positive, it has some unique qualities that are divergent from most Gram-positive bacteria. Its cell wall contains mycolic acids, long, branched fatty acids that are normally present in acid-fast bacteria. The acids prevent proper Gram staining

that would normally identify the cell as a Gram-positive cell because they create a waxy coating so the crystal violet has difficulty entering the cell, therefore making it seem Gram-negative. The cell wall is also abnormal because it is irregularly thick for a Gram-positive bacterium and its hydrophobicity reduces desiccation. This feature in addition to its slow cell growth (in comparison to most other bacteria) attribute to *M. smegmatis* low response to antibiotics (Antony *et al*., 2020).

2.4 Transmission and Symptoms of Tuberculosis

2.4.1 Transmission of Mycobacterium tuberculosis

Tuberculosis can spread from person to person through the air by droplet nuclei particles 1 to 5 µm in diameter that contain *M. tuberculosis* complex (Edwards and Kirkpatrick, 2018). Droplet nuclei are produced when persons with pulmonary or laryngeal tuberculosis cough, sneeze, speak, or sing. They also may be produced by aerosol treatments, sputum induction, aerosolization during bronchoscopy, and through manipulation of lesions or processing of tissue or secretions in the hospital or laboratory. Droplet nuclei, containing two to three *M. tuberculosis* organisms, are so small that air currents normally present in any indoor space can keep them airborne for long periods (Riley, 2019). Droplet nuclei are small enough to reach the alveoli within the lungs, where the organisms replicate.

Although patients with tuberculosis also generate larger particles containing numerous bacilli, these particles do not serve as effective vehicles for the transmission of infection because they do not remain airborne, and if inhaled, do not reach alveoli. Organisms deposited on intact mucosa or skin do not invade tissue. When large particles are inhaled, they impact the wall of the upper airways, where they are trapped in the mucous blanket, carried to the oropharynx, and swallowed or expectorated. Four factors determine the

likelihood of transmission of *M. tuberculosis*: (1) the number of organisms being expelled into the air, (2) the concentration of organisms in the air determined by the volume of the space and its ventilation, (3) the length of time an exposed person breathes the contaminated air, and (4) presumably the immune status of the exposed individual.

The HIV-infected persons and others with impaired cell mediated immunity are thought to be more likely to become infected with *M. tuberculosis* after exposure than persons with normal immunity; also, HIV-infected persons and others with impaired cell-mediated immunity are much more likely to develop the disease if they are infected. However, they are no more likely to transmit *M. tuberculosis* (Horsburgh, 2018).

There are five closely related mycobacteria grouped in the *M. tuberculosis* complex: *M. tuberculosis, M. bovis, M. africanum, M. microti*, and *M. canetti* (Soolingen *et al*., 2019). *Mycobacterium tuberculosis* is transmitted through the airborne route and there are no known animal reservoirs. *Mycobacterium bovis* may penetrate the gastrointestinal mucosa or invade the lymphatic tissue of the oropharynx when ingested in milk containing large numbers of organisms. Human infection with *M. bovis* has decreased significantly in developed countries as a result of the pasteurization of milk and effective tuberculosis control programs for cattle. Airborne transmission of both *M. bovis* and *M. africanum* can also occur. *Mycobacterium bovis* BCG is a live-attenuated strain of *M. bovis* and is widely used as a vaccine for tuberculosis. It may also be used as an agent to enhance immunity against transitional-cell carcinoma of the bladder. When used in this manner, adverse reactions such as dissemination may be encountered, and in such cases *M. bovis* BCG may be cultured from non-urinary tract system specimens, i.e., blood, sputum, bone marrow, etc. (Scully *et al*., 2019).

2.4.2 Symptoms of tuberculosis

The classic clinical features of pulmonary tuberculosis include chronic cough, sputum production, appetite loss, weight loss, fever, night sweats, and hemoptysis. Extrapulmonary tuberculosis occurs in 10 to 42 % of patients, depending on race or ethnic background, age, presence or absence of underlying disease, the genotype of the *M. tuberculosis* strain, and immune status (Caws *et al*., 2018). Extrapulmonary tuberculosis can affect any organ in the body, has varied and protean clinical manifestations, and therefore requires a high index of clinical suspicion. The HIV co-infection poses special challenges to clinical management in patients with active tuberculosis. The risk of active tuberculosis increases soon after infection with HIV, and the manifestations of pulmonary tuberculosis at this stage are similar to those in HIV-negative persons (Temu *et al.,* 2023)

Asymptomatic, subclinical tuberculosis, with negative findings on a sputum smear and chest radiography and positive culture results, is a common feature of HIV-associated tuberculosis and may account for 10 % of cases in regions in which tuberculosis is endemic. Up to 25 % of patients presenting for HIV care in such regions have undiagnosed active tuberculosis (Global tuberculosis report, 2020).

2.5 Diagnosis of Tuberculosis

Tuberculosis is diagnosed firstly by establishing a case definition, sputum samples are obtained from suspected individuals. Persons with prolonged coughing for an extended period of 2 weeks or more with or without the general symptoms associated with TB such as shortness of breath, loss of appetite, coughing up of blood, weight loss, tiredness, fever, night sweats, chest pain are examined as cases of pulmonary TB (Kwaghe *et al*., 2020) while for extra-pulmonary cases, fluid samples are obtained from individuals with suspected symptoms of pain and swellings on the vertebral spine, bones joints, loins, upper respiratory tract,

painless swelling of the lymph node, painful urination, bloody urination, frequent urination, meninges of the brain and some general symptoms earlier mentioned (Kwaghe *et al*., 2020).

2.5.1 Smear microscopy

Smear microscopy (SM) is one of the several methods of diagnosing TB and it is otherwise known as sputum smear microscopy (SSM) or phlegm smear microscopy (PSM) (Ogbaini-Emovon, 2009; Azadi *et al*., 2018). It is regarded by WHO as the basic diagnostic approach for TB identification and diagnosis. Although developed countries of the world focus on novel diagnostic approaches in TB diagnosis and management, developing countries (such as Nigeria) solely adopt the SSM as their basic laboratory approach for TB diagnosis (Azadi *et al*., 2018). This is due to the lack of facilities and equipment suitable for culturing these slow growing Mycobacterial species. Sputum samples obtained from a patient with established symptoms of TB are smeared directly on a clean grease free slide and stained with the Ziehl Neelsen staining technique for acid fast bacilli (AFB) or the Fluorochrome stain (to aid visualization) (Ogbaini-Emovon, 2009; National institute for pharmaceutical research and development, 2020). The slides are viewed on a Light microscope or Fluorescence microscope as positive samples retain the primary dye while negative samples retain the counter stain. The sensitivity of this procedure depends on several factors such as the experience of the scientist performing the act, the quality of the stain used, instrument quality, and the bacilli in each mL of sputum sample to become positive (Azadi *et al*., 2018).

2.5.2 Culture method

The cultural or culture method is regarded as a golden standard for tuberculosis diagnosis by WHO, it is not as rapid as the smear microscopy due to the slow growth rate of *Mycobacterium* causing tuberculosis (EL Kechine and Drancourt, 2011; Azadi *et al*., 2018).

Nonetheless, the rate of discovering acid-fast bacilli in a mL of phlegm in smear microscopy is lower compared to the culture method i.e the sensitivity of positive samples is 10 to 100 acid-fast bacilli per mL of phlegm in the culture method while 10-1000 in smear microscopy (Azadi *et al*., 2018). Samples obtained from patients are decontaminated with soda or chlorhexidine (a chemical substance used in the decontamination of microbial flora and or non-tuberculous organisms in samples) and then cultured on solid media: either blood agar, Lowenstein Jensen agar, stone brink medium, Middlebrook 7H10 and 7H11 (semi-synthetic agar) or Ogawa medium, liquid medium: Middlebrook 7H9 and further incubated invertedly at 37 °C in an atmosphere of 5 to 10 % of carbon dioxide. Once feasible growth or colonies is observed, then phenotypical and biochemical identification such as the pigment production test, growth rate calculation, niacin reduction test potassium tellurite reduction test, tween 80 hydrolysis test, Arylsufatase test, catalase test (semi-quantitative and 68 °C catalase test), iron uptake test of the Mycobacterial species is being carried out (Azadi *et al*., 2018).

2.5.3 Molecular method

The molecular approach for microbial detection is a very rapid, expensive, and painstaking method of detecting microorganisms; it is commonly and usually used in developed countries with high technological inclination. There are arrays of molecular diagnostic approaches nonetheless, the rapid TB diagnostic approach works based on targeting and multiplication of different areas in mycobacterial genome (Azadi *et al*., 2018). This approach such as nucleic acid hybridization techniques permits rapid identification of certain common mycobacterial species. Nucleic acid probes are commercially available for *Mycobacterium tuberculosis* complex, *M. avium* complex, *M. kansasii,* and *M. gordonae*. Specifically labelled acridine ester-labeled nucleic acid probes are used in this test for specific

mycobacterial ribosomal RNA (rRNA). Sonication occurs, and the RNA released from the cell afterward reacts with the DNA probe. A stable hybridization complex of RNA and DNA probe is established probably if the specific Mycobacterial RNA is present. This complex is detected by alkaline hydrogen peroxide solution which causes a chemi-luminescence reaction of the hybrid bound acridine ester resulting in the emission of light. The amount of light emitted is proportional to the amount of the hybridized probe (Jagielski *et al*., 2014; Jagielski *et al*., 2016).

Nucleic acid amplification assay is also, another approach designated to directly determine species of Mycobacteria by a transcription mediated amplification of specific 16S rRNA in positive and negative samples of patients, at a constant temperature (Chitnis *et al*., 2015). This approach has the potential to improve the detection of *M. tuberculosis* and other NTM's within a few hours and offers the reporting of the result the same day of performing the approach (Xie *et al*., 2018; Cantera *et al*., 2019). Lastly, gene sequencing analysis is also a form of molecular diagnostic approach to TB detection and determination. Several important genes are used as a good targets for identifying mycobacterial species. Particularly 16S rRNA, rpoB, and Internal Transcribed Spacers (ITSs) have been useful for the rapid identification of many mycobacterial species (Azadi *et al*., 2018).

Table 2.1: Genes used for differentiation of mycobacterial species

Gene	Product
Rrs	16S Rrna
ITS	Internal transcribed spacer region
hsp65	Heat shock protein 65
groES	10-kDa chaperonin
recA	Recombination protein
rpoB	DNA-directed RNA polymerase beta chain
dnaJ	Chaperone protein
oxyR	Hydrogen peroxide-inducible gene activator
pncA	Pyrazinamidase/nicotinamidase
rnpB	Catalytic subunit of RNase P
Soda	Superoxide dismutase
gyrB	DNA gyrase subunit B
SecA1	Preprotein translocase

Source: Azadi *et al.*, 2018

Table 2.2: Major genes of *Mycobacterium tuberculosis* linked with the acquisition of drug resistance

Drug	Gene	Product
Isoniazid	katG	Catalase-peroxidase-peroxynitritase T
	inhA	NADH-dependent enoyl-acyl carrier protein reductase
	ndh	NADH dehydrogenase
	ahpC	Alkyl hydroperoxide reductase C
Rifampin	rpoB	DNA-directed RNA polymerase β chain
Pyrazindamide	pncA	Pyrazinase/nicotinamidase
Streptomycin	rpsL	30S ribosomal protein S12
	rrs	16S rRNA
	gidB	Glucose-inhibited division protein B
Amikacin-kanamycin	Rrs	16S rRNA
	Eis	Enhanced intracellular survival protein
Ethionamide	ethA	Monooxygenase
	inhA	NADH-dependent enoyl-acyl carrier protein reductase
	ethR	TetR family transcriptional repressor
	ndh	NADH dehydrogenase
Fluoroquinolones	gyrAB	DNA gyrase
Para-Aminosalicyclic acid	thyA	Thymidylate synthase
	folC	Folylpolyglutamate synthase C

Source: Azadi *et al.,* 2018

2.6 Pathogenesis of Tuberculosis

Mycobacterium tuberculosis infection is a serious and delicate disease sometimes it could be life threatening and the resulting infection could persist throughout the life time of the infected individual. After inhalation, the droplet nucleus is carried down the bronchial tree and implants in a respiratory bronchiole or alveolus. Whether or not an inhaled tubercle

bacillus establishes an infection in the lung depends on both the bacterial virulence and the inherent microbicidal ability of the alveolar macrophage that ingests it (Dannenberg *et al.*, 2019). If the bacillus can survive initial defences, it can multiply within the alveolar macrophage. The tubercle bacillus grows slowly, dividing approximately every 25 to 32 hours within the macrophage. *Mycobacterium tuberculosis* has no known endotoxins or exotoxins; therefore, there is no immediate host response to infection.

The organisms grow for 2 to 12 weeks until they reach 103 to 104 in number, which is sufficient to elicit a cellular immune response that can be detected by a reaction to the tuberculin skin test.

Before the development of cellular immunity, tubercle bacilli spread via the lymphatics to the hilar lymph nodes and then through the bloodstream to more distant sites (Smith and Wiengeshaus, 2018). In persons with intact cell-mediated immunity, collections of activated T cells and macrophages form granulomas can limit the multiplication and spread of the organism. Antibodies against *M. tuberculosis* are formed but do not appear to be protective. The organisms tend to be localized in the centre of the granuloma, which is often necrotic. For the majority of individuals with normal immune function, the proliferation of *M. tuberculosis* is arrested once cell-mediated immunity develops, even though small numbers of viable bacilli may remain within the granuloma. Although a primary complex can sometimes be seen on chest radiographs, the majority of pulmonary tuberculosis infections are clinically and radiographically inapparent (Dannenberg *et al.*, 2019).

Most commonly, a positive tuberculin skin test result is the only indication that infection with *M. tuberculosis* has taken place. The risk of developing tuberculosis also appears to be greater during the first 2 years of life. The HIV infected persons, especially those with low CD4 1 cell counts, develop tuberculosis rapidly after becoming infected with *M. tuberculosis*;

up to 50 % of such persons may do so in the first 2 years after infection with *M. tuberculosis*. Conversely, an individual who has a prior latent infection with *M. tuberculosis* (not treated) and then acquires HIV infection will develop tuberculosis disease at an approximate rate of 5–10 % per year. In a person with intact cell-mediated immunity, the response to infection with the tubercle bacillus protects against reinfection. The likelihood of reinfection is a function of the risk of re-exposure, the intensity of such exposure, and the integrity of the host's immune system (Markowitz *et al.,* 2018).

2.7 Ethnobotany of Medicinal Plant Used

2.7.1 Description of *Curcuma longa* L. (Turmeric)

Turmeric is a perennial plant belonging to the ginger family which can be found in several countries of South East Asia as well as all of the Caribbean islands. Turmeric as a Medicinal plant has provided a reliable source for the preparation of new drugs as well as for combating diseases, from the dawn of civilization. The extensive survey of the literature revealed that *Curcuma longa* L. or turmeric (from *Zingiberaceae* family) is highly regarded as a universal panacea in herbal medicine with a wide spectrum of pharmacological activities (Namdeo *et al.,* 2023).

Turmeric is a plant distributed throughout tropical and subtropical regions of the world. It is widely cultivated in Asian countries, mainly in China and India. The plant measures up to 1 m high with a short stem. Turmeric is an essential spice all over the world with distinguished human use particularly among Eastern people (Ravindran *et al*., 2018).

Table 2.3: Taxonomy of *Curcuma longa*

Kingdom	**Plantae**
Subkingdom	Tracheobionta
Super division	Spermatophyta
Division	Magnoliophyta
Subclass	Zingiberidae
Order	Zingiberales
Family	Zingiberaceae
Genus	*Curcuma*
Species	*longa*
Scientific name	*Curcuma longa*

Source: Chanda and Ramachandra, 2019

2.7.2 Medicinal use of *Curcuma longa*

Curcuma longa is a plant that has traditional and medicinal relevancy and has been tagged as one of nature's most powerful healers due to its richness in secondary metabolites such as curcumin (Gahtori *et al.*, 2023), flavonoids, polyphenols, antioxidants, alkaloids, tannins, steroids and saponins (Oghenejobo *et al*., 2017; Ayati *et al*., 2019; Kasta, 2020). It is known as Ata ile pupa by Yorubas, Gangamau by the Hausas, Turi by Nupe, Iblue by the Urhobos, and Girgir by the Tivs. These metabolites could be responsible for the treatment of digestive disorders, Atherosclerosis, diabetes, respiratory diseases, cancer, liver diseases, Osteoarthritis, and menstrual problems (Ayati *et al*., 2019). The curcumin present in Tumeric may be proven to be a corticosteroid which may aid the anti-inflammation of the Sclerotic, middle, and inner layers of the eyes (Debjit-Bhowmik *et al*., 2009). More so, *C. longa* can

help in decongesting and preventing inflammation of the mucous membrane which coats the lungs, throat, stomach, and intestine. It is effective in skin treatment, detoxification of toxic waste from the body, healing wounds, and boosting immunity (Ayati *et al*., 2019). Apart from its medicinal use, it can also be used in the food industry for spicing and preserving foods and in the textile industry as a dyeing agent (Debjit-Bhowmik *et al*., 2009; Ayati *et al*., 2019).

2.7.3 Description of *Saccharum officinarum*

Saccharum officinarum (Sugarcane) is a monocotyledonous, perennial plant of the grass family 'poaceae' and subfamily 'panicoideae' (Uchenna *et al*., 2015). It is known as ireke by Yorubas, arakke by the Hausas, kpansannako by Nupe, and okpete in Igbo. Sugarcane is grown in all tropical and subtropical regions of the world. In 2007, the main sugarcane-producing countries were Brazil, India, China, and Thailand. The currently cultivated sugarcane plants are hybrids derived from crossings mainly between plants of *S. officinarum* and *S. spontaneum* (Dillon *et al*., 2019). The plants are perennial grasses that form stools of stalks or culms that can be several meters in length and are juicy, with high concentrations of sucrose. The sugarcane root system consists of adventitious and permanent shoot root types. Adventitious roots emerge from the culm root zone and are responsible for water uptake during bud sprouting and plant support until the permanent roots develop. Permanent roots are fasciculated at the base of growing shoots and are classified into support or anchor roots and the more network like absorption roots. The ratio between one root type and another is somewhat species specific. *Saccharum officinarum* generally contains fewer support roots than *S. spontaneum*, which could explain the increased vigor and resistance to environmental stresses characteristic of *S. spontaneum*. The stalk or culm consists of alternating nodes and

internodes. On the node, there is a leaf scar, an axillary bud, and a circumferential band of axillary root primordia.

Table 2.4: Taxonomy of *Saccharum officinarum*

Kingdom	**Plantae**
Division	Magnoliophyta
Class	Liliopsida
Order	Poales
Family	Poaceae
Genus	*Saccharum* L.
Species	*Officinarum*
Scientific name	*Saccharum Officinarum* L.

Source: Zahro *et al.,* 2023

2.7.4 Medicinal uses of *Saccharum officinarum*

Saccharum officinarum can be used for various purposes and the juice has nutritional value. it possesses medicinal and pharmaceutical properties which help to fight against sore throat, cold influenza, and low glycemic index (Rajendran *et al*., 2017) while the bark is known to treat urinary and bronchial tract infections, anaemia, constipation and regulates blood pressure (Adjatin *et al*., 2019). It also is used as a sweetener of drugs and as an ingredient in some cosmetics while the bark has also been reported to possess antimicrobial activities against microorganisms such as *Escherichia coli*, *Pseudomonas aeruginosa,* and in the treatment of the diseases that they cause (Adjatin *et al*., 2019).

2.7.5 Toxicological studies of medicinal plant used

The general scope of toxicology or toxicological studies is to establish the safety of substances being taken into the body as medication. Substances can either be chemically synthesized or extracted from either natural or artificial sources. The test substance (substance under investigation) is injected into animals at higher doses for a shorter period (mostly 1day) to get the Lethal dose (LD_{50}) that could cause damage in the animal system and then, administered with lower dose for long99er period (mostly 4 weeks) to also establish the effect of low concentration of the test substance on the animal model over an extended period. This is also referred to as acute and sub-acute toxicity (Mohammed *et al*., 2016). Principally, Lorke's method is mostly adopted for this approach. This method envisages two phases (i.e phase one and phase two) and is categorized so due to the difference in doses per kg body weight of the animals to be administered (Kasmu *et al*., 2019).

2.8 Nanotechnology and Nanoparticles

Nanotechnology is defined as the use of various engineering, physical, chemical, and biological methods in the exploitation of metallic substances at the atomic level to produce the metallic nanoparticles of their equivalence. Nanoparticles as described by the international union of pure and applied chemistry (IUPAC) are particles that cannot be seen with the naked eye and range in size from 1-100 nanometers (nm) in dimension (Agbebati-Maleki *et al*., 2020). The nanoscale material has new, unique, and superior physical and chemical properties compared to its bulk structure, due to an increase in the ratio of the surface area per volume of the material/particle (Swetha *et al.,* 2020).

2.8.1 Applications of nanoparticulate delivery systems

- **Nanoparticles as drug delivery systems:** The use of pharmacological agents is frequently limited by drug resistance at the target level owing to physiological barriers to cellular mechanisms encountered. In addition, many drugs have poor solubility and low bioactivity and they can be quickly cleared in the body by the reticuloendothelial system. Further, the efficacy of different drugs, such as chemotherapeutical agents, is often limited by dose-dependent side effects (Raj *et al.*, 2022).
- **Gastrointestinal tract:** Other portals for entry are GI and Skin. It is known that the kinetics of particle uptake in the GI tract depends on diffusion and accessibility through mucus initial contact with enterocytes, cellular trafficking, and post translocation events. The smaller the particle diameter is, the faster they could diffuse through GI secretion to reach the colonic enterocytes. Following uptake by the GI tract nanoparticles can translocate to the bloodstream and distribute all over the body. Targeting strategies to improve the interaction of nanoparticles with adsorptive sites (enterocytes and M-cells of Peyer's patches) in the GI tract, utilizes specific binding to ligands or receptors and nonspecific adsorptive mechanism. The surface of enterocytes and M cells shows cell-specific carbohydrates, which can serve as binding sites to nanoparticle drug carriers with appropriate ligands. Certain glycoproteins and lectins bind selectively to this type of surface structure by a specific receptor-mediated mechanism (Hedley and Curley, 2020).
- **Tumor cell targeting:** Anticancer drugs, which usually have a large volume of distribution, are toxic to both normal and cancer cells. Therefore, precise drug release into highly specified targets involves miniaturizing the delivery systems to become

much smaller than their targets. With the use of nanotechnology, targeting drug molecules to the site of action is becoming a reality resulting in personalized medicine, which reduces the effect of the drug on other sites while maximizing the therapeutic effect. This goal is mainly achieved by the small size of these particles, which can penetrate across different barriers through small capillaries into individual cells.

- **Respiratory tract:** One of the most common entry passages for nanoparticles is the respiratory tract. Nanoparticles could avoid normal phagocytic defences in therein respiratory tract and gain access to the systemic circulation and may reach CNS. Aerosol therapy using nanoparticles as a drug carrier is gaining importance for delivering therapeutic compounds. The lung is an attractive target for drug delivery due to non-invasive administration via inhalation aerosols, avoidance of first-pass metabolism, direct delivery to the site of action for the treatment of respiratory diseases, and the availability of a huge surface area for local drug action and systemic absorption of drug (Giri, 2022).

- **For gene delivery:** The key ingredient of polynucleotide vaccines, DNA, can be produced cheaply and has much better storage and handling properties than the ingredients of the majority of protein-based vaccines. However, there are several issues related to the delivery of polynucleotides that limit their application. These issues include efficient delivery of the polynucleotide to the target cell population and its localization to the nucleus of these cells and ensuring that the integrity of the polynucleotide is maintained during delivery to the target site. Nanoparticles loaded with plasmid DNA could also serve as an efficient sustained release gene delivery

system due to their rapid escape from the degradative endolysosomal compartment to the cytoplasmic compartment (Gurunathan *et al*., 2020).

- **Tissue repair:** Tissue repair using iron oxide nanoparticles is accomplished either through welding, apposing two tissue surfaces then heating the tissues sufficiently to join them, or through soldering, where the protein or synthetic polymer-coated nanoparticles are placed between two tissue surfaces to enhance the joining of the tissues. Temperatures greater than 50°C are known to induce tissue union induced by the denaturation of proteins and the subsequent entanglement of adjacent protein chains (Fried, 2019). There are believed to be nanoparticles that strongly absorb light corresponding to the output of a laser are also useful for tissue-repairing procedures.

2.8.2 Method of synthesis of nanoparticles

There are majorly three methods of synthesizing nanoparticles and these are physical method, chemical method, and biological method (also known as green synthesis).

Physical methods involve the use of a method such as evaporation-condensation, and laser ablation in synthesizing nanoparticles. Synthesis of nanoparticles using ceramic heaters with a heat source, and cooling down the evaporated vapor at a fast rate synthesizes nanoparticles by evaporation-condensation method. Likewise, the nanoparticle can be synthesized from metallic bulk materials in solution by laser ablation method. The effectiveness of this method (laser ablation), and the characteristics of the nanoparticles synthesized depend on factors such as the wavelength of the laser impinging the metallic target, the duration of the laser pulses, the laser fluence, the ablation time duration, the effective liquid medium, with or without the presence of surfactants (Xu *et al.,* 2020).

The chemical method involves the use of organic and inorganic chemicals as capping and stabilizing agents to reduce metal ions to nanoparticles of their equivalence. These chemical agents although reduce metal ions, constitute a high degree of toxicity to the environment and even to the human system if used as a drug delivery agent.

The biological method is the cheapest and safest of all three methods, it utilizes primary and secondary metabolites embedded in plant extracts, microorganisms, and animal secretion, such as proteins, enzymes, carbohydrates, fat, nucleic acid, phenolic compounds, amines, alkaloids and pigments as capping and stabilizing agents to bio-reduce metal ion to a valence of zero and precipitate nanoparticles either intracellularly or extracellularly). These primary and secondary metabolites embedded in plants, animals, and microorganisms are also responsible for reducing the risk of toxicity of the process to the environment and controlling undesired agglomeration of the product formed. Some microorganisms for example yeast and algae are good detoxifiers of heavy metals and thereby reducing them to nanoparticles of good morphology and size (Raj *et al.*, 2022).

2.8.3 Role of nanotechnology in drug delivery

The prefix “nano” has found in the last decade an ever-increasing application to different fields of knowledge. Nanoscience, nanotechnology, nanomaterials, or nanochemistry are only a few of the new nano-containing terms that occur frequently in scientific reports, in popular books as well as in newspapers, and that have become familiar to a wide public, even among non-experts. It is the use and manipulation of matter on a tiny scale. At this size, atoms and molecules work differently and provide a variety of surprising and interesting uses. Nanotechnology and Nanoscience studies have emerged rapidly during the past years in a broad range of product domains. It provides opportunities for the development of materials,

including those for medical applications, where conventional techniques may reach their limits (Hedley and Curley, 2020).

2.8.4 Synthesis and characterization of silver nanoparticles

Silver occurs in four different oxidation states: Ag^0, Ag^+, $Ag^{2+,}$ and Ag^{3+}. Ag^0 and Ag^+ are the most predominantly abundant in nature while Ag^{2+} and Ag^{3+} are unstable in an aquatic environment. Metallic silver is insoluble in water, but salts of metallic silver such as $AgNO_3$ and AgCl are very much soluble in water (Christopher *et al.,* 2018). Silver nanoparticles (AgNps) can be synthesized through the three major methods but most recently, it is predominantly synthesized biologically. It is then characterized using several parameters such as energy dispersive x-ray spectrophotometer (EDS), which is used alongside an emission scanning electron microscope, x-ray photoelectron spectroscopy (XPS), x-ray diffractometry (XRD), fourier transformation infrared spectroscopy (FTIR) and UV-vis spectroscopy which is used to confirm the formation of AgNps. The XRD is used in the determination of the crystallinity of the nanoparticles synthesized. While FTIR is used to characterize the functional group of organic compounds responsible for the biogenic reduction of the $AgNO_3$ to Ag^+. Scanning Electron Microscopy and Transmission Electron Microscopy are used in the shape, size, and structure of the NP and how relatively dispersed or uniform they are (Raj *et al.,* 2022).

CHAPTER THREE

3.0 MATERIALS AND METHODS

3.1 Collection and Identification of Plant Materials

Fresh turmeric rhizomes were purchased from Kure market, Minna, Niger State in November, 2019 and purple sugarcane peels were collected from sugarcane market in Madalla, Suleja, Niger State in February, 2021. Samples were transferred into sterile labelled plastic containers and transported to the Laboratory of the Department of Biological Sciences, Federal University of Technology, Minna, for identification by an Ethnobotanist. Turmeric rhizomes were identified as *Curcuma longa* (*Zingiberacea*) while purple sugarcane peels were identified as *Saccharum officinarum* (Poaceae). Voucher specimens were deposited in the Department for future reference.

Plate 1: Turmeric Rhizome

Source: Fieldwork

Plate 2: Purple sugarcane

Source: Fieldwork

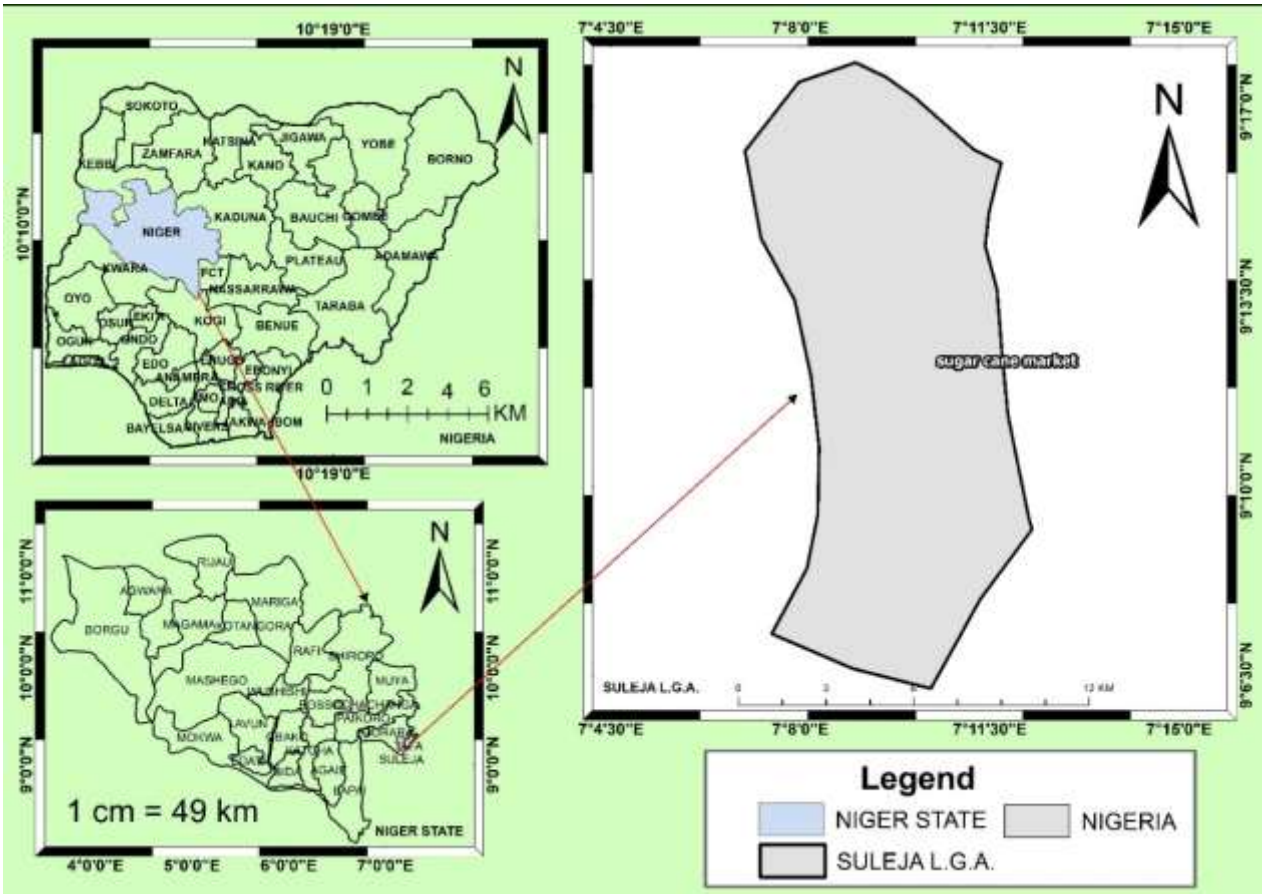

Figure 3. 1: Map of Sugarcane market, Suleja L.G.A. Niger State

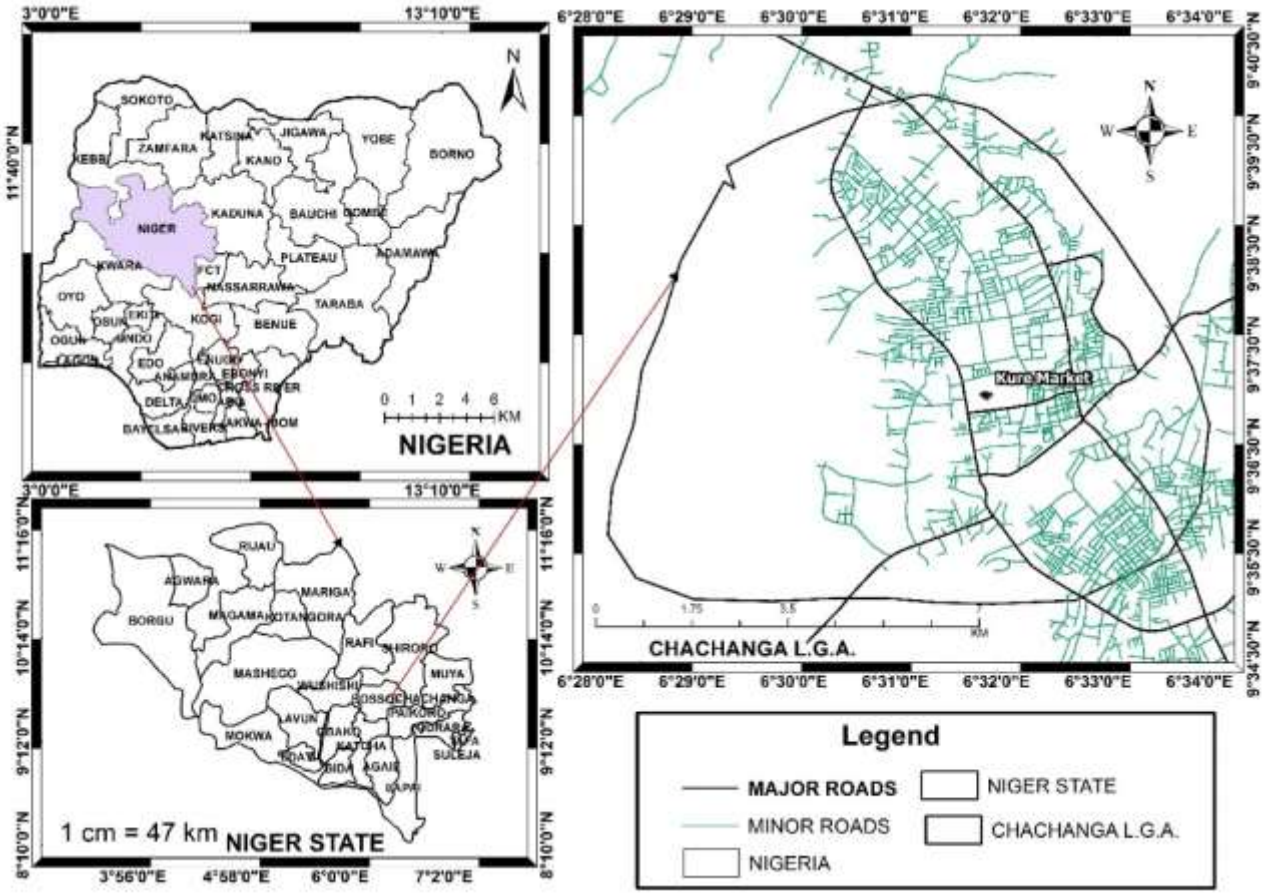

Figure 3.2: Map of Kure market, Chachanga L.G.A. Niger State.

3.2 Preparation and Extraction of Plant Materials

Niger State is situated in the north-central of Nigeria with Minna as its State capital. Other major local government areas include Suleja, Bida, and Kantagora. Minna consists of two major ethnic groups, Gbagyi and Nupe. The people there are mainly involved in agriculture, shea nut processing, gold mining, and leather work. Suleja is the location of ladi kwali pottery center, cotton weaving and dyeing, with locally grown indigo and mat making are traditional activities, but farming remains the chief occupation. Both communities comprise of people from other parts of the country such as the Yoruba and Igbo.

The plant materials used were washed to remove dirt, after which they were cut into smaller pieces and dried for two weeks at room temperature (28 $\pm 2^{o}$c). An electric blender

(brentwood JR-920R) was used to pulverize each plant into powder. *Curcuma longa* powder (400g) was extracted by cold maceration with 70% ethanol (2000 mL) for 5 days to yield a crude ethanol extract (coded E). Successive and exhaustive partitioning of extract E with petroleum ether and ethyl acetate gave rise to petroleum ether (coded P), ethyl acetate (coded AE) soluble fractions as well as aqueous residual fraction (coded A) which were freeze dried at -20 ℃. The resulting weights were 21.7g for crude ethanol, 5.62g for petroleum ether fraction, 10.6g for ethyl acetate fraction, and 1.78g aqueous residual fraction respectively. *Saccharum officinarum* peel (500 g) was similarly extracted and crude ethanolic extract (Es 8.17 g), petroleum ether fraction (Ps 2.20g), ethyl acetate fraction (AEs 2.07g), and aqueous residual fraction (As 5.35g) were obtained. All extracts/fractions were stored in a well labeled air tight sample bottles at 4 ˚C until required for use (Olatunji *et al.,* 2021).

3.3 Qualitative Phytochemical Screening of the Medicinal Plants Extracts and Fractions

Curcuma longa and Saccharum officinarum peel crude extracts and fractions were screened to detect the presence or absence of various secondary metabolites (alkaloids, saponins, flavonoids, tannins, phenolic acids, reducing sugar) using the method employed by Bahar *et al.,* (2018) and Sayantani and Ramachandra (2021).

3.3.1 Test for saponins

Five milliliter (5 mL) of distilled water were added to 0.2 g of extract in a test tube and agitated vigorously for 2 minutes. Persistent frothing or foaming indicated the presence of saponins.

3.3.2 Test for alkaloids

The plant extract was dissolved in 5 mL of distilled water, 0.2 mL of filtrate was measured into a beaker, and 1–2 mL of Dragendorff's reagent was added. The formation of prominent reddish-brown precipitate indicated the presence of alkaloids.

3.3.3 Test for flavonoids (Shinoda test)

About 5 mL of each of the samples was dissolved in alcohol with fragments of Magnesium ribbon and a few drops of Conc. HCl was added. The development of pink scarlet or crimson red color indicated the presence of flavonoids.

3.3.4 Test for tannins

Two-point five (2.5) milliliter of distilled water was added to each of the samples (0.2 g), filtered and a few drops of 10% ferric chloride solution was added to each filtrate. A blue color indicated the presence of tannins.

3.3.5 Test for phenols

Each sample (0.2 g) was treated with 1.0 mL of 10% ferric chloride solution. A deep-bluish green solution indicated the presence of phenols.

3.3.6 Reducing sugar

Benedict's test: filtrate of each of the sample was treated with Benedict's reagent and heated until an orange red precipitate appeared which indicated the presence of reducing sugar (Bahar *et al.*, 2018).

3.4 Sources of Test Organisms

The microorganisms used for this study were the clinical isolates of *Mycobacterium tuberculosis* ($H_{37}Rv$), an organism obtained from sputa of TB patients, *Mycobacterium bovis* (ATCC 27290), and *Mycobacterium smegmatis* (ATCC 607) which are typed cultures and

surrogate used for experimental purpose. *Mycobacterium tuberculosis* were obtained from Directly Observed Treatment Strategy (DOTS) Unit of the Diagnostic Laboratory of National Institute for Pharmaceutical Research and Development (NIPRD) while *M. bovis* and *M. smegmatis* were obtained from Microbiology Laboratory of Pharmaceutical Microbiology Department, NIPRD Idu, Abuja, Nigeria.

3.5 Identification and Characterization of Test Organisms

Identification and confirmation of the organisms were carried out according to the method described by NIPRD standard operating procedure (2020). *Mycobacterium tuberculosis* stock solution obtained from centrifuged sputum mixture while cultures of *Mycobacterium bovis* (ATCC 27290) and *Mycobacterium smegmatis* (ATCC 607) above were inoculated into 10 mL sterile Middle Brook 7H9/Tween/ADC (Becton Dickinson and company France) broth each. The setup was incubated at 37˚C for 7 days with daily observation for turbidity and monitored for AFB with Ziehl-Neelsen staining technique.

3.5.1 Digestion and decontamination of *Mycobacterium tuberculosis* clinical isolate

Two gram (2 g) of sodium hydroxide was dispensed into 50 mL of sterile distilled water labeled A. The mixture was homogenized, in a separate conical flask. Specifically, 50 mL of the sterile distilled water, 1.45 g of sodium citrate was added and homogenized, and the reagent N-acetyl-L-cysteine was added labeled B. Equal volume of the reagents A and B above and the positive acid-fast bacilli (AFB) sputum sample was measured and homogenized with a votex mixer and allowed to stand for 15 minutes to digest and decontaminate the bacilli. Phosphate buffer was added to the broth to neutralize it and was centrifuged at 3000 rpm for 15 minutes (Izebe *et al*., 2020).

3.5.2 Resuscitation of *Mycobacterium* species

Old stock of *Mycobacterium bovis* and *Mycobacterium smegmatis* were sub cultured in middlebrook 7H9/ADC broth. It was incubated at 37℃ for 5-7 days in a shaker incubator at 150 rpm. The optical density of the culture was measured with UV/ spectrophotometer at 540 nm to be between 0.2 nm-0.3 nm. The culture was standardized by further dilution in ratio 1:1000 by inoculating 50 µL culture into 50 mL middlebrook 7H9/ADC broth.

3.5.3 Ziehl-Neelsen acid fast stains

Ziehl-Neelsen staining enhances the isolation of acid-fast bacilli, *Mycobacterium* species from other upper respiratory tract microflora in the sputa samples (Izebe *et al.*, 2020). The sputum from patients containing *Mycobacterium tuberculosis* and cultures of *M. bovis* and *M. smegmatis* were smeared on clean slides and heat-fixed, carbol-fuchsin was poured on the smeared slide, heat fixed and allowed to remain for 3 to 5 minutes before washing it off with water. An acid alcohol decolourizer was added in drops continuously on the smeared glass until the carbol-fuchin faded away. The smeared glass was then washed with water and methylene blue was applied and allowed to stay for 10-30 seconds. Furthermore, the methylene blue was washed off from the smeared glass and allowed to dry. The slide was observed under microscope (x 100) using oil immersion (objective lens).

3.5.4 Standardization of *Mycobacterium* species

The method of NIPRD (2020) was employed for standardizing the organisms. A measured quantity of 50 µL of *Mycobacterium tuberculosis* stock culture was inoculated into 50 mL of sterile 7H9/Tween/ADC broth. The setup was incubated at 30˚C for 7 days to obtain optical density of 0.2-0.3 nm using uv spectrophotometer at 650 nm. This was further diluted in ratio 1:1000 by diluting 50 uL culture in 450 broths. The turbidity of the culture was compared

with 0.5 McFarland turbidity standards (approximately 1.5×10^7 cfu/mL). The culture was standardized to 10^6 cfu/mL. The standardized culture was then used for anti-tubercular screening (NIPRD, 2020). The procedure was repeated for *M. bovis* and *M. smegmatis.*

3.6 Screening of Extract and Fractions for Anti-tubercular Activities of Medicinal Plants

All the plant extract and fractions were dried thoroughly in an oven at 40˚C to ensure that any residual solvent evaporated completely in order to eliminate the toxic effects of solvents on the organisms which could interfere with the results. About 100000 µg/mL of each of the extract and fractions labelled 1-4 (turmeric) was dissolved in 0.5 mL DMSO to aid dissolution and 0.5 mL sterile Middlebrook 7H9/ADC broth to give a stock concentration of 100000µg/mL. The stock concentration of samples was further diluted 1:10 by diluting 0.1mL of stock to 0.9 mL 7H9/ADC broth to give a final concentration of 10000 µg/mL. Fractions in oil form were dissolved with tween-80 in place of DMSO that was used for paste.

Fifty microliter of sterile middlebrook 7H9/ADC broth was introduced into well 2-12 of 96 micro broth well plate, 100 µL of extract prepared in middlebrook 7H9/ADC broth was introduced into well one (1), from which 50 µL was taken to the next well using a multichannel pipette repeatedly to well 11, then 50 µL was discarded to have equal volume. The well(s) were inoculated with 50µL of already standardized test organisms [well 1-12]. The plates were incubated for 7 days at 37^0C. After the seven days incubation period, the wells were stained by adding 25 µL of tetrazolium dye and allowed to stand for 2 hours. The plates were observed for presence of microbial growth by color change in the wells. Colourless wells were recorded as no growth of test organisms (activity of extract/fraction) while a change in the initial colourless form to pink indicated growth of test organism (no

activity of extract /fraction). Well 12 was the Organism Viability Control. The efficacy of extract and each fraction was compared with Rifampicin (0.04µg/mL). The procedure was repeated in triplicate. Sugarcane peel extract and fractions were similarly treated.

3.7 Determination of Minimum Inhibitory Concentration

Minimum inhibitory concentration (MIC) of the extract and fractions was determined using the micro broth dilution method of NIPRD (2020). The MIC of turmeric extract/fraction was taken as the least concentration that inhibited the growth of *Mycobacterium* species after incubation for 7 days.

3.8 Determination of Minimum Bactericidal Concentration

The minimum bactericidal concentration (MBC) of the extract and fractions was determined using the method of NIPRD (2020) that employed prolonged incubation technique. Specifically, 50µL of the last well before the MIC was diluted in peptone water to neutralize the antimicrobial agent. The diluted solution was inoculated into 10mL 7H9 middle brook broth and incubated for 3 weeks. Post incubation of the sample was observed for turbidity. Absence of turbidity was taken as bactericidal activity at the concentration before the MIC well. The MIC of sugarcane peel was similarly determined.

3.9 Preparation and Synthesis of Silver Nanoparticles ($AgNO_3$)

Curcuma longa (turmeric) was selected for the synthesis of nanoparticles because it had better activity than sugarcane peels. Ethyl acetate fraction of turmeric was selected because of its efficacy, yield and texture. Silver nitrate ($AgNO_3$) powder, 0.17 g was dissolved in distilled 100 mL water to prepare a 2 mm $AgNO_3$ stock solution. Two grams of ethyl acetate (AE) fraction of turmeric were measured in separate beakers and dissolved with 100 mL distilled water. One hundred milliliter (100 mL) of $AgNO_3$ solutions was mixed with 100 mL

ethyl acetate (AE) fractions at a ratio of 1:1 (v/v) respectively in each beaker. The beaker was placed in the sun for 30 minutes to observe for colour change, ethyl acetate (AE) gave an ash colour indicating the formation of AgNPs. The mixture was freeze dried at -20^{0}C and stored in the refrigerator for the anti-tubercular activity (Swetha *et al.*, 2020).

3.10 Characterization of Synthesized Nanoparticles

Synthesized silver nanoparticles were characterized using ultraviolet-visible spectroscopy (UV-VIS spec), X-ray diffraction (XRD), transmission electron microscopy (TEM), selected area electron diffraction (SAED), energy dispersive spectroscopy (EDS) (Paul *et al*., 2023).

3.10.1. UV–visible spectroscopy

The Ag nanoparticles synthesized were analyzed using UV-Vis spectroscopy. This was done by using a Shimadzu UV-Visible spectrophotometer (1800-series) which is a spectrophotometer at a resolution of 1 nm from 190 to 800 nm and absorption peaks. The characteristics of Ag nanoparticles appeared at a wavelength interval of 400–600 nm. This showed that the Ag nanoparticles have formed in the extract, where the Ag^+ has been reduced to Ag^0 (Khan *et al.*, 2023). For X-ray Diffraction (XRD) the crystalline nature of the greenly synthesized AgNPs was done by using the XRD pattern analysis. A thin film of the silver nanoparticle was made by dipping a glass plate in a solution and used for X-ray diffraction studies. The dry powder of the silver nanoparticles (SNPs) were used. The main diffraction peaks were observed at the 2Θ value. A Siemens X-ray diffractometer, model D5000 (Munich, Germany), was used for that aim.

$$D = \frac{K\lambda}{\beta cos\Theta} \qquad (3.1)$$

Where, *D* denotes crystal size, *k* is the shape factor (0.94), the full width in radians at half maximum is denoted by β. The λ represents the X-ray wavelength (1.5418 Å) and Θ is the Bragg's angle (Ajala *et al.*, 2020).

3.10.2. Transmission electron microscopy (TEM)

It provides the most accurate and high-resolution imaging information about the size, shape, morphology, state of aggregation and distribution which were evaluated by a Philips GM-30 transmission electron microscope (Hillsboro, OR, USA). For the preparation of the samples, the cleaned AgNPs were re-dispersed in a solution, and one drop of this solution was placed on a copper grid, followed by the evaporation of solvent under an infrared lamp. The Digimizer software (version 4.1.1.0) was applied for the measurement of the particles size distribution, using the TEM images at nanometer resolution.

3.10.3. Selected area electron diffraction

Selected area electron diffraction (SAED) is to characterize the crystallinity, crystal structure and lattice parameters of nanoparticles from the diffraction pattern where a thin sample is targeted with a parallel beam of high-energy electron.

3.10.4 Energy dispersive spectroscopy

It analyse the elemental compositions of the sample. It is detected by using energy dispersive X-ray spectrometer (EDS) using x-act with INCA and Aztec EDS analysis software oxford instrument, London, UK) (Masi *et al.*, 2020).

3.11 Anti-tubercular Screening of Ethyl Acetate Silver Nanoparticles from Turmeric Fractions

The anti-tubercular activity of synthesized nanoparticles from turmeric ethyl acetate fraction (AEAgNPs) of silver nanoparticles, were investigated against the *Mycobacterium* species as described for the crude extract and fractions of turmeric.

3.12 Determination of MIC and MBC of Ethyl Acetate Silver Nanoparticles from Turmeric Fractions

Minimum inhibitory concentration (MIC) of the synthesized turmeric fraction were determined using the micro broth dilution method of NIPRD (2020) as described for the crude extract and fractions. The minimum bactericidal concentration (MBC) of the synthesized turmeric fraction were determined using the method of NIPRID (2020) that employed prolonged incubation for the crude extract and fractions.

3.13 Toxicological Studies of Ethyl Acetate Silver Nanoparticles

3.13.1 Experimental animals

Forty (48) healthy Albino rats (100-150 g) were used for this study. The animals were purchased from Animal Farm, Vom, Plateau State, Nigeria. The rats were kept in clean plastic cages bedded with dry clean wood shaving, a well-ventilated room and allowed to acclimatize for 2 weeks before the commencement of the experiment.

3.13.2 Toxicity profile of ethyl acetate silver nanoparticles

The method of Lorke's (1983) as described by Ibrahim *et al*. (2022) was adopted for the acute toxicity study of the silver nanoparticles. The method involved two phases (phases I and II). In phase I, nine (9) rats were distributed into three groups of three rats each and administered doses of 10, 100 and 1000 mg/kg bw of each of the nanoparticles. The animals were then observed for 24 hours for signs of toxicity which include decreased activities, licking of paw,

body weakness, sleeping and mortality. In the absence of mortality in phase I, another set of rats were grouped for phase II of the method. In phase II, a total of nine (9) rats were distributed into three groups of three rats each as in phase I and administered 1600, 2900, and 5000 mg/kg bw. The animals were again observed for 24 hours for signs of toxicity and mortality after which the LD_{50} will be calculated using equation 3.2:

$$\text{LD50} = \sqrt{(D0 \times Dm)} \qquad (3.2)$$

Where D0= minimum tolerated dose, Dm= minimum lethal dose.

3.13.3 Sub-chronic toxicity studies of ethyl acetate silver nanoparticles

The sub-chronic toxicity study of the AEAgNPs was conducted in accordance with Organization of Economic Co-operation and Development (OECD) guidelines. A total of twenty-five (30) rats were distributed into six groups of five (5) rats each. Groups 1, 2, 3 and 4 were orally administered 25, 50,100 and 1000 mg/kg bw of AEAgNPs, group 5 were orally administered 0.2 mL of rifampicin and 0.2 mL normal saline to group 6 respectively for a period of 28 days. The animals were fasted overnight but given free access to water before the administration of the extract throughout the experimental days. The weight variations of the experimental animals were also monitored on a weekly basis throughout the experimental days. The experimental animals were fasted overnight on the 28^{th} day, they were sacrificed on the 29^{th} day and the blood sample was collected for hematological analysis in ethylenediamine tetraacetic acid bottles (Ibrahim *et al.,* 2022).

3.14 Collection of Serum and Organs from Rats

The collection of blood, serum and organs were done as described by Shittu (2015). At the end of the four weeks treatment, the animals were starved for 24 hours. They were sacrificed under diethyl ether anesthesia. Blood for biochemical parameters were collected in a clean,

EDTA –free (plain) tubes which were allowed to stand for 10 minutes at room temperature before been centrifuged at 3000 revolution per minute (rmp) for 15 minutes to obtain the serum. The animals were thereafter quickly dissected and the organs (liver, kidney, lungs, spleen and heart) were removed, cleaned, weighed and observed for gross pathological changes. The organs were then fixed in 10% formalin solution for preservation. The organs were weighed and relative organ weights were recorded using equation 3.3:

$$ROW = \frac{Absolute\ organ\ weight\ (kg)}{Body\ weight\ of\ rat\ on\ sacrifices\ day\ (kg)} \times \frac{100}{1} \qquad (3.3)$$

Where ROW= Relative Organs Weight

3.15 Biochemical Analysis

3.15.1 Aspartate transaminase activity

Test-tubes were set on a rack and each test-tube contained 0.25 cm^3 of solution 1 (RI) and 0.05 cm^3 of the sample was dispensed into the test-tubes. It was then incubated for 30 minutes at 37℃. After 30minutes, 0.25 cm^3 solution 2 (R2) was added to the content of the test-tube and 0.05 cm^3 of distilled water was added to the blank and allowed to stand for 20 minutes at 20-25℃, 2.5 cm^3 of (0.4 M) sodium hydroxide was added to the mixture (Zaitsev *et al.*, 2020). The absorbance of the reaction mixture was determined at 546 nm after 5 minutes.

R1 NADH 0.18mmol/l: LDH 500 U/L;

R2 L-alanine, 5000 mmol/l- ∞ ketoglutarate

3.15.3 Determination of serum alanine phosphatase

Test-tubes were labelled as test, test-blank standard and standard blank, to the test- tubes labelled test, 1 cm^3 of alkaline buffer and 1 cm^3 of phenyl phosphate substrate was added. The mixture was incubated at 37 ºC for a minute. Serum, 0.1 cm^3 was added into the tube in

the incubator. The mixture was homogenized and incubated at 37 ºC for 5 minutes. The test-tube was removed and sodium hydroxide (0.5M), 0.8 cm^3 was added. Sodium bicarbonate (0.5M), 1.2 cm^3, para-(4)-amino antipyrine, 1.0 cm^3 and finally 1.0 cm^3 potassium ferricyanide were added. The mixture was homogenized and absorbance determined at 510 nm. The test blank was treated as test serum was added after the addition of sodium hydroxide. To the test-tube labelled, standard, 1.2 $cm^3$of buffer was pipetted. Phenol, 1.0 cm^3, was added and was treated as test after incubation. To the test labelled blank, 1.2 cm of buffer was taken Water, 1.0 cm^3 was added and was treated as test after incubation serum alkaline phosphatase activity was obtained.

3.15.4 Total protein determination

Total protein was determined using the RANDOX standard manual for *in vivo* quantitative plasma/serum total protein diagnostic kit (cat No. TP254 – Randox laboratories, UK). The principle of assay is based on the interaction of cupric ion in alkaline media with protein peptide bonds resulting in the formation of a colored complex, read against a protein standard at 530 nm (Zaitsev *et al.,* 2020).

3.15.5 Serum urea

One-hundred-centimeter cube (100 cm^3) of the test serum was accurately dispensed into a clean dry universal bottle while 10 cm^3 distilled water was added bringing the dilution to 1:100, 1 cm^3 of the resulting mixture was then withdrawn into a clean test tube. Distilled water (1 cm^3) was added, urea (2 cm^3) was added, followed by 2 cm^3 of the urea color reagent. The resulting mixture was homogenized, incubated at 100 ˚C for 20 minutes and then cooled in water bath at room temperature for 10 minutes and absorbance read spectrophotometrically at 520 nm. The value of measured serum urea was deduced using the formula:

$X = T \infty Cs$

Where:

T = test serum septrophoto-metric value

S = standard (normal) serum level

Cs = conversation of the standard = 10

3.15.6 Creatinine concentration

Creatinine concentration was assayed according to the method of Ibrahim *et al*. (2022). The content of the kit was R1a (picric acid), R1b (sodium hydroxide) and creatinine standard. The working reagent contained equal volume of R1a and R1b. one hundred microliters (100 µL) of plasma, 100 µL of creatinine standard and 100 µL of dH_2O were separately placed in different test tubes and 10.00 µL of working reagent was added. The reaction mixtures were swilled gently and absorbance of sample and that of standard were monitored after 30 seconds at 492 nm. Thereafter, 2 minutes of initial reading, Absorbance of sample and that of standard were recorded.

3.16 Serum lipid Profile

3.16.1 Estimation of serum cholesterol

Serum total cholesterol was estimated by cholesterol oxidase/peroxidase (CHOD/POD) colorimetric endpoint method, using liquizyme kit (Bates *et al.,* 2019). Cholesterol esterase hydrolyzed by cholesterol esterase to produce free cholesterol and fatty acid. This free cholesterol oxidized in the presence of cholesterol oxidase to liberate cholestenone and hydrogen peroxide. Liberated hydrogen peroxide combines with hydroxyl benzoate and 4 animoantipyrine in the presence of peroxidase to form red colored quinonimine complex, the intensity of which was measured at 505 nm (490-430).

3.16.2 Estimation of serum triglycerides

Serum triglycerides was estimated by glycerol phosphate oxidase/peroxidase (GPO/POD) colorimetric endpoint method using liquizyme kit as described by (Sakarde *et al.*, 2022). Triglyceride is hydrolyzed by lipoprotein lipase to free fatty acids and glycerol. Glycerol kinase convert glycerol to glycerol phosphate, which get oxidized to dihydroxy actone phosphate and hydrogen peroxide by glycerol phosphate oxidase. Hydrogen peroxide so formed react with 4 aminoantipyrine in the presence of peroxidase to give a purple coloured complex whose absorbance is determined at 546 nm.

3.16.3 Estimation of serum high density lipoprotein cholesterol (HDL-C)

Serum high density lipoprotein (HDL-C) was estimated by direct method using. Liquizyme kit (national committee for clinical laboratory, standard, NCCLS, 1995). The system utilizes a combination of surfactants, phosphoric, organic and inorganic acids. Specifically binging LDL-C

VLDL-C and chylomicrons. Only HDL, cholesterol is detected by the enzymatic CHOD/POD method.

3.16.4 Estimation of serum low density lipoprotein cholesterol (LDL-C)

Low density lipoprotein cholesterol is obtained using the friedwaid equation

LDL-C = Total cholesterol – (HDL-C).

3.17 Effect of Ethyl Acetate Silver Nanoparticles on Haematological Parameters in Rats

The effect of the silver nanoparticles on Haematological parameters of the Packed Cell Volume (PCV), Mean Cell Volume (MCV), Haemoglobin (Hb), Mean Cell Haemoglobin (MCH), Mean Cell Haemoglobin Concentration (MCHC), Red Blood Cell Count (RBC),

Platelet Count (PLC), White Blood cell Count (WBC), Neutrophils (N), Eosinophil (E), Lymphocytes (L) and Monocytes (M) were analysed using Auto-haematological Analyzer (produced by Abacus) (Shittu *et al.,* 2021).

3.18 Histopathological Studies

The organs comprising of kidney, spleen, heart, liver and lungs were collected after sacrificing the rats. The organs were washed in normal saline and fixed immediately in 10 % normal saline for a period of 24 hours. Grossing was achieved by selection of tissues to be processed. The organs were placed on tissue cassette alongside their identification number. The selected tissues were processed using automatic tissue cassette alongside the identification number. The selected tissues were processed using automatic tissue processor (SLEE MTP Tissue processor), which involved four major stages; fixation, dehydration, clearing and impregnation. An embedding machine was used to dispense wax into an embedding mould, unto which the processed tissues and tissue cassettes are placed and allowed to solidify. The solidified tissue in the cassette was placed in MR3500 microtome and tiny sections were cut at 5 microns. The tissue sections were flooded on a heated water bath maintained at 3 ˚C below melting point of the wax. Tissue sections were picked using microscopic slides angled at about 45 ˚C for water to drain and dry. The slide was then placed on hot plate and allowed to fix at maintained temperature of 3 ˚C above the melting point of wax. This was done to ensure bond between the tissue and slides and allowed fixing for minimum of 30 minutes. Thereafter, the slides were stained using Harris's haematoxylin and eosin method and allowed to air dry (Tietz, 1995). The dried slides were mounted with Distyrene Plasticizer Xylene (DPX) mountant and cover slips and examined under the

microscope. Any alterations compared to the normal structures were recorded (Paul *et al.*, 2023).

3.19 Data Analysis

Result were expressed as mean value ± standard deviation (S. E. M.). Within groups, comparisons were performed using one way ANOVA. Significant difference control and experimental groups were assessed by Duncan- test using SPSS version 26.1.0

CHAPTER FOUR

4.0 RESULTS AND DISCUSSION

4.1 Results

4.1.1 Characteristics of medicinal plants extract/fractions

Table 4.1a shows the physical appearances and percentage recovery of *Curcuma longa* crude ethanol (E), ethyl acetate (AE), petroleum ether (P) and aqueous fractions (A). Crude ethanolic extract had the highest yield of (21.79g) followed by ethyl acetate (10.60g), petroleum ether (5.62g) and aqueous (1.78g) fractions. Table 4.1b shows the physical appearances and percentage recovery of sugarcane peel extract and fractions. Crude ethanolic extract (Es) had the highest yield of (10.00g) followed by petroleum ether (Ps) (4.35g), ethyl acetate (AEs) (3.63g) and aqueous (As) (2.02g), crude ethanolic extract (Es) (10.00g) and respectively.

Table 4.1a: Characteristics and Percentage Recovery of Turmeric Extract and Fractions

Extract/fractions	Code	Colour	Appearance	Weight(g)	(%) Recovery
Crude ethanol	E	Reddish brown	Sticky paste	21.79	5.00
Petroleum ether	P	Yellowish	Oily	5.62	58.90
Ethyl acetate	AE	Reddish	Rocky paste	10.60	31.20
Aqueous	A	Dark brown	sticky paste	1.78	9.90

%: percentage, g: gram

Table 4.1b: Characteristics and Percentage Recovery of Sugarcane Peel Extract and Fractions

Extract/fractions	Code	Colour	Appearance	Weight(g)	(%) Recovery
Crude ethanol	Es	Brown	Sticky paste	10.00	5.00
Petroleum ether	Ps	Brown	Paste	4.35	43.50
Ethyl acetate	AEs	Brown	Rocky paste	3.63	36.30
Aqueous	As	Dark brown	Paste	2.02	20.20

%: percentage, g: gram, s: sugarcane

4.1.2 Qualitative phytochemical components of turmeric extract and fractions

The phytochemical components in crude extract and fractions of turmeric are shown in Table 4.2. Alkaloids were present in all the extract and fractions. Flavonoids were present in ethanolic extract, petroleum ether and ethyl acetate fractions. Saponins were present in ethanolic extract and ethyl acetate fraction. Tannins were only present in ethanolic extract while phenols were only detected in ethyl acetate fraction.

Table 4.2: Qualitative Phytochemical Components of Turmeric Extract and Fractions

Phytochemical Components	E	P	AE	A
Saponins	+	-	+	-
Alkaloids	+	+	+	+
Flavonoids	+	+	+	-
Phenols	-	-	+	-
Tannins	+	-	-	-

+: present, - : not detected, AE: ethyl acetate fraction, A: aqueous fraction, E: crude ethanol extract, P: petroleum ether fraction

4.1.3 Qualitative phytochemical components of sugarcane peels extract and fractions

The phytochemical components in crude extract and fractions of sugarcane peels are shown in Table 4.3. Flavonoids were present in all the extract and fractions, while saponins were absent in all the extract and fractions. Reducing sugar was detected in ethanolic extract, ethyl acetate and aqueous fraction. Tannins were detected in ethanolic extract and ethyl acetate. Phenols were present in ethanolic extract and petroleum ether while alkaloids were present only in crude ethanolic extract.

Table 4.3: Qualitative Phytochemical Components of Sugarcane Peel Extract and Fractions

Phytochemical Components	Es	Ps	AEs	As
Phenols	+	+	-	-
Alkaloids	+	-	-	-
Flavonoids	+	+	+	+
Tannins	+	-	+	-
Saponins	-	-	-	-
Reducing sugar	+	-	+	+

+: present, - : not detected, AEs: ethyl acetate fraction, As: aqueous fraction, Es: crude ethanol extract, Ps: petroleum ether fraction, s: sugarcane peel

4.1.4 Identities of *Mycobacterium* species

Clinical isolate of *Mycobacterium tuberculosis* was obtained from sputa of TB patients attending the diagnostic Centre while *M. bovis* (ATCC 27290) and *M. smegmatis* (ATCC 607) are typed cultures and surrogates used for experimental purpose as summarized in Table 4.4.

Table 4.4: Identities and Isolate number of *Mycobacterium* Species

Test organisms	Zielh-Neelsen	Isolate Number	Morphology
Mycobacterium tuberculosis	+	H37Rv	Bright red in colour, slightly curved, thin rod shape with beaded appearance
Mycobacterium smegmatis	+	ATCC 607	Red in colour, slender, curve rod with barrel appearance
Mycobacterium bovis	+	ATCC 27290	Red in colour, straight, slender, slightly curved, short rods occurring singly or in clusters

+: positive

4.1.5 Anti-tubercular activities of crude extract and fractions of medicinal plants

Tables 4.5 to 4.13 depicts the anti-tubercular activities of the medicinal plants extract and fractions against the *Mycobacterium* species. In Table 4.5, crude ethanolic extract (E) and aqueous (A) fractions inhibited the growth of *Mycobacterium tuberculosis* with MIC at 39 µg/mL (0.039 mg/mL), ethyl acetate (AE) was at 20 µg/mL (0.02 mg/mL). The MBC of crude ethanolic extract (E), and aqueous (A) fractions was 78 µg/mL (0.078 mg/mL) and the MBC of ethyl acetate (AE) was 39 µg/mL (0.039 mg/mL). While in table 4.6 petroleum ether (P) inhibited the growth of *M. tuberculosis* with MIC value of 0.781 %v/v, and the MBC was 1.562 %v/v.

Table 4.7 shows the anti-tubercular activities of turmeric extract and fractions against *Mycobacterium bovis.* Crude ethanolic extract (E), and ethyl acetate (AE) fractions inhibited the growth of *M. bovis* with MIC at 20 µg/mL (0.02 mg /mL) while for aqueous (A), the MIC was 78 µg/mL (0.078 mg /mL). The MBC of crude ethanolic extract (E),

and ethyl acetate (AE) fractions on *M. bovis* was 39 µg/mL (0.039 mg /mL) while the MBC of aqueous (A) was 165 µg/mL (0.165 mg/mL). For petroleum ether (P) the MIC was 0.390 %v/v, and the MBC was 0.781 %v/v as shown in table 4.8.

Table 4.9 depicts the anti-tubercular activities of turmeric extract and fractions against *Mycobacterium smegmatis*. Crude ethanolic extract (E), ethyl acetate (AE) and aqueous (A) fractions inhibited the growth of *M. smegmatis* with MIC at 78 µg/mL (0.078 mg/mL). The MBC for ethanolic extract, ethyl acetate and aqueous fractions was 165 µg/mL (0.165 mg/mL).

While in table 4.10, petroleum ether (P) inhibited the growth of M. smegmatis with MIC value of 0.390 %v/v and the MBC was 0.781 %v/v.

Table 4.11 shows the anti-tubercular activities of sugarcane peel extract and fractions against *Mycobacterium tuberculosis*. Crude extract inhibited the growth of *M. tuberculosis* with MIC at 1250 µg/mL (1.25 mg/mL), petroleum ether (Ps) and aqueous (As) fraction had MIC of 310 µg/mL (0.31 mg/mL) while ethyl acetate (AEs) was 20 µg/mL (0.02 mg/mL). The MBC of crude ethanolic extract (Es) was 2500 µg/mL (2.5 mg/mL), while petroleum ether and aqueous fractions had MBC value of 625 µg/mL (0.625 mg/mL) for ethyl acetate the MBC value was 39 µg/mL (0.039 mg/mL).

Table 4.12 shows the anti-tubercular activities of sugarcane peel extract and fractions against *Mycobacterium bovis*. Crude extract (Es) and aqueous fraction (As) inhibited the growth of *M. bovis* with MIC at 313 µg/mL (0.313 mg/mL), ethyl acetate (AEs) with MIC at 625 µg/mL (0.625 mg/mL) while for petroleum ether (Ps) the MIC was 1250 µg/mL (1.25 mg/mL). The MBC of crude ethanolic extract and aqueous fraction was 625 µg/mL (0.625 mg/mL) that of ethyl acetate was 1250 µg/mL (1.25 mg/mL) while the MBC for petroleum ether was 2500 µg/mL (2.5 mg/mL).

Table 4.13 shows the anti-tubercular activities of sugarcane peel extract and fractions against *Mycobacterium smegmatis*. Crude extract, ethyl acetate and aqueous fractions inhibited the growth of *M. smegmatis* with MIC at 313 µg/mL (0.313 mg/mL), while for petroleum ether the MIC was 165 µg/mL (0.165 mg/mL). The MBC of crude ethanolic extract, ethyl acetate and aqueous fraction was 625 µg/mL (0.625 mg/mL), while that of petroleum ether was 313 µg/mL (0.313 mg/mL).

Table 4.5: Anti-tubercular Activities of Turmeric Crude Extract and Fractions against *Mycobacterium tuberculosis*

	Concentration (µg/mL)											
Agents	**5000**	**2500**	**1250**	**625**	**313**	**165**	**78**	**39**	**20**	**10**	**5**	**MIC**	**MBC**
Crude (Ethanol)	+	+	+	+	+	+	+	+	-	-	-	40	80
Ethyl Acetate	+	+	+	+	+	+	+	+	+	-	-	20	40
Aqueous	+	+	+	+	+	+	+	+	-	-	-	40	80
Rifampicin	+	+	+	+	+	+	+	+	+	+	+	0.04	

-: No activity; +: Activity; MIC: Minimum inhibitory concentration; MBC: Minimum bactericidal concentration

Table 4.6 Anti-tubercular Activities of Turmeric Fraction (liquid) against *Mycobacterium tuberculosis*

	Concentration (%v/v)											
Agent	**50**	**25**	**12.5**	**6.25**	**3.125**	**1.562**	**0.781**	**0.390**	**0.195**	**0.097**	**MIC**	**MBC**
Petroleum Ether	+	+	+	+	+	+	+	-	-	-	0.781	1.562

-: No activity; +: Activity; MIC: Minimum inhibitory concentration; MBC: Minimum bactericidal concentration

Table 4.7: Anti-tubercular Activities of Turmeric Crude Extract and Fractions against *Mycobacterium bovis*

	Concentration (µg/mL)												
Agents	**5000**	**2500**	**1250**	**625**	**313**	**165**	**78**	**39**	**20**	**10**	**5**	**MIC**	**MBC**
Crude (Ethanol)	+	+	+	+	+	+	+	+	+	-	-	20	40
Ethyl Acetate	+	+	+	+	+	+	+	+	+	-	-	20	40
Aqueous	+	+	+	+	+	+	+	-	-	-	-	80	160
Rifampicin	+	+	+	+	+	+	+	+	+	+	+	0.04	

-: No activity; +: Activity; MIC: Minimum inhibitory concentration; MBC: Minimum bactericidal concentration

Table 4.8: Anti-tubercular Activities of Turmeric Fraction (liquid) against *Mycobacterium bovis*

	Concentration (%v/v)											
Agent	**50**	**25**	**12.5**	**6.25**	**3.125**	**1.562**	**0.781**	**0.390**	**0.195**	**0.097**	**MIC**	**MBC**
Petroleum Ether	+	+	+	+	+	+	+	+	-	-	0.390	0.781

-: No activity; +: Activity; MIC: Minimum inhibitory concentration; MBC: Minimum bactericidal concentration

Table 4.9: Anti-tubercular Activities of Turmeric Crude Extract and Fractions against *Mycobacterium smegmatis*

	Concentration (µg/mL)												
Agents	**5000**	**2500**	**1250**	**625**	**313**	**165**	**78**	**39**	**20**	**10**	**5**	**MIC**	**MBC**
Crude (Ethanol)	+	+	+	+	+	+	+	-	-	-	-	80	160
Ethyl Acetate	+	+	+	+	+	+	+	-	-	-	-	80	160
Aqueous	+	+	+	+	+	+	+	-	-	-	-	80	160
Rifampicin	+	+	+	+	+	+	+	+	+	+	+	0.04	

Table 4.10: Anti-tubercular Activities of Turmeric Fraction (liquid) against *Mycobacterium smegmatis*

Agents (%/v)	**50**	**25**	**12.5**	**6.25**	**3.125**	**1.562**	**0.781**	**0.390**	**0.195**	**0.097**	**MIC**	**MBC**
Petroleum ether	+	+	+	+	+	+	+	+	-	-	0.390	0.781

-: No activity; +: Activity; MIC: Minimum inhibitory concentration; MBC: Minimum bactericidal concentration

Table 4.11: Anti-tubercular activities of Sugarcane Peel Crude Extract and Fractions against *Mycobacterium tuberculosis*

	Concentration (µg/mL)												
Agents	**5000**	**2500**	**1250**	**625**	**313**	**165**	**78**	**39**	**20**	**10**	**5**	**MIC**	**MBC**
Crude (Ethanol)	+	+	+	+	-	-	-	-	-	-	-	630	1250
Ethyl Acetate	+	+	+	-	-	-	-	-	-	-	-	1250	2500
Petroleum Ether	+	+	+	+	+	-	-	-	-	-	-	310	630
Aqueous	+	+	-	-	-	-	-	-	-	-	-	2500	5000
Rifampicin	+	+	+	+	+	+	+	+	+	+	+	0.04	

-: No activity

+: Activity

MIC: Minimum inhibitory concentration

MBC: Minimum bactericidal concentration

Table 4.12: Anti-tubercular Activities of Sugarcane Peel Crude Extract and Fractions against *Mycobacterium bovis*

	Concentration (µg/mL)												
Agents	**5000**	**2500**	**1250**	**625**	**313**	**165**	**78**	**39**	**20**	**10**	**5**	**MIC**	**MBC**
Crude (Ethanol)	+	+	+	+	+	-	-	-	-	-	-	310	630
Ethyl Acetate	+	+	+	+	-	-	-	-	-	-	-	630	1250
Petroleum Ether	+	+	+	-	-	-	-	-	-	-	-	1250	2500
Aqueous	+	+	+	+	+	-	-	-	-	-	-	310	630
Rifampicin	+	+	+	+	+	+	+	+	+	+	+	0.04	

-: No activity

+: Activity

MIC: Minimum inhibitory concentration

MBC: Minimum bactericidal concentration

Table 4.13: Anti-tubercular Activities of Sugarcane Peel Crude Extract and Fractions against *Mycobacterium smegmatis*

	Concentration (µg/mL)												
Agents	**5000**	**2500**	**1250**	**625**	**313**	**165**	**78**	**39**	**20**	**10**	**5**	**MIC**	**MBC**
Crude (Ethanol)	+	+	+	+	-	-	-	-	-	-	-	630	1250
Ethyl Acetate	+	+	+	+	+	-	-	-	-	-	-	310	630
Petroleum Ether	+	+	+	+	+	+	-	-	-	-	-	160	310
Aqueous	+	+	+	+	+	-	-	-	-	-	-	310	630
Rifampicin	+	+	+	+	+	+	+	+	+	+	+	0.04	

-: No activity

+: Activity

MIC: Minimum inhibitory concentration

MBC: Minimum bactericidal concentration

4.1.6 Characteristics of silver nanoparticles synthesized from turmeric fractions

The change in colour in plate III (ethyl acetate) from orange to ash, indicates the conversion of ionic silver (Ag^{+}) to metallic silver (Ag^{o}) that combines into colloidal particles (AgNPs). The synthesized AgNPs exhibited distinctive UV–Visible Spectroscopy absorption bands with maximum absorbance peak. As shown in Figure 4.1, the absorption peak of silver nanoparticles synthesized from ethyl acetate fraction (AEAgNPs) occurred at 438nm. The transmission electron microscopy (TEM) micrograph of the synthesized AEAgNPs was spherical in shape, with an average particle size of 19.24 nm represented in Figure 4.2. The XRD pattern of the synthesized nanoparticles AEAgNPs shown in (Figure 4.4), with the peaks recorded at 2θ from 20˚ to 90˚ angle. The sharp peaks obtained was at 38˚, 44˚, 65˚, 77˚and 82˚ which correspond to the (111), (200), (220), (311), and (222) Miller indices, respectively. These indices indicated the face-centered cubic (FCC) structure of Ag based on the data base of Joint Committee on Powder Direction Standards (JCPDS), file No. 04-0783.

The selected area of electron diffraction pattern (SAED), reveals the presence of bright ring pattern, signifying the presence of various planes of AgNPs and also indicating the crystalline nature Figure 4.5. The patterns demonstrate fringes with bright circular rings related to the (111), (200) and (311) Bragg's reflection planes of AgNPs which also indicates the crystallinity of nanoparticles. Energy dispersive spectrum (EDS) assessed the elemental compositions showing Ag and O and confirmed the presence of silver nanoparticle in (Figure 4.6).

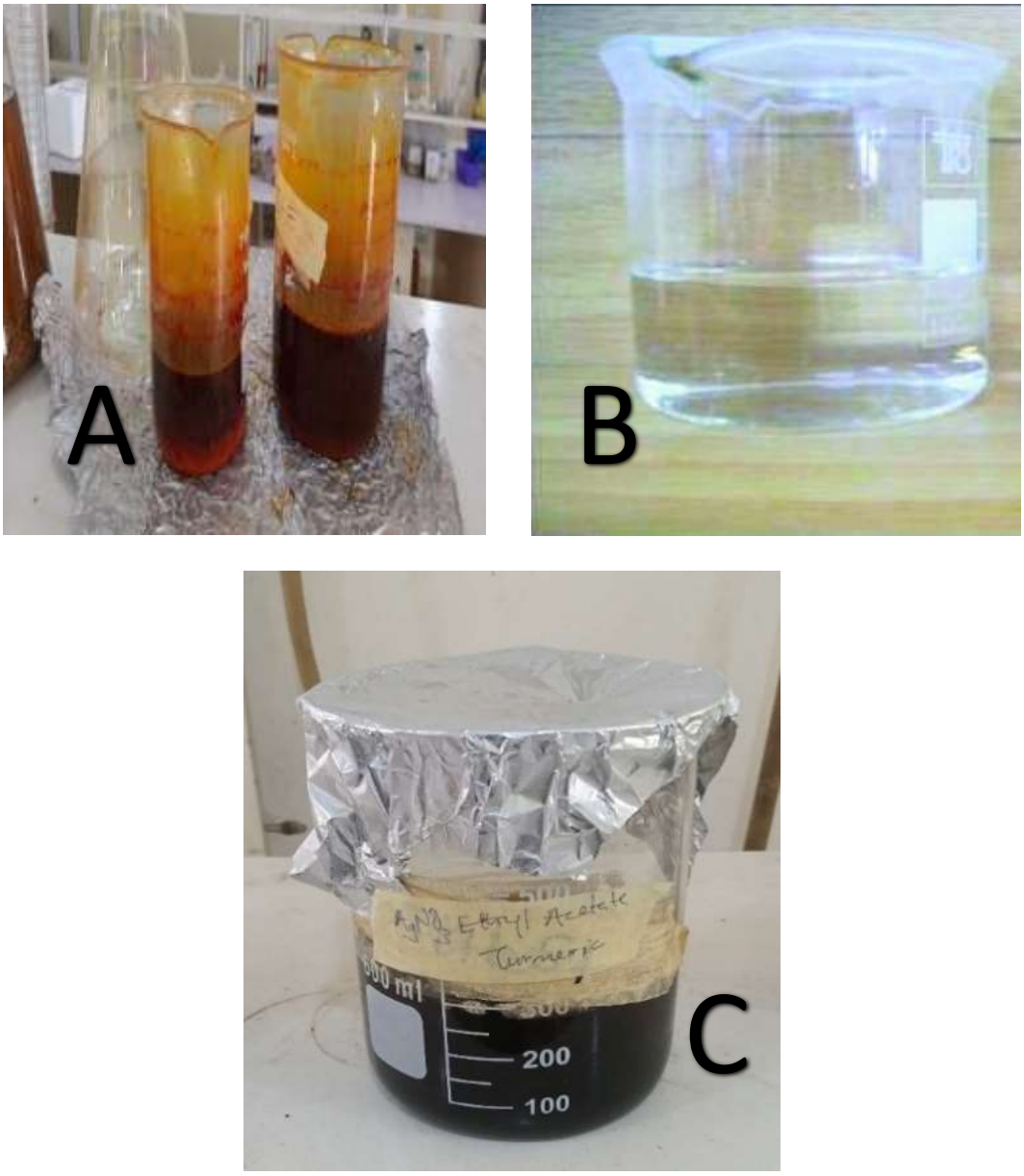

Plate III: Showing (A) Silver nitrate solution ($AgNO_3$), (B) Ethyl acetate fraction and (C) Ethyl acetate synthesized silver nanoparticles (AEAgNPs)

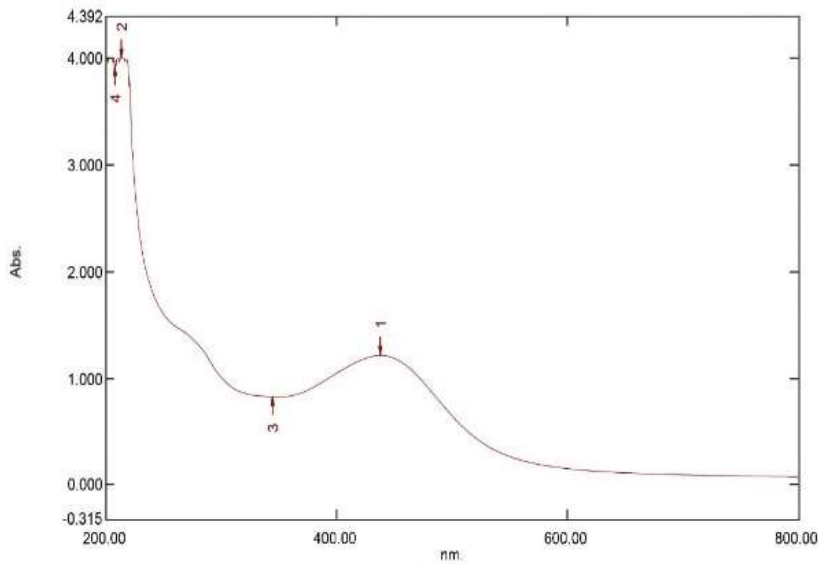

Figure 4.1: Ultra - violet-visible spectrum of nanoparticles synthesized from ethyl acetate fraction

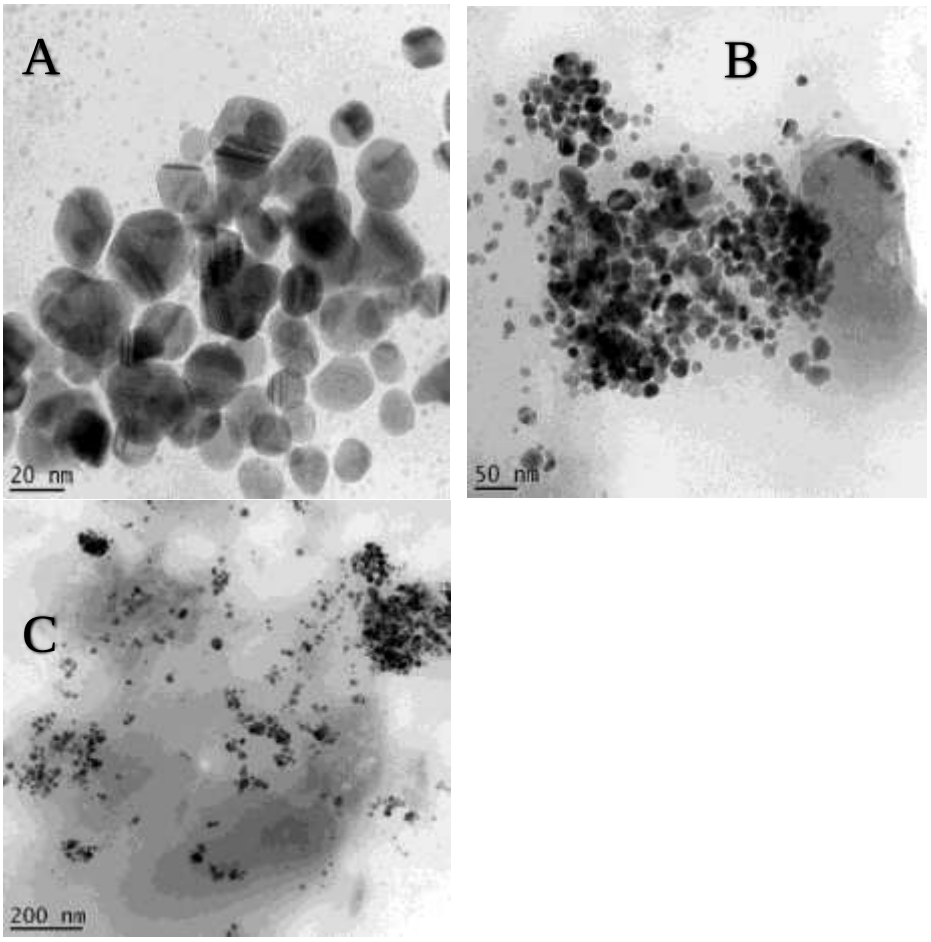

Figure 4.2a: Transmission Electron Microscopy of AEAgNPs with different sizes 20nm (b) 50nm (c) 200nm

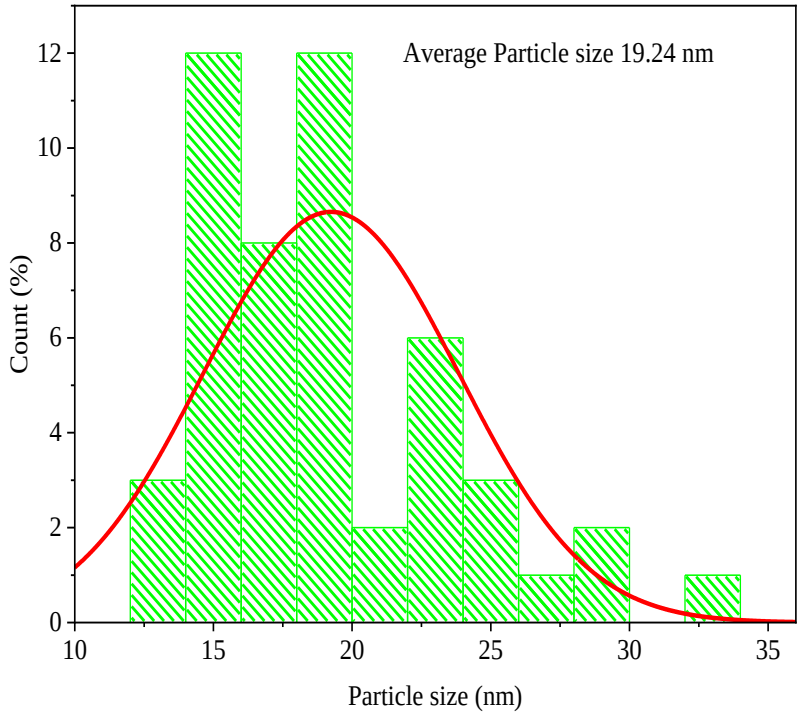

Figure 4.2b: Transmission Electron Microscopy of AEAgNPs graph showing the average particle size.

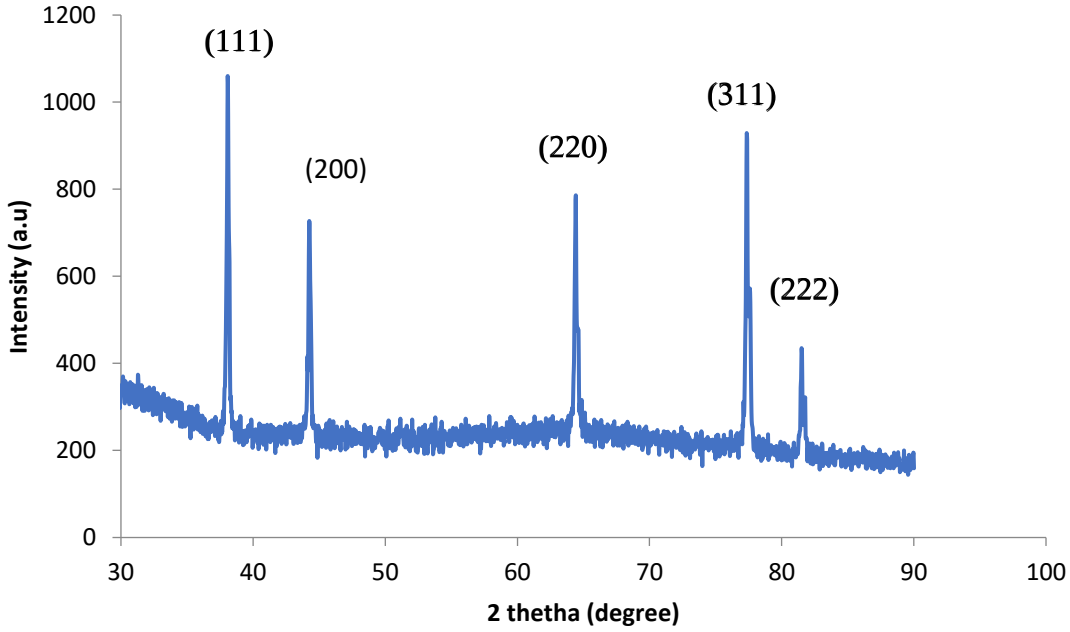

Figure 4.3 X-ray diffraction of AEAgNPs

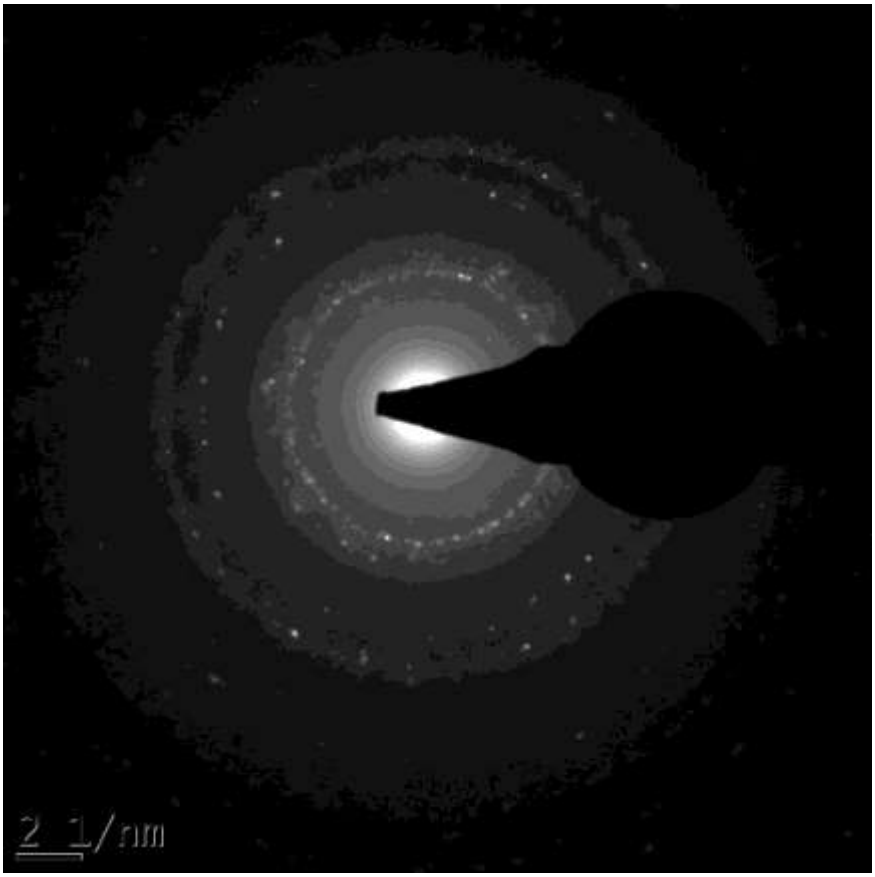

Figure 4.4: selected area of electron diffraction pattern of AEAgNPs

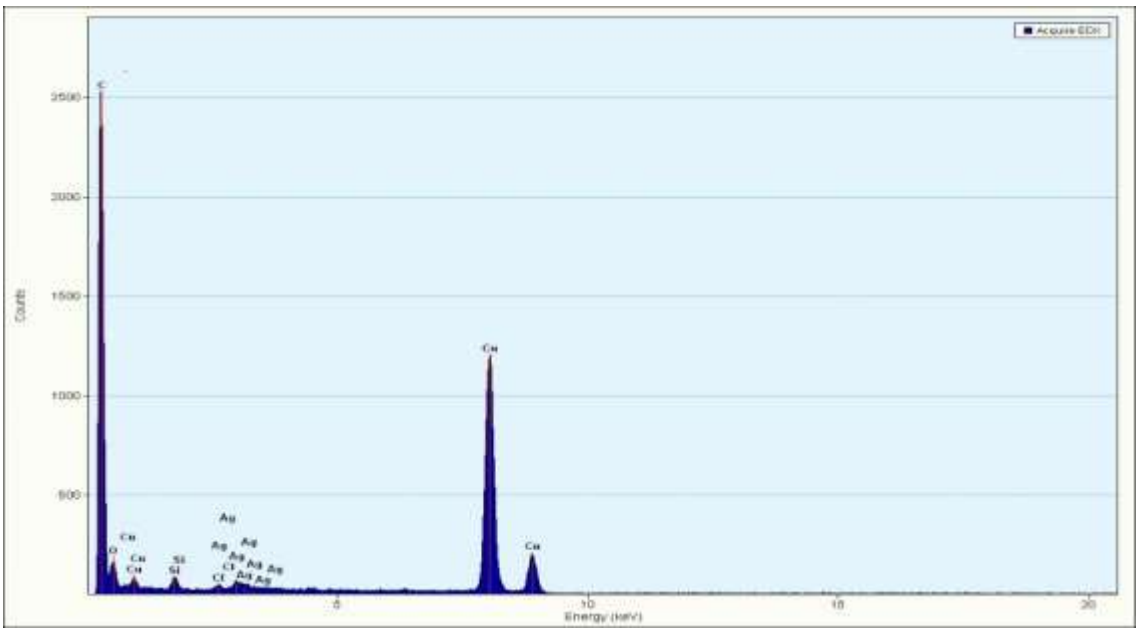

Figure 4.5: Energy dispersive spectrum of AEAgNPs.

4.1.7 Anti-tubercular activities of synthesized nanoparticles from turmeric fraction

Tables 4.14 to 4.16 indicates the anti-tubercular activities of synthesized nanoparticles from turmeric fraction against the *Mycobacterium* species. Synthesized ethyl acetate (AEAgNPs) fraction inhibited the growth of *Mycobacterium tuberculosis* with MIC at 39 µg/mL (0.039 mg/mL) while the MBC of ethyl acetate (AE) fraction was 78 µg/mL (0.078 mg/mL) as represented in Table 4.14.

In Table 4.15 the anti-tubercular activities against *Mycobacterium bovis,* showed that the synthesized ethyl acetate (AEAgNPs) fraction inhibited the growth of *M. bovis* with MIC at 20 µg/mL (0.02 mg /mL) while the MBC was 39 µg/mL (0.039 mg /mL). Table 4.16 shows the anti-tubercular activities against *Mycobacterium smegmatis.* Synthesized ethyl acetate (AEAgNPs) had MIC value at 39 µg/mL (0.039 mg/mL) while the MBC for ethyl acetate was 78 µg/mL (0.078 mg/mL).

Table 4.14: Anti-tubercular Activities of Synthesized Nanoparticles against *Mycobacterium tuberculosis*

	Concentration (µg/mL)												
Agents	**5000**	**2500**	**1250**	**625**	**313**	**165**	**78**	**39**	**20**	**10**	**5**	**MIC**	**MBC**
Ethyl Acetate	+	+	+	+	+	+	+	+	-	-	-	40	80
Rifampicin	+	+	+	+	+	+	+	+	+	+	+	0.04	

-: No activity

+: Activity

MIC: Minimum inhibitory concentration

MBC: Minimum bactericidal concentration

Table 4.15: Anti-tubercular Activities of Synthesized Nanoparticles against *Mycobacterium bovis*

	Concentration (µg/mL)												
Agents	**5000**	**2500**	**1250**	**625**	**313**	**165**	**78**	**39**	**20**	**10**	**5**	**MIC**	**MBC**
Ethyl Acetate	+	+	+	+	+	+	+	+	+	-	-	20	40
Rifampicin	+	+	+	+	+	+	+	+	+	+	+	0.04	

-: No activity

+: Activity

MIC: Minimum inhibitory concentration

MBC: Minimum bactericidal concentration

Table 4.16: Anti-tubercular Activities of Synthesized Nanoparticles against *Mycobacterium smegmatis*

	Concentration (µg/mL)												
Agents	**5000**	**2500**	**1250**	**625**	**313**	**165**	**78**	**39**	**20**	**10**	**5**	**MIC**	**MBC**
Ethyl Acetate	+	+	+	+	+	+	+	+	-	-	-	40	80
Rifampicin	+	+	+	+	+	+	+	+	+	+	+	0.04	

-: No activity

+: Activity

MIC: Minimum inhibitory concentration

MBC: Minimum bactericidal concentration

4.1.8 Toxicity profile of ethyl acetate silver nanoparticles

In the oral acute toxicity study as shown in Table 4.17 below, no death or toxicity symptoms was recorded in phase I and phase II. As such, the LD50 of AEAgNPs is greater than 5000 mg/kg body weight.

Table 4.17: Toxicity Profile of Ethyl acetate Silver Nanoparticles

Group	Dosage	Mortality/ No of Rat	Observation
1	10	0/3	No apparent changes
2	100	0/3	No apparent changes
3	1000	0/3	No apparent changes
4	1900	0/3	Sleeping
5	3600	0/3	Sleeping
6	5000	0/3	Sleeping

4.1.9 Effect of ethyl acetate silver nanoparticles on biochemical parameters of rats

The effect of AEAgNPs on some biochemical parameters in rats are shown in Table 4.18. The administration of AEAgNPs (1000 mg/kgbw) to the rats for 28 days significantly ($p< 0.05$) increased the aspartate amino transaminase (AST), alanine amino transaminase (ALT), ALP and bilirubin concentration when compared with the control (normal saline).

Treatment group 25,50 and 100 mg/kgbw showed no significant ($p> 0.05$) difference in protein concentration, but there was significant ($p< 0.05$) decrease in protein and albumin concentration in rats treated with AEAgNPs (1000 mg/kgbw) when compared with the control (normal saline). However, there was no significant ($p< 0.05$) difference in AST, ALT and ALP treated with AEAgNPs (1000 mg/kgbw) when compared with rifampicin.

Table 4.18: Effect of Ethyl Acetate Silver Nanoparticles on Liver Function Indices in Rats

Dose (mg/kg bw)	AST (µ/L)	ALT (µ/L)	ALP (µ/L)	Total protein (mg/dL)	Total bilirubin (mmol/L)	Albumin (mg/dL)
25	35.11 ± 2.09^{bc}	25.49 ± 0.96^{a}	68.85 ± 1.00^{a}	7.58 ± 0.41^{bc}	0.53 ± 0.02^{a}	4.59 ± 0.40^{b}
50	32.68 ±1.07^{ab}	23.19 ± 1.43^{a}	69.83 ± 1.09^{a}	6.92 ± 0.54^{b}	0.51 ± 0.05^{a}	3.73 ± 0.17^{a}
100	29.20 ± 0.53^{a}	22.85 ± 0.79^{a}	69.90 ± 2.28^{a}	8.37 ±0.25^{c}	0.50 ± 0.02^{a}	3.84 ± 0.10^{a}
1000	42.61 ±1.65^{d}	42.30 ±1.74^{b}	86.79 ± 0.77^{b}	5.42 ±0.27^{a}	0.71 ± 0.01^{b}	3.83 ± 0.16^{a}
Rifampicin	42.55±0.45^{d}	32.50±0.50^{b}	84.20±0.20^{b}	7.12±0.60^{bc}	0.75 ±0.02^{c}	4.33±0.13^{b}
Normal saline	37.68 ±1.48^{c}	24.93 ±1.84^{a}	69.12 ±0.58^{a}	7.96 ±0.04^{bc}	0.58 ± 0.04^{a}	4.81 ± 0.17^{b}

Values are presented as mean ± standard error of mean (SEM) of three replicates. Values with different superscripts in a column are significantly different at $p < 0.05$.Mg/kgbw: milligram per kilogram body weight of animals, µ/L: micro per liter, mg/dL: milligram per deciliter, AST: Aspartate amino transaminase, ALT: Alanine amino transaminase, ALP: Alkaline phosphatase.

4.1.10 Effect of ethyl acetate silver nanoparticles on Kidney function indices of rats

Creatinine and uric acid concentration were not significantly ($p< 0.05$) different in rats administered AEAgNPs (25, 50 and 100 mg/kgbw) when compared with the control (normal saline). There was significant ($p< 0.05$) increase in all the kidney function indices of rats treated with AEAgNPs (1000 mg/kgbw) when compared with the control (normal saline).

Urea concentration was significantly ($p< 0.05$) lowered in rats treated with AEAgNPs (50 mg/kgbw) when compared with the control. Similarly, urea concentration was significantly lowered in rats treated with rifampicin when compared with the treatment group's 25-1000 mg/kgbw (Table 4.19).

Table 4.19: Effect of Ethyl Acetate Silver Nanoparticles on Kidney Function Indices of Rats

Dose (mg/kg bw.)	Creatinine (mg/dL)	Urea (mg/dL)	Uric acid (mg/dL)
25	7.05 ± 0.16^{a}	45.03 ± 1.26^{ab}	7.87 ± 0.19^{a}
50	6.78 ± 0.19^{a}	41.71 ± 0.88^{a}	7.64 ± 0.40^{a}
100	6.66 ± 0.20^{a}	43.46 ± 1.56^{ab}	8.09 ± 0.48^{a}
1000	8.46 ± 0.44^{b}	57.67 ± 0.90^{c}	11.25 ± 0.62^{b}
Rifampicin	7.25 ± 0.07^{a}	32.10 ± 0.10^{a}	6.97 ± 0.02^{a}
Normal saline	7.56 ± 0.25^{a}	46.31 ± 1.75^{b}	8.83 ± 0.36^{a}

Values are presented as mean ± standard error of mean (SEM) of three replicates.

Values with different superscripts in a column are significantly different at $p < 0.05$. Mg/dL: milligram per deciliter, mg/kgbw: milligram per kilogram body weight of animals.

4.1.11 Effect of the ethyl acetate silver nanoparticles on Lipid profile of rats

Administration of AEAgNPs daily to the rats, at dose (1000 mg/kgbw) significantly ($p< 0.05$) increased the cholesterol, triglycerides and LDL-Cholesterol concentration when compared with the control (normal saline). However, there was no significant ($P>0.05$) difference in triglycerides concentration in rats treated with 25, 50 and 100 mg/kgbw respectively.

HDL-Cholesterol decreased significantly ($p< 0.05$) in rats treated with 25 and 1000 mg/kgbw of AEAgNPs when compared to the control (normal saline) Table 4.20.

Table 4.20: Effect of Ethyl Acetate Silver Nanoparticles on Lipid Profile of Rats

Dose (mg/kgbw.)	Total cholesterol (mg/dL)	Triglycerides (mg/dL)	HDL-C (mg/dL)	LDL-C (mg/dL)
25	252.65 ± 1.00^{bc}	133.05 ± 1.65^{a}	5.52 ± 0.93^{bc}	121.29 ± 2.10^{b}
50	248.97 ± 2.09^{ab}	139.71 ± 3.59^{a}	97.06 ± 0.64^{d}	108.08 ± 1.35^{a}
100	245.51 ± 3.08^{a}	135.59 ± 2.16^{a}	89.04 ± 0.87^{c}	112.60 ± 1.09^{a}
1000	282.27 ± 1.20^{d}	154.56 ± 1.28^{b}	70.32 ± 1.63^{a}	131.50 ± 1.51^{c}
Rifampicin	261.50 ± 0.50^{d}	140.20 ± 0.20^{a}	81.50 ± 0.50^{b}	109.30 ± 0.20^{a}
Normal saline	256.92 ± 1.52^{c}	140.08 ± 1.71^{a}	84.44 ± 2.13^{b}	119.62 ± 2.44^{b}

Values are presented as mean ± standard error of mean (SEM) of three replicates.

Values with different superscripts in a column are significantly different at $p < 0.05$, mg/kgbw: milligram per kilogram body weight of animals, milligram per decilitre, HDL-C: High density lipoprotein cholesterol, LDL-C: Low density lipoprotein cholesterol

4.1.12 Effect of ethyl acetate silver nanoparticles on haematological parameters of rats

Group treated with synthesized ethyl acetate nanoparticles (50 mg/kgbw) showed no significant ($p< 0.05$) effect on packed cell volume (PCV) while the groups treated with 100 and 1000 mg/kgbw showed significant increase in PCV when compared with the control (normal saline).There was no significant ($p< 0.05$) effect in the haemoglobin count (HB), red blood cell (RBC) and mean corpuscular haemoglobin concentration (MCHC), monocytes and eosinophils of all the treatment groups, while there was significant decrease in blood platelet, mean corpuscular volume (MCV) and neutrophils when compared with the control (normal saline).

There was significant ($p>0.05$) elevation in packed cell volume (PCV) and white blood cell (WBC) while there was a significant decrease in haemoglobin (HB) and mean corpuscular volume (MCV) when compared with Rifampicin as shown in tables 4.21 and 4.22.

Table 4.21: Effect of Ethyl Acetate Silver Nanoparticles on Haematological Parameters of Rat

Dose (mg/kg bw.)	PCV	HB (g/dL)	RBC ($x10^9$/L)	Platelet ($x10^6$/L)	WBC ($x10^6$/L)	MCV (FL)	MCHC (g/dL)
25	30.00±2.31^{a}	10.00±0.91^{a}	4.10±0.12^{a}	314.00±4.62^{d}	5.90±0.43^{a}	131.00±3.46^{d}	33.30±1.97^{a}
50	40.00±1.15^{bc}	13.30±1.22^{ab}	5.00±0.58^{a}	215.00±3.46^{a}	4.00±0.58^{a}	30.00±1.73^{a}	33.20±2.23^{a}
100	45.00±2.31^{c}	15.00±1.15^{b}	4.00±0.12^{a}	250.00±3.46^{b}	4.10±0.08^{a}	112.00±2.89^{c}	33.30±1.80^{a}
1000	46.00±1.73^{c}	13.30±1.24^{ab}	4.20±0.12^{a}	324.00±4.62^{d}	4.00±2.89^{b}	109.00±2.31^{c}	33.90±1.73^{a}
Rifampicin	50.50±0.50^{d}	16.57±0.04^{c}	3.25±0.05^{a}	252.50±2.50^{b}	5.20±0.50^{c}	151.50±0.50^{e}	33.22±0.02^{a}
Normal saline	38.00±1.73^{b}	12.60±1.22^{ab}	4.00±0.58^{a}	280.00±4.04^{c}	6.30±0.72^{a}	95.00±2.89^{b}	33.10±1.97^{a}

Values are presented as mean ± standard error of mean (SEM) of three replicates. Values with different superscripts in a column are significantly different at $p < 0.05$. HB: Haemoglobin count, RBC: Red blood cell count, WBC: White blood cell count, MCHC: mean corpuscular haemoglobin concentration, MCV: Mean corpuscular volume, g/dL: gram per deciliter, mg/kgbw: milligram per kilogram body weight of animals, FL: Femtolitre, PCV: Packed cell volume

Table 4.22: Effect of Ethyl Acetate Silver Nanoparticles on Differential Count in Rats

Dose (mg/kg bw.)	Neutrophils (%)	Lymphocytes (%)	Monocytes (%)	Eosinophils (%)
25	38.00 ± 2.31^{b}	40.00 ± 2.31^{b}	8.00 ± 1.15^{c}	4.00 ± 0.58^{b}
50	30.00 ± 2.31^{a}	50.00 ± 4.04^{c}	6.00 ± 1.15^{bc}	4.00 ± 0.58^{b}
100	45.00 ± 2.31^{bc}	40.00 ± 1.73^{b}	3.00 ± 0.58^{a}	2.00 ± 0.58^{a}
1000	50.00 ± 2.31^{c}	41.00 ± 2.31^{b}	6.00 ± 0.58^{bc}	3.00 ± 0.58^{ab}
Rifampicin	55.50 ± 0.50^{c}	40.50 ± 0.50^{b}	3.00 ± 0.01^{a}	4.78 ± 0.01^{c}
Normal saline	60.00 ± 2.31^{d}	31.00 ± 1.73^{a}	5.00 ± 0.58^{ab}	3.00 ± 0.58^{ab}

Values are presented as mean ± standard error of mean (SEM) of three replicates.

Values with different superscripts in a column are significantly different at $p < 0.05$ %: percentage, mg/kgbw: milligram per kilogram body weight of animals

4.1.13 Effect of the ethyl acetate silver nanoparticles on body weight of rats

The effect of the synthesized ethyl acetate fraction on the body weight gain of rats. There was no significant ($p > 0.05$) difference on the body weight gain of rats from week 0 – week 2 in all the treatment groups when compared with the control (normal saline). In week 3, rats administered 1000 mg/kgbw showed significant ($p < 0.05$) difference and weight loss when compared with the control (normal saline). From week 0-3 there was weight loss in rats treated with Rifampicin when compared with the treatment groups Table 4.23.

Table 4.23: Weight Gain of Rats Treated with Ethyl Acetate Silver Nanoparticles

Dose (mg/kg bw.)	Body weight (g)			
	W 0	**W 1**	**W 2**	**W 3**
25	123.03 ± 3.43[a]	131.32 ± 2.28[a]	138.60 ± 2.56[ab]	147.88 ± 3.17[b]
50	122.29 ± 2.42[a]	132.63 ± 2.91[a]	142.60 ± 2.16[ab]	149.97 ± 2.51[b]
100	124.72 ± 2.12[a]	135.24 ± 1.58[a]	144.63 ± 1.63[b]	156.80 ± 1.38[b]
1000	124.33 ± 3.32[a]	130.08 ± 3.13[a]	133.77 ± 2.56[a]	138.44 ± 2.62[a]
Rifampicin	108.25±2.00[a]	104.53±12.50[a]	110.63±4.60[a]	123.35±4.00[a]
Normal saline	123.43 ± 2.95[a]	130.92 ± 3.24[a]	140.85 ± 4.04[ab]	148.99 ± 3.69[b]

Values are presented as mean ± standard error of mean (SEM) of three replicates. Values with different superscripts in a column are significantly different at $p < 0.05$. mg/kgbw: milligram per kilogram body weight of animals, w: week.

4.1.14 Effect of organ weight gain of rats treated with ethyl acetate silver nanoparticles

The effect of AEAgNPs on the organ weight gain of rats. There was no significant ($p > 0.05$) difference in the weight of spleen and lungs, while the liver, kidney and heart, at dose 1000 mg/kgbw significantly ($p < 0.05$) increased when compared with the control (normal saline). However, there was decrease in all the organ weight of rats treated with 0.2mL of Rifampicin when compared with the treatment groups Table 4.24.

Table 4.24: Organ Weight Gain of Rats Treated with Ethyl Acetate Silver Nanoparticles

Grouping	Organ weight (g)				
	Liver	**Kidney**	**Spleen**	**Heart**	**Lungs**
25	6.85±0.05[a]	0.64±0.07[a]	0.57±0.07[a]	1.22±0.08[a]	1.32±0.11[a]
50	6.94±0.07[a]	0.60±0.06[a]	0.54±0.05a	1.18±0.12[a]	1.28±0.09[a]
100	7.32±0.06[a]	0.65±0.06[a]	0.43±0.10[a]	1.20±0.09[a]	1.30±0.13[a]
1000	8.25±0.09[b]	0.79±0.08[b]	0.56±0.06[a]	1.35±0.07[b]	1.45±0.10[a]
Rifampicin	4.01± 0.07[a]	0.61± 0.03[a]	0.20± 0.02[a]	0.29± 0.02[a]	0.73± 0.01[a]
Normal saline	6.98±0.08[a]	0.58±0.05[a]	0.48±0.08[a]	1.12±0.13[a]	1.30±0.12[a]

Values are presented as mean ± standard error of mean (SEM) of three replicates. Values with different superscripts in a column are significantly different at $p < 0.05$, g: gram.

4.1.15 Histological studies of the organs treated with synthesized fraction of AEAgNPs

The microscopic assessment of the organs on the administration of 25 to 1000 mg/kgbw of AEAgNPs and Rifampicin produced histological alteration in the organs of the rats. Pulmonary haemorrhage, thickened inter-alveoli septa with mononuclear cellular infiltration, hemosiderosis and caseous necrosis when treated with AEAgNPs (25 -1000 mg/kgbw) and Rifampicin was detected in the lungs (A) when compared with the control (normal saline) plate IV. In the liver (B), hepatic necrosis with mononuclear cellular infiltration at dose 25 and 1000 mg/kgbw. Hepatic congestion at dose 25 mg/kgbw when compared with the control. Rifampicin caused hepatic necrosis when compared with the control (normal saline) Plate V.

In the kidney (C) at dose 25, 1000 mg/kgbw and Rifampicin, renal congestion, at dose 25 mg/kgbw interstitial haemorrhage while dose 25,100 and 1000 mg/kgbw, interstitial tubular necrosis with mononuclear cellular infiltration was detected when compared with the control Plate VI. Treatment given at doses 25 -1000 mg/kgbw and Rifampicin caused mycocardial haemorrhage in the heart (D) when compared with the control (Plate VII). The spleen (E) had splenic vacuolation at dose 50 mg/kgbw and lymphocytic depletion with increased reticulation at dose 25 and 1000 mg/kgbw while splenic congestion was occurred in rats treated with Rifampicin when compared with the control respectively Plate VIII.

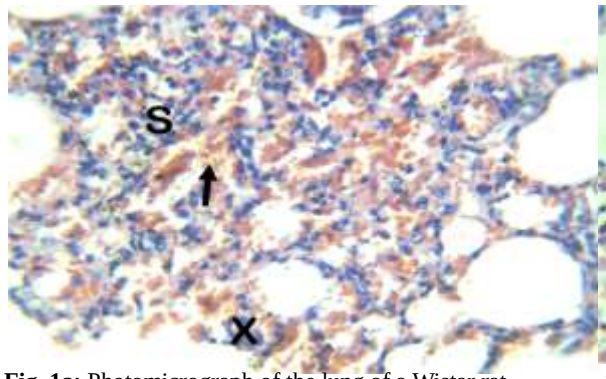

Fig. 1a: Photomicrograph of the lung of a Wistar rat exposed to AEAgNPs (25 mg/kg). Note the pulmonary haemorrhage (arrow) and the thickened inter-alveoli septa (X) with mononuclear cellular infiltration (S). H & E 400

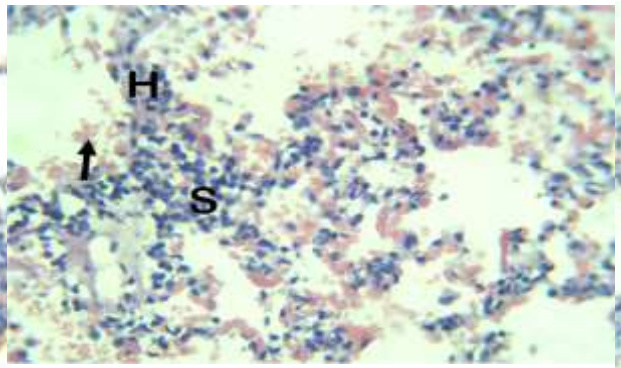

Fig. 1b: Photomicrograph of the lung of a Wistar rat exposed to AEAgNPs (50 mg/kg). Note the pulmonary haemorrhage (arrow) and the thickened inter-alveoli septa (X) with mononuclear cellular infiltration (S). H & E x 400.

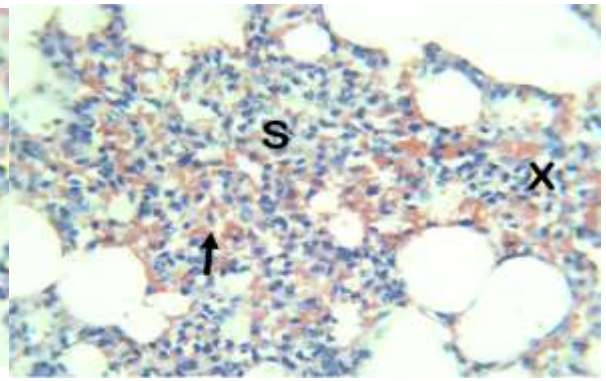

Fig. 1c: Photomicrograph of the lung of a Wistar rat exposed to AEAgNPs (100 mg/kg). Note the pulmonary haemorrhage (arrow) and the thickened inter-alveoli septa (X) with mononuclear cellular infiltration (arrowheads). H & E x 400.

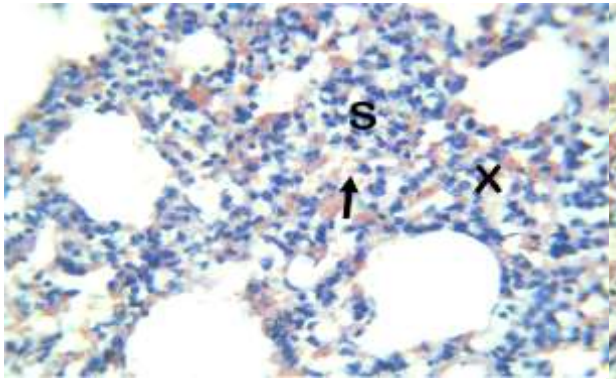

Fig. 1d: Photomicrograph of the lung of a Wistar rat exposed to AEAgNPs (1000 mg/kg). Note the pulmonary haemorrhage (arrow) and the thickened inter-alveoli septa (X) with mononuclear cellular infiltration (arrowheads).H & E x 400.

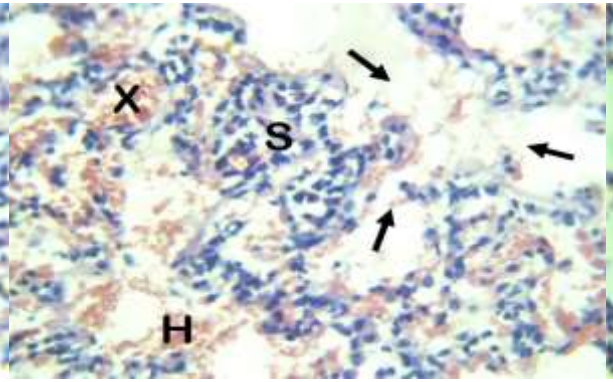

Fig. 1e. Photomicrograph of the lung of a control Wistar rats exposed to Rifampicin (0.2 mL). Note the pulmonary congestion (X), pulmonary haemorrhage (H), thickened inter-alveoli septa with mononuclear cellular infiltration (S), and emphysema (arrows). H & E x 400.

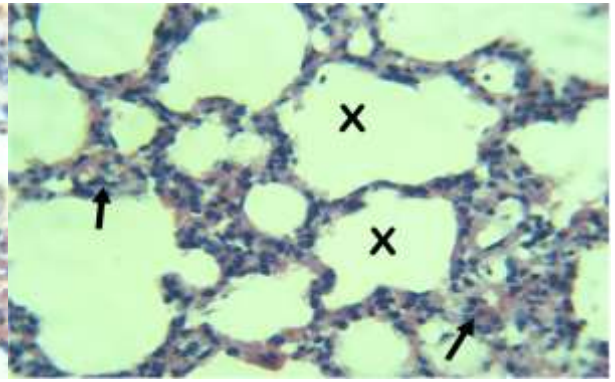

Fig. 1f: Photomicrograph of the lung of a control unexposed Wistar rat. H & E x 400.

Plate IV: Photomicrographs of the lungs section of rat treated with ethyl acetate silver nanoparticles

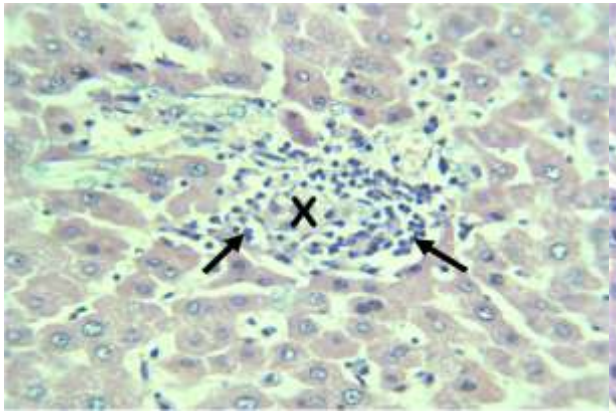

Fig. 2a: Photomicrograph of the liver of a Wistar rat exposed to AEAgNPs (25 mg/kg). Note the hepatic necrosis (x) with mononuclear cellular infiltration (arrows). H & E x 400.

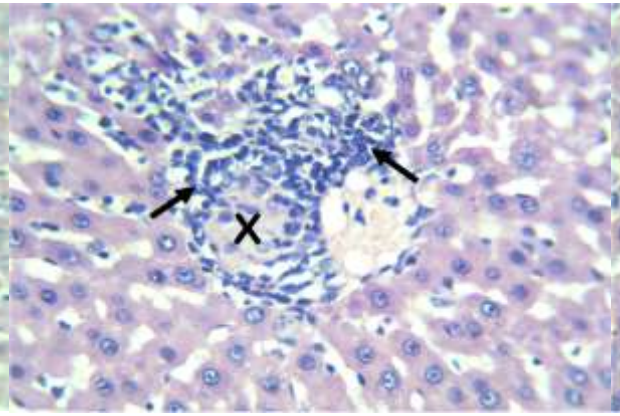

Fig. 2b: Photomicrograph of the liver of a Wistar rat AEAgNPs (50 mg/kg). Note the hepatic necrosis (x) with mononuclear cellular infiltration (arrows). H & E x 400.

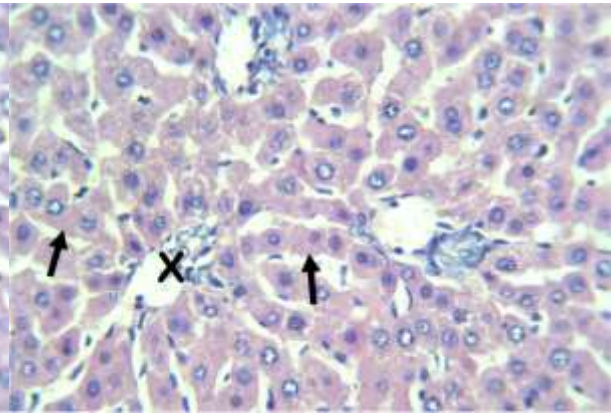

Fig. 2c: Photomicrograph of the liver of a Wistar rat exposed AEAgNPs (100 mg/kg). Note the portal triad (X) and the hepatocytes (arrows). H & E x 400.

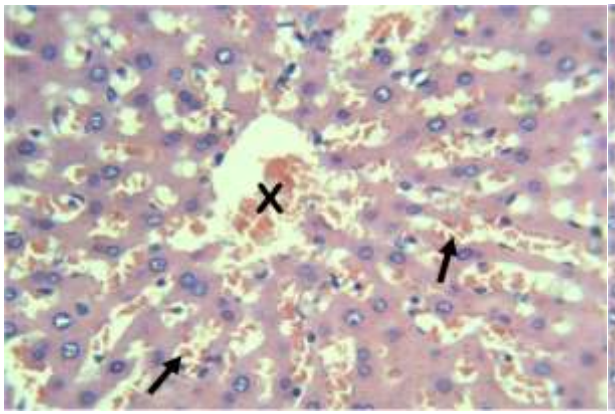

Fig. 2d: Photomicrograph of the liver of a Wistar rat exposed to AEAgNPs (1000 mg/kg). Note the hepatic congestion of the central vein (X) and the hepatic sinusoids (arrows). H & E x 400.

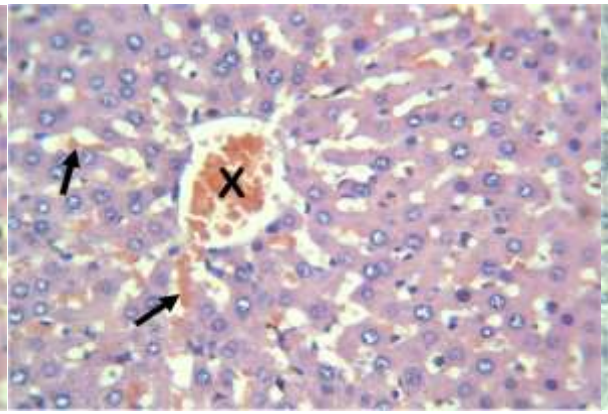

Fig. 2e: Photomicrograph of the liver of a control Wistar rats exposed to Rifampicin (0.2 mL). Note the hepatic congestion of the central vein (X) and the hepatic sinusoids (arrows). H & E x 400.

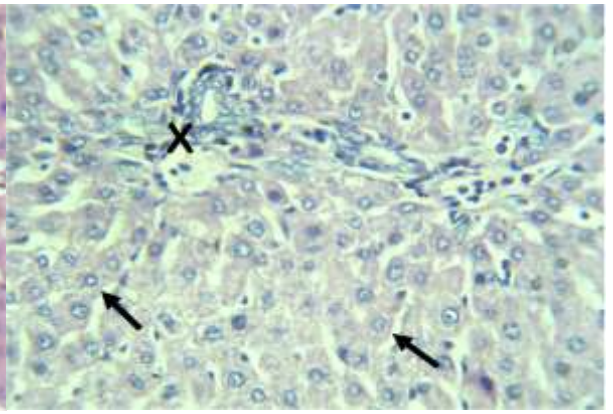

Fig. 2f: Photomicrograph of the liver of a control unexposed Wistar rat. H & E x 400.

Plate V: Photomicrographs of the liver section of rat treated with ethyl acetate silver nanoparticles

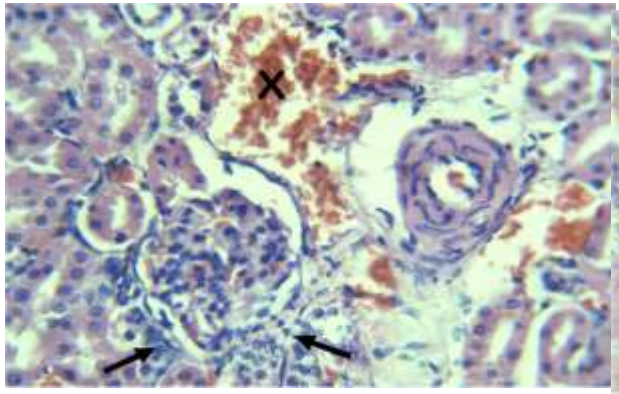

Fig. 3a: Photomicrograph of the kidney of a Wistar rat exposed to ……..…… (25 mg/kg). Note the renal congestion (X), interstitial tubular necrosis with mononuclear cellular infiltration (arrows). H & E x 400.

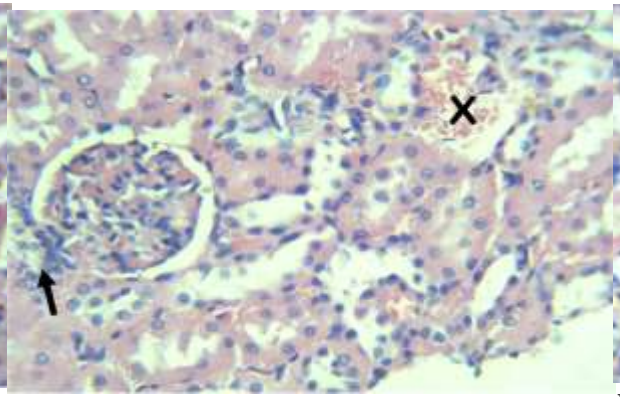

Fig. 3b: Photomicrograph of the kidney of a Wistar rat exposed to ……..…… (50 mg/kg). Note the renal congestion (X), interstitial tubular necrosis with mononuclear cellular infiltration (arrow). H & E x 400.

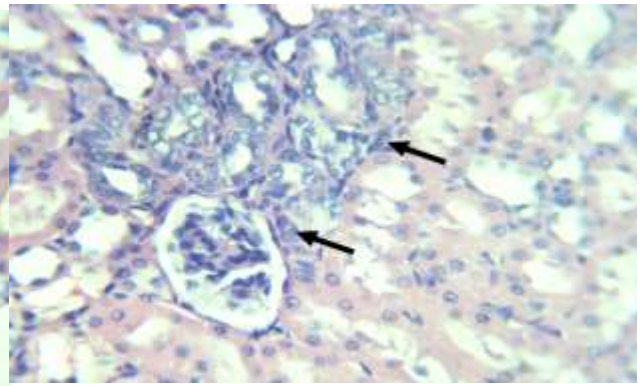

Fig. 3c: Photomicrograph of the kidney of a Wistar rat exposed to ……. (100 mg/kg). Note the interstitial tubular necrosis with mononuclear cellular infiltration (arrows). H & E x 400.

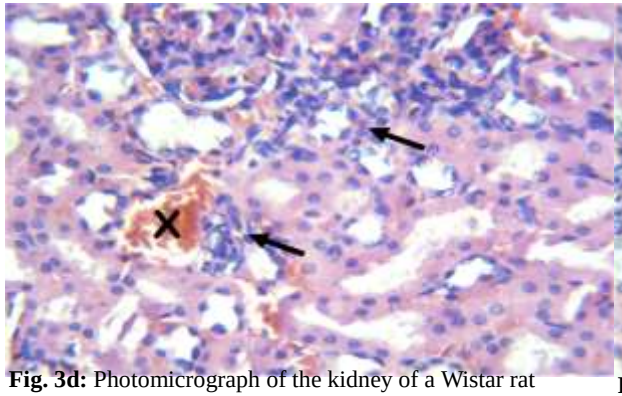

Fig. 3d: Photomicrograph of the kidney of a Wistar rat exposed to ……..…… (1000 mg/kg). Note the renal congestion (X), interstitial tubular necrosis with mononuclear cellular infiltration (arrows). H & E x 400.

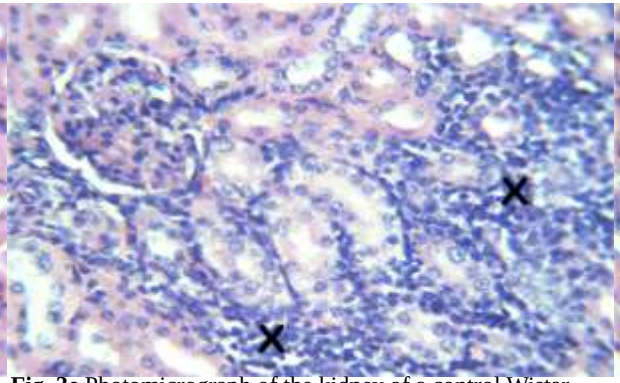

Fig. 3e Photomicrograph of the kidney of a control Wistar rats exposed to Rifampicin (0.2 mL). Note the tubular necrosis with interstitial mononuclear cellular infiltration (X). H & E x 400.

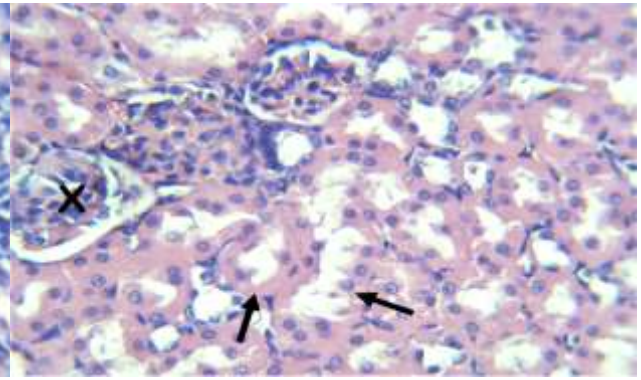

Fig. 3f: Photomicrograph of the kidney of a control unexposed Wistar rat. H & E x 400.

Plate VI: Photomicrographs of the Kidney section of rat treated with ethyl acetate silver nanoparticles

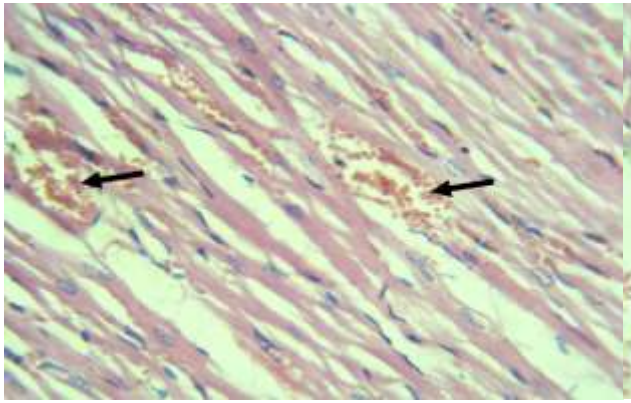

Fig. 4a: Photomicrograph of the heart of a Wistar rat exposed to ……..……. (25 mg/kg). Note the haemorrhages within the heart musculature (arrows). H & E x 400.

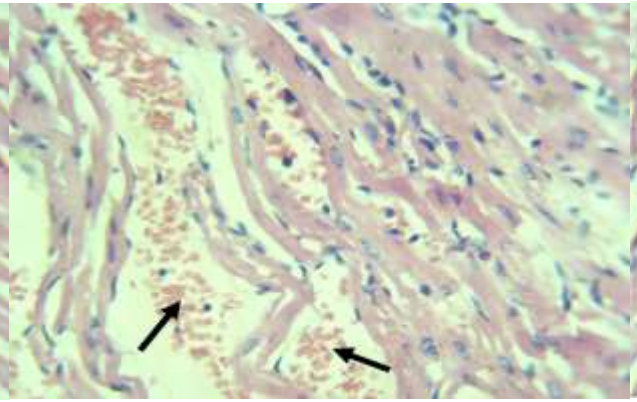

Fig. 4b: Photomicrograph of the heart of a Wistar rat exposed to ……..……. (50 mg/kg). Note the haemorrhages within the heart musculature (arrows). H & E x 400.

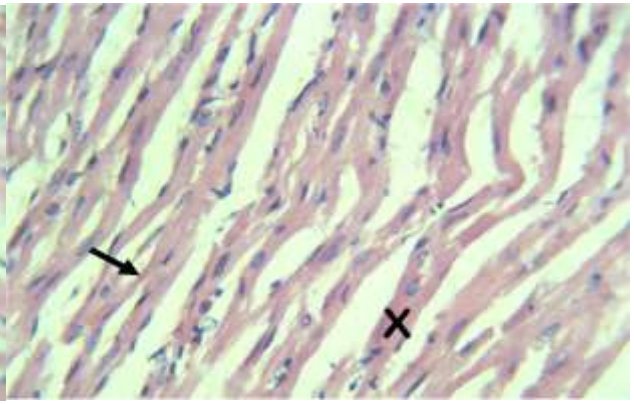

Fig. 4c: Photomicrograph of the kidney of a control Wistar rats exposed to …… 100 mg/kg). Note the cardiomyocyte (X) and the intercalated discs (arrow). H & E x 400.

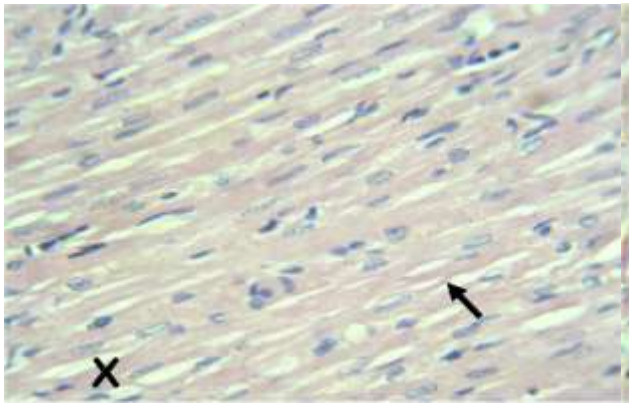

Fig. 4d: Photomicrograph of the kidney of a control Wistar rats exposed to …… 1000 mg/kg). Note the cardiomyocyte (X) and the intercalated discs (arrow). H & E x 400.

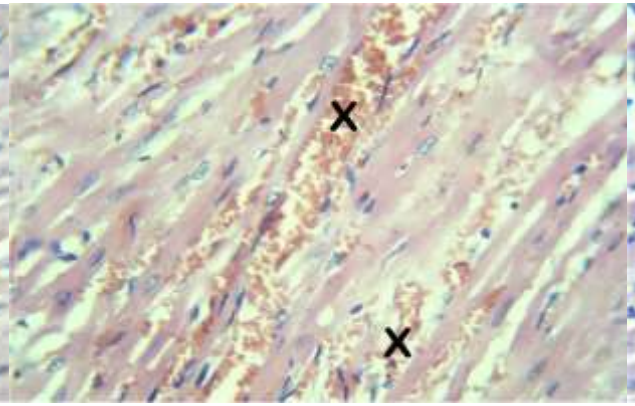

Fig. 4e Photomicrograph of the kidney of a control Wistar rats exposed to Rifampicin (0.2 mL). Note the diffuse haemorrhages within the heart musculature (X). H & E x 400.

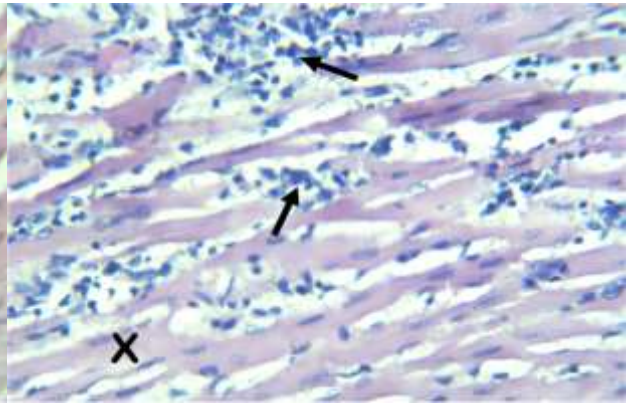

Fig. 4f: Photomicrograph of the heart of a control unexposed Wistar rat. Note the cardiomyocytes (X) with mononuclear cellular infiltration (arrows). H & E x 400.

Plate VII: Photomicrographs of the heart section of rat treated with ethyl acetate silver nanoparticles

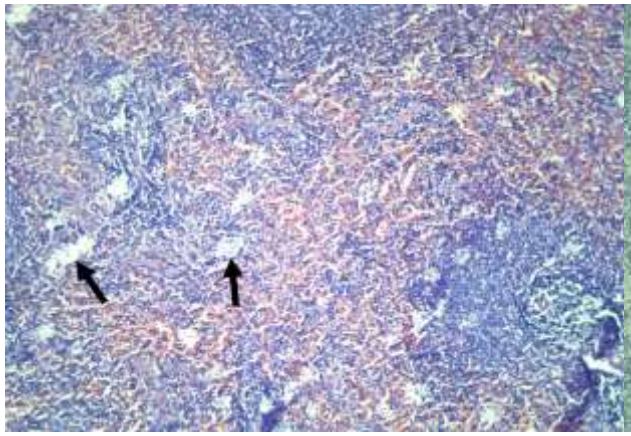

Fig. 5a: Photomicrograph of the spleen of a Wistar rat exposed to (25 mg/kg). Note the vacuolations (arrows). H & E x 100.

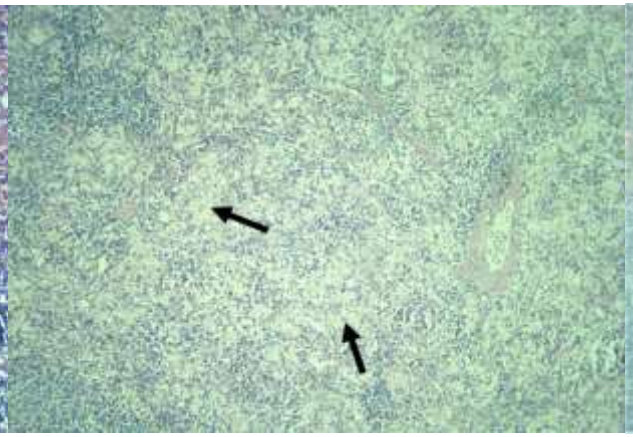

Fig. 5b: Photomicrograph of the spleen of a Wistar rat exposed to (50 mg/kg). Note the lymphocytic depletion with prominent reticulation (X). H & E x 100.

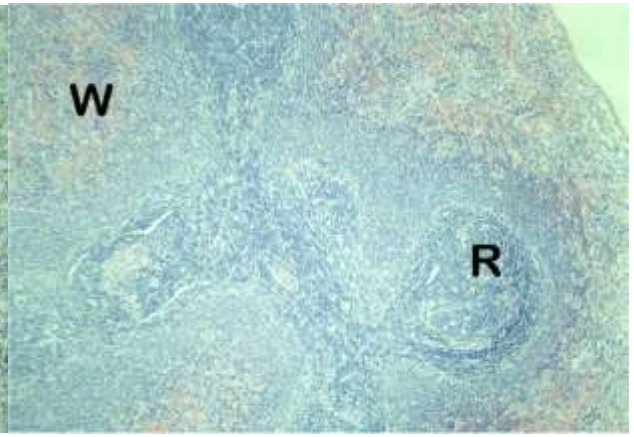

Fig. 5c: Photomicrograph of the spleen of a Wistar rat exposed to (100 mg/kg). Note the white pulp (W) and the red pulp (R). H & E x 100.

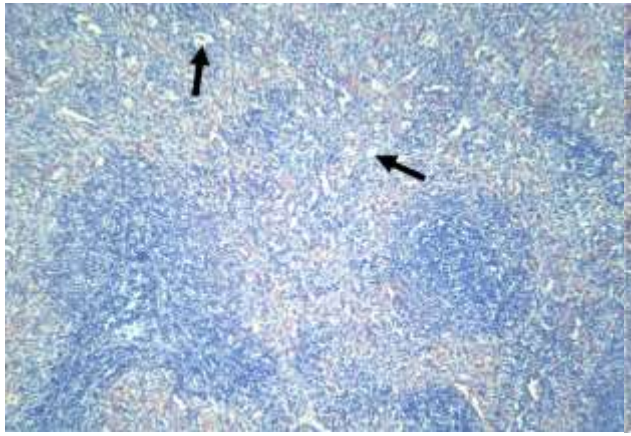

Fig. 5d: Photomicrograph of the spleen of a Wistar rat exposed to (1000 mg/kg). Note the vacuolations (arrows). H & E x 100.

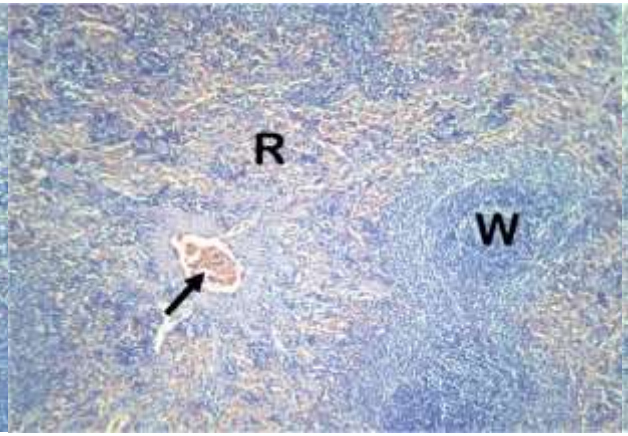

Fig. 5e: Photomicrograph of the spleen of a wistar rat exposed
to Rifampicin (0.2 mL). Note the congested splenic vein (arrow), white pulp (W) and the red pulp (R). H & E x 100.

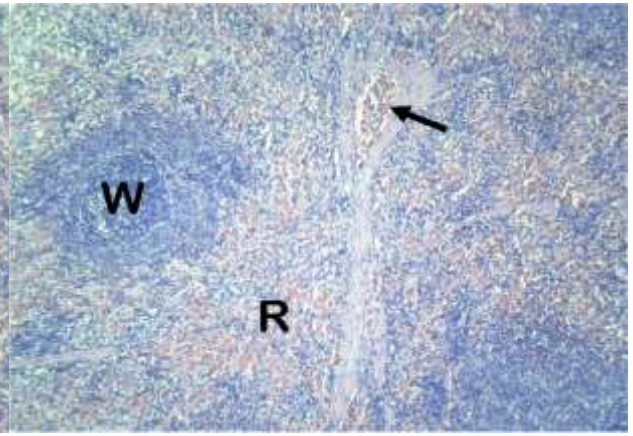

Fig. 5f: Photomicrograph of the spleen of a control unexposed Wistar rat. H & E x 100.

Plate VIII: Photomicrographs of the Spleen section of rat treated with ethyl acetate silver nanoparticles

4.2 Discussion

4.2.1 Qualitative phytochemical components of the medicinal plants

The current investigation revealed the presence of flavonoids, phenols, saponins, alkaloids, and tannins in the extract and fractions of *Curcuma longa* and *Saccharum officinarum* (Tables 4.2 and 4.3). This result corresponds with the findings of Ngadino *et al.* (2018) and Muhammad and Fathuddin (2021) who reported the presence of flavonoids, alkaloids, tannins, phenols, and saponins in *Curcuma longa*. The presence of saponins, alkaloids, tannins, and phenols has been reported in medicinal plants such as *Curcuma longa* (Ferrar *et al.*, 2021), *Tetrapleura tetraptera* (Poro *et al.*, 2021). The sugarcane peel revealed the presence of reducing sugar, alkaloids, phenols, flavonoids, and tannins. This is similar to the findings of Uchenna *et al.* (2015), who reported the presence of saponins, tannins, phenols, flavonoids, and reducing sugars.

Flavonoids induce cell death and inhibit the growth of *Mycobacteria*, it has an inhibitory effect on fatty acid and also inhibit the mycolic acid biosynthesis of *Mycobacterium tuberculosis* (Alka *et al*., 2020). Flavonoids and tannins act on reactive oxygen species, phenol possesses free radical scavenging properties (Mangwani *et al.* 2020). While saponins are bioactive compounds produced mainly by plants, they generally occur chemically as glycosides of steroids or polycyclic triterpenes. According to Olatunji *et al.* (2021), saponins stimulate the immune system and ease coughing by making the bronchial secretion less viscous and reducing the congestion of the bronchi. Phenols can inhibit efflux pumps (Mazlun *et al*., 2019). Tannins have been found to form irreversible complexes with proline proteins resulting in the inhibition of cellular protein synthesis (Olatunji *et al.*, 2021). Reducing sugar and non-reducing sugar plays an important role in the central metabolic

pathways and help in the production of secondary metabolites that enhance the medicinal properties of plants (Ashraf *et al*. 2022). Arya *et al*. (2018) reported that alkaloids showed the inhibition of ATP-dependent transport of compounds across the cell membrane and disrupt the peptidoglycan component of the bacterial cell, preventing the formation of an intact cell wall. It also affects the amino acids of the cell wall and bacterial DNA.

According to Ferrar *et al*. (2021), the inhibitory activity of turmeric extract and fractions could be a result of the extraction method used, the location in which the plant materials were collected, and the type of turmeric used. Thus, cold maceration used for the extraction of the plant in the absence of heat may be a suitable technique as components of extract and fractions that may be heat labile are retained. Many researchers have reported that the activity of different plant extracts depends on the solvent used for extraction (Radhika *et al*., 2020). Ethyl acetate fraction displayed a good spectrum of activity which may be due to, the solvent high affinity for different bioactive components that are now concentrated in ethyl acetate fraction. The solvent being a mid-polar one, was able to extract both hydrophobic and hydrophilic compounds. The presence of these compounds in the fraction enhanced the penetration of the hydrophobic outer membrane of *Mycobacterium tuberculosis* species to exert marked inhibitory effects (Martin *et al.,* 2015). Samreen and Prakash, (2021) reported that *Curcuma longa* acts effectively to eliminate *Mycobacterium tuberculosis* in TB-infected patients. Curcumin which is the major component of *Curcuma longa* is reported to prevent anti-TB drug-induced hepatic damage. According to Bai *et al.* (2016), Barua and Buragohain, 2021), *Curcuma longa* was proven to increase the ability of human monocytic cells (THP-I cell line) infected with *Mycobacterium tuberculosis* $H_{37}R_v$ to control infection via inhibition of nuclear factor kappa-light-chain-enhancer of activated B cells (NF_{KB}).

4.2.3 Anti-tubercular activities of crude extract and fractions of medicinal plants

In this study, all the crude extract and fractions of turmeric rhizomes were able to inhibit the growth of *Mycobacterium tuberculosis* at 5000 µg/mL as shown in (Table 4.5), which is in line with the findings of Poro *et al*. (2021) on inhibition of *Mycobacterium tuberculosis* with *Carissa edulis* extract at 5000 µg/mL. This observation supported our findings of turmeric as a potent anti-tubercular extract. The inhibitory potential exhibited by the crude extract and fractions may be due to the presence of phytoconstitutents (Izebe *et al*., 2020), which may be acting singly or in combination to inhibit the growth of the organisms (Ehiobu *et al*., 2021). The ethyl acetate fraction of turmeric at 50 %v/v concentration inhibited the growth of *M. tuberculosis* M. *bovis,* and *M. smegmatis.* In agreement with Babayi *et al.* (2022) the extract of *Syzygium aromaticum* at 50 %v/v concentration inhibited the growth of *Mycobacterium bovis, M. smegmatis* and *M. tuberculosis.*

According to Poro *et al*. (2021), crude extract and fractions are considered to have antimicrobial activity during a susceptibility test if its minimum inhibitory concentration (MIC) is in the range of 100-1,000 µg/mL. The activity is significant when the MIC is less than 100 µg/mL, moderate when the MIC is between 100 - 625 µg/mL, and low when is higher than 625 µg/mL. The extract and fractions used in this study were able to inhibit the growth of *Mycobacterium tuberculosis* with MIC within 20 µg/mL – 39 µg/mL and the MBC within 39 µg/mL- 78 µg/mL. Therefore, the extracts and fractions of *Curcuma longa* have significant activity while that of sugarcane peels have moderate activity. In a similar study, Safitri *et al*. (2017) reported that *Curcuma longa* rhizomes inhibited the growth of *Mycobacterium tuberculosis* ($H_{37}R_v$) at MIC of 187.5 µg/mL, Ngadino *et al.* (2018) also reported that *Curcuma xanthorrhiza* ethanolic extract inhibited the growth of *Mycobacterium*

tuberculosis ($H_{37}R_v$) at MIC of 1600 µg/mL. In contrast to the result obtained in this present study, Sivakumar and Jayaraman (2011) reported that ethanol and aqueous extracts of *Curcuma longa* were not able to inhibit the growth of *Mycobacterium tuberculosis* ($H_{37}R_v$). The MBC results for the extract and fractions of turmeric was within 39 µg/mL - 78 µg/mL, which showed better inhibition at a lower concentration than the research carried out by Mohammad *et al*. (2018) on *Costus speciosus* stem chloroform and n- hexane fractions which inhibited the growth of *Mycobacterium tuberculosis* with MBC at 200 µg/mL.

The MIC of petroleum ether fraction against *M. tuberculosis* was 0.781 %v/v and MBC was 1.562 %v/v. While the MIC of *M. bovis* and *M. smegmatis* were 0.390 %v/v and MBC were 0.781 %v/v respectively. Babayi *et al.* (2022) reported that the extract of *S. aromaticum* at 50 % v/v concentration inhibited the growth of *Mycobacterium bovis, M. smegmatis* and *M. tuberculosis* with minimum inhibitory concentration of 0.2 % v/v, 0.1 % v/v and 0.2 % v/v respectively and MBC of the extracts were 0.39 % v/v, 0.2 % v/v and 0.39 % v/v respectively. The reason for this activity in the result could be the choice of solvent, how the plant material was dried and the method of extraction (Mueller-Harvey, 2019).

The inhibitory activity of extract and fractions against *Mycobacterium bovis* revealed all the crude extract and fractions of turmeric rhizomes were able to inhibit the growth of *Mycobacterium bovis* at 5000µg/mL (Table 4.7), which is in line with the findings of Ankomah (2020) using *Lantana hispida* plant extract. Activity was reported on *Mycobacterium bovis* with MIC at 5000 µg/mL. The MIC ranged from 20 µg/mL -78 µg/mL. Therefore, the rhizomes of *C. longa* extract and fractions have significant activity. The ethyl acetate fraction of *Curcuma longa* was able to inhibit the growth of *Mycobacterium bovis* with MIC of 78 µg/mL, which was the same to that obtained, by Aro *et al*. (2019) who

reported that the crude extracts of *Plantago lanceolata* and *Psychotria zombamontana* had MIC value of 78 µg/mL against *Mycobacterium bovis*. The MBC value of *C. longa* extract and fractions ranged from 39 µg/mL – 165 µg/mL. Donfack *et al.* (2014) reported that *Annickia chlorantha* stem had a minimum bactericidal concentration of 313 µg/mL against *M. bovis,* a value higher than the result obtained in this study, could be as a result of the choice of plants (Nguta *et al.,* 2016)

For *Smegmatis,* all the crude extract and fractions of turmeric rhizomes inhibited the growth of *Mycobacterium smegmatis* at 5000 µg/mL (Table 4.9). Nugta *et al*. (2016) made a similar observation using *M. smegmatis* hydroethanolic leaf extract from *Aloe vera* and *Drosera rotundifolia at* 5000 µg/mL. The plant extract and fractions used in this study (turmeric) was able to inhibit the growth of *M. smegmatis* with MIC ranging from 20 µg/mL to 78 µg/mL. Therefore, the rhizomes of *C. longa* extract and fractions have significant activity, which was comparable to the ethyl acetate extract of *Piper longum* that inhibited the growth of *M. smegmatis* with MIC of 32 mg/mL as reported by Ravindran *et al*. (2020). Kumar *et al*. (2022) reported that the ethanolic extract of *Solanum torvum* leaves exhibited a MIC of 12.5 µg/mL and was effective against *Mycobacterium smegmatis,* a value that is lower than the MIC of *C. longa* recorded in this study. *Combretum hereroense* hexane extract exhibited MIC of 1600 µg/mL against *M. smegmatis,* a value higher than the MIC of *C. longa* recorded in this study. The activity may be due to the presence of phytochemical components detected in them (Array, 2019). Ethyl acetate fraction of turmeric had MBC value of 1600 µg/mL against *M. smegmatis*. This was in contrast to the research undertaken by Sanusi *et al*. (2018) on *Cynanchum auriculatum* ethyl acetate extract which exhibited activity on *M. smegmatis* with MBC value of 6.25 mg/mL (630 µg/mL).

The difference in the results obtained and other reports, by researchers could be due to different extraction methods, different choices and concentrations of solvents, plant materials used, time of sample collection, soil nutrient available, temperature, water quality, rooting, aeration and the type of turmeric rhizome (Ngadino *et al.,* 2018).

The MIC results obtained from all the *Mycobacterium* species as compared to the standard drug Rifampicin with MIC of 0.04 µg/mL showed that possibly further purification to eliminate impurities which may interfere with and reduce the potency of the crude extract and fractions of the plant, *Curcuma longa* can serve as a lead in research and development of new drugs to combat resistant strains of *Mycobacterium*.

Sugarcane is edible and so will potentially produce antimicrobial compounds that are safe and more tolerable by living systems and a large volume of sugarcane bark is produced yearly thereby constituting a huge raw material base for the production of the antimicrobial compound. For sugarcane peels, all the crude extract and fractions of sugarcane inhibited the growth of all *Mycobacterium* species at 5000 µg/mL (Tables 4.11 to 4.13). The plant extract and fractions of sugarcane peels used in this study were able to inhibit the growth of *Mycobacterium tuberculosis* with MIC ranging from 165 µg/mL – 625 µg/mL and MBC within the range of 313 µg/mL -1250 µg/mL. Ethyl acetate fraction of sugarcane inhibited the growth of *M. tuberculosis* with MIC at 1250 µg/mL, agrees with the findings of Ravidran *et al*., (2020) who reported that *Glycyrrhiza glabra* inhibited the growth of *M. tuberculosis* with MIC at 1.25 mg/mL (1250 µg/mL). Kahaliw *et al.* (2017) reported the methanolic extract of *Combretum spp* with MIC of 1250 µg/mL against *M. tuberculosis.*

Furthermore, all extracts of sugarcane were active against *Mycobacterium bovis* with MIC values ranging from 313 – 1250 µg/mL which was in contrast with the study of Gemechu *et*

al. (2013) who reported the antimycobacterial activity against *M. bovis* strain with MIC value ranging from 6.25 -100 µg/mL which was lower than the result obtained in the present study. This could be as a result of the extraction process, the place where the plant was collected and the plant part used (Abubakar and Haque, 2020). And also the antimycobacterial activities of extracts are dependent on their lipophilic nature (Gemechu *et al.,* 2013, Izebe *et al.,* 2020).

The use of the non-pathogenic rapidly growing *M. smegmatis* permits the use of low-cost rapid methods. It has also been noted that at least 12 of the 19 known virulence genes of M. tuberculosis share close homology with genes of *M. smegmatis* (Ekundayo *et al.,* 2020). Sugarcane peel extract and fractions inhibited the growth of *Mycobacterium smegmatis* at 5000 µg/mL (Table 4.13). Enas *et al*. (2020) reported similar observation stating that the ethyl acetate fraction of *Anogeissus leiocarpa* inhibited the growth of *M. smegmatis* at 5000 µg/mL. The plant extract and fractions used were able to inhibit the growth of *M. smegmatis* with MIC ranging from 165 µg/mL – 625 µg/mL and the MBC ranging from 625 µg/mL-2500 µg/mL. The ethanolic extract of sugarcane peel inhibited the growth of *M.smegmatis* with MIC value of 625 µg/mL. In contrast, Bhunu *et al.* (2017) reported, the ethanolic extract of *P. curatellifolia* inhibited the growth of *M.smegmatis* with MIC value of 12.5 µg/mL. The activity obtained in this study could be due to the absence of some phytochemical or synergistic effect of two or more phytochemicals and the location and duration of the experimental study (Ngadino *et al.,* 2018; Das *et al.,* 2023). *G. africana* showed minimum bactericidal concentration (MBC) of 1.56 mg/mL against *M. smegmatis* (Dembetembe *et al.,* 2023). The bark of sugarcane has been demonstrated as a strong antibacterial (Uchenna *et al*., 2015), Khan *et al*. (2023) also observed that sugarcane extract was able to curb hazardous

side effects of standard drugs. In the present investigation, the potent anti-tubercular activity of rifampicin (0.04 μg/mL) was expected in selecting rifampicin as control drug due to its specificity to *Mycobacterium* species.

4.2.4 Characteristics of synthesized silver nanoparticles

Silver nanoparticles have a wide range of applications because of their unique characteristics such as optical, electrical, and magnetic properties, which can be incorporated into antibacterial, antiviral, and antifungal agent. The ultraviolet-visible spectrum absorption peak (Figure 4.1) for AEAgNPs occurred at 438nm. This result was compared with the report of Moges and Goud, (2022) who stated that the UV-Visible spectrum of methanolic *Azadiracta indica* showed an absorbance peak at 428nm. This demonstrates that silver nanoparticles with a surface plasmon resonance occurred in the reaction mixtures. Sharifi-Rad *et al*. (2020) recorded a peak of 430nm for *Astragalus tribuloides* root extract.

The morphology of synthesized AEAgNPs observed with transmission electron microscopy (TEM) was spherical with an average particle size of 19.24 nm. Ejidike and Clayton, (2022) reported a spherical shape with an average particle size of 18.26nm for nanoparticles mediated by *Daucus caroti*. This confirms the nano-particulate nature of the synthesized materials and supports the observation from the UV- Visible spectrum. For the XRD pattern of the synthesized ethyl acetate fraction (Figure 4.4), sharp peaks of 38˚, 44˚, 65˚, 77˚and 82˚ were obtained. This is similar to the findings of Khan *et al*. (2023) who recorded sharp peaks at 38.25°, 43.70°, 64.8°, and 77.51°. The XRD pattern showed that the silver nanoparticles synthesized by the turmeric ethyl acetate fraction were crystalline in nature (Nampoothiri *et al.,* 2018). In addition, the extra peaks appearing in the diffractogram may be due to the biomass residue capping of AgNPs as reported by Khan *et al*. (2023).

In this study, EDS showed an optical absorption peak of silver at 3 keV due to the surface plasmon resonance (Figure 4.6). Silver peaks were the most prominent while the presence of carbon, copper, silicon, and oxygen atoms in the nanoparticle samples might be due to their presence in plants. In accordance, Konappa *et al.* (2021) reported that synthesized silver nanoparticles from *Trichoderma harzianum* ethyl acetate filtrate revealed the presence of a maximum amount of AgNPs, followed by carbon, oxygen, and chlorine. Kitimu *et al.* (2022) reported that EDS showing the element of silver, carbon, silicon, and oxygen are weak signals. It might be originated from macromolecules and fatty acids present in the plant and oxygen could appear during the preparation process.

The selected area of the electron diffraction (SAED) pattern of the biogenic AgNPs confirmed the crystalline nature of the synthesized nanoparticles in the sample, as evidenced by the presence of bright dots. Four bright rings correlated to the lattice planes ((111, 200, 220 and 311) of FCC silver confirmed that biosynthesized AgNPs had good crystallinity which is similar to Yu *et al*. (2019) findings on green-synthesized nanoparticles by using *Eriobotrya japonica*.

4.2.5 Anti-tubercular activities of ethyl acetate silver nanoparticles from turmeric fraction

Silver nanoparticles using ethyl acetate fraction of turmeric exhibited marked activities on the three strains of *Mycobacterium* spp represented in Tables (4.11 to 4.13) with MIC ranging from 20 - 39 µg/mL and the MBC ranging from 39 - 78 µg/mL respectively. This study exhibited better growth inhibition at low concentration than the study carried out by Sudjarwo *et al*. (2019) who observed that *Pinus merkusii* ethanolic nanoparticle inhibited the growth of *Mycobacterium tuberculosis* at 2000 µg/mL. This could be as a result of the plant

genotype, physical and chemical soil conditions, harvest time, plant maturity, drying technology, storage period, and extraction.

The synthesized fraction AEAgNPs and crude ethyl acetate fraction of turmeric had the same inhibitory effect on *M. bovis* with MIC at 20 µg/mL and the MBC at 39 µg/mL (Table 4.12). This could be as a result of the plant collection site, type and part of plant materials used and the extraction method (Ferrar *et al.,* 2021). The MIC and MBC value of AEAgNPs against M. *smegmatis* was 39 µg/mL and 78 µg/mL as shown in Table 4.13 which had better inhibition than the crude extraction which might be because, AgNPs contains a large surface area that facilitates ameliorating contact with bacterial cell wall (Khadka *et al.,* 2020). Devi *et al.* (2020) also stated that AgNPs have a widespread application in the design of resistant drugs because of their unusual stability and ease to release silver ions to delay or prevent the growth of bacterial cells by creating reactive hydrogen peroxide.

4.2.6 Toxicity profile of ethyl acetate silver nanoparticles

There was no death or toxicity symptoms and the LD_{50} was greater than 5000 mg/kgbw (Table 4.14). This is similar to the report by Nghilokwa *et al*. (2020) on nanosynthesized methanolic extract of *Azardirachta indica* after 28 days of treatment.

4.2.7 Effect of ethyl acetate silver nanoparticles on biochemical parameters of rats

Biochemical indices are significant in monitoring chemical symptoms produced by a toxicant. Moreover, enzyme assays play a crucial role in toxicological evaluation (Adeyemi and Aanji, 2012). Serum amino transferases analyses have become a standard measure of hepatotoxicity because of the significance of these enzymes. Normally, these enzymes are present in the liver and other tissues where they function in energy metabolism involving transamination of amino acids. In this study, the administration of AEAgNPs at a dose of

1000 mg/kgbw for 28days had an increase in alanine amino transaminase (ALT), aspartate amino transaminase (AST) and alkaline phosphatase (ALP) levels when compared to the control (normal saline), which was similar to the findings of Rathore *et al*. (2021) who observed an increase in AST, ALP, and ALT when 1ug/animal/day of AgNP *Spirulina platensis* was administered on rats for 28 days. This might be a result of liver damage, infiltrative liver disease and hepatocellular disease (Mendiratta-Lala *et al*., 2022). The decrease in total protein at doses 50 and 1000 mg/kgbw when compared with the control (normal saline), was in accordance with the work of Wen *et al*. (2017) who administered 60nm of AgNPs in doses of 30, 300, and 1000 mg/kgbw for 28 days. The decrease in the level of protein might be due to a liver disease, malabsorption syndrome and kidney disease (Tufan *et al.,* 2023).

Rifampicin is a core drug in the standard six month first-line treatment and it comes with side effects such as hepatitis, hypersensitivity and gastrointestinal disturbance. This study revealed that there was an elevation in the biochemical parameters of rats treated with Rifampicin when compared with the control (normal saline), which is similar to the findings of Maiti *et al. (*2019) who administered 50 mg/kgbw of rifampicin where several biomarkers such as AST, ALP, ALT, and bilirubin elevated significantly. The elevation could be due to hepatotoxicity (Pandit *et al.,* 2012).

4.2.8 Effect of ethyl acetate silver nanoparticles on Kidney function indices of rats

Creatinine and uric acid concentrations showed no significant differences between the control group and the test groups administered with AEAgNPs (25, 50 and 100 mg/kgbw). Nghilokwa *et al.* (2020) gave a similar report that the administration of *Azadirachata indica* (AgNPs) to rats for 28 days showed no significant difference when compared with the control

group. However, there was an increase in all the kidney function indices of rats treated with AEAgNPs (1000 mg/kgbw). According to Banaee *et al*. (2021), urea, creatinine and uric acid are major by-products excreted by the kidneys, and increased levels of these parameters are indicative of kidney damage. There was a decrease in serum urea which is in line with Adeyemi and Akanji (2012) who recorded a decrease in the concentration of urea which might be attributed to decreased amino acid degradation by the liver.

4.2.9 Effect of ethyl acetate silver nanoparticles on Lipid profile of rats

The administration of AEAgNPs daily to the rats, at the highest dose significantly increased the cholesterol, triglycerides and LDL-Cholesterol concentration when compared with the control (normal saline). In accordance, Sulaiman *et al*. (2015) reported that daily administration of Ag nanoparticles to rats reveals significant elevation LDL- cholesterol at a dose of 10 mg kg^{-1} when compared to the control. When the level of total cholesterol, triglycerides, and LDL- cholesterol is elevated it could raise the risk of cardiovascular disorder. The administration of nanoparticles decreased the HDL-C in the serum with the highest dose which may increase the risk of cardiovascular diseases (Sulaiman *et al*., 2015).

4.2.10 Effect of ethyl acetate silver nanoparticles on haematological parameters of experimental rats

Haematological profile reveals valuable information on cellular elements, the extent of damage to the blood, and therapeutic responses to treatment (Okonkwo *et al*., 2019). The packed cell volume (PCV) is a measurement of the proportion of blood that is made up of cells. Red blood cells are created by blood stem cells in the bone marrow through the maturation process with the help of erythropoietin. The main function is to transport oxygen around the body.

The group treated with synthesized ethyl acetate nanoparticles (100 and 1000 mg/kgbw) produced a significant increase in packed cell volume (PCV) when compared with the control (normal saline). Previous studies (Lee *et al*., 2018) suggest that when AgNP is ingested, it circulates in particulate form, thus interacting with blood components and cells to induce coagulative reaction

According to Venkatesh and Kalaivani (2017), an increase in the count of RBC, HB and PCV suggest polycythemia and positive erythropoiesis while reduction is an indication of either the destruction of RBC or decreased production, which may lead to anaemia.

There was no significant ($p< 0.05$) effect in red blood cell (RBC), haemoglobin count (HB), mean corpuscular haemoglobin concentration (MCHC), monocytes and eosinophils of all the treatment groups. Marais *et al*. (2019) reported similar results that the PCV, RBC, HB, MCHC, monocytes and eosinophils values were not different from the control when treated with silver nanoparticles synthesized from *Calopogonium mucunoides* aqueous leaf extract.

There was a significant decrease in blood platelet, mean corpuscular volume (MCV), and neutrophils when compared with the control (normal saline). Olugbodi *et al*. (2020) observed that MCV, platelet count was significantly low at a dose of 50 mg/kgbw which is an indication of hematopoietic properties. Blood platelets are known to play a major role in blood clotting. When there is elevation, it causes thrombocytosis while a low platelet could cause difficulty for the blood to clot which can lead to excessive bleeding (Periayah *et al.*, 2017).

4.2.11 Effect of ethyl acetate silver nanoparticles on body weight of rats

The results demonstrated that there were no significant dose-related changes in the bodyweight gains of the rats treated with AEAgNPs from week 0-2 in all treatment groups. These result is in line with Nosrati *et al.* (2021) showing no significant changes in bodyweight of rats treated with various concentrations of AgNPs during the 28-day experiment through oral and inhalation exposure. From week 0-3 there was weight loss in rats treated with Rifampicin when compared with the treatment groups. In contrast doses of rifampicin did not affect the body weight of mice negatively with an increase in the mean body weight of the mice (Ofori *et al.*, 2022).

4.2.12 Effect of organ weight gain of rats treated with ethyl acetate silver nanoparticles

This investigation showed that the liver, kidney and heart at dose 1000 mg/kgbw increased when compared to the control. In contrast De Jong *et al*.(2013) the heart, kidneys, adrenals, brain, and epididymis were weighed and showed no differences in the different dose groups (Ag-NP 20 nm) compared to the control.

4.2.13 Histological studies of the organs treated with synthesized fraction of AEAgNPs

Histological study helps to examine the changes in any tissue of animals associated with disease or disorder. The liver showed hepatic necrosis with mononuclear cellular infiltration and Hepatic congestion which is in agreement with the study of shittu *et al.* (2022) who reported a toxic effect on the liver sections. Necrotic cell death can be triggered by the deposition of silver nanoparticles in the liver leading to alterations seen as necrosis. In the kidney renal congestion, interstitial haemorrhage and interstitial tubular necrosis with mononuclear cellular infiltration were present. Similar to Wen *et al.* (2017) who stated extensive organ damage, such as necrosis and hemorrhage in the kidney and liver. But

disagrees with Nghilokwa *et al*. 2020 who recorded the kidney of the treated rats to be normal.

In this study pulmonary haemorrhage, thickened inter-alveoli septa with mononuclear cellular infiltration, hemosiderosis and caseous necrosis were detected in the lungs. Also treatment given at doses 25 -1000 mg/kgbw and Rifampicin caused mycocardial haemorrhage in the heart when compared with the control. The spleen had splenic vacuolation at dose 50 mg/kgbw and lymphocytic depletion with increased reticulation at dose 25 and 1000 mg/kgbw while splenic congestion was occurred in rats treated with Rifampicin when compared with the control. These results obtained were in contrast with that of Srisrimal *et al.* (2023) whose results indicated that AgNPs did not show any visible signs of histopathological changes in the kidney, lung, heart and spleen.

Most of the toxic effects caused by AgNP were contributed by the dissolved Ag, and the possible mechanisms include activation of lysosomal acid phosphatase activity, disruption of actin cytoskeleton and stimulation of phagocytosis, increase of MXR transport activity, inhibition of Na-K-ATPase (Wen *et al.,* 2017). the release of AgNPs into the environment during manufacturing, washing, and disposal of the product enables the NPs to enter into the human respiratory system through inhalation, following inhalation the transport and deposition of NPs that are not uniform and it's influenced by the flow rate, the structure of the airway, age and most importantly particle size (Ferdous and Nemmar, 2020).

CHAPTER FIVE

5.0 CONCLUSION, RECOMMENDATIONS AND CONTRIBUTION TO KNOWLEDGE

5.1 Conclusion

i. The phytochemical components of *Curcuma longa* and *Saccharum officinarum* include saponins, alkaloids, phenols, tannins, flavonoids and reducing sugar.

ii. The extracts, fractions and nanoparticles of the medicinal plants exhibited potent antitubercular activities against *Mycobacterium* species.

iii. The MIC and MBC of *C. longa* for *M. tuberculosis, M. bovis* and *M.smegmatis* ranged from 20 µg/mL- 78 µg/mL and 39 µg/mL-165 µg/mL. Petroleum ether fraction ranged from 0.390 – 0.781 %v/v and MBC 0.781 -1562 %v/v. While the MIC and MBC of *S.officinarum* ranged from 165 µg/mL – 2500 µg/mL and 313 µg/mL - 5000 µg/mL respectively.

iv. The MIC for the synthesized nanoparticles (AEAgNPs) for *M. tuberculosis, M.bovis* and *M. smegmatis* was between 20 µg/mL and 39 µg/mL and 39 µg/mL to 78 µg/mL respectively.

v. The AEAgNPs was ash in colour having a maximum absorbance peak at 438nm with a spherical shape and particle size of 19.24nm. The sharp peaks obtained was at 38˚, 44˚, 65˚, 77˚and 82˚. The SAED, showed the presence of bright ring pattern, signifying the presence of various planes of AgNPs and also indicating the crystalline nature. Energy dispersive spectrum (EDS) revealed the presence of Ag and O.

vi. The LD_{50} of the synthesized nanoparticles of turmeric was 5000 mg/kgbw however the kidney, lungs, liver, spleen and heart affected causing (Pulmonary haemorrhage, hepatic necrosis, renal congestion and splenic vacuolation).

5.2 Recommendations

i. Due to the inhibitory effects of *C. longa and S.officinarum* on some *Mycobacterium* species, it can serve as a lead compound in the development of novel drugs against tuberculosis.

ii. Further studies should also be carried out on other parts of the plants such as the leaves and seeds to determine the anti-tubercular activity against *M. tuberculosis* and other *Mycobacterium* complex.

iii. Individuals should be cautious in the intake of nanosynthesized turmeric extracts due to its toxic effect on the liver, lungs, kidney, spleen and heart.

5.3 Contribution to Knowledge

i. The research established that the medicinal plants contained important phytochemicals (alkaloids, flavonoids, saponins, reducing sugar, phenols and tannins).

ii. This study established that nanoparticles synthesized from *Curcuma longa* exhibited an inhibitory effect on *M. tuberculosis*, *M. smegmatis* and *M. bovis* at a low concentration.

iii. This study has established the use of *Saccharum officinarum* peel in the treatment of tuberculosis.

REFERENCES

Abbas, S. R., Sabir, S. M., Ahmad, S. D., Boligon, A. A., & Athayde, M. L. (2014). Phenolic profile, antioxidant potential and DNA damage protecting activity of sugarcane (*Saccharum officinarum*). *Food Chemistry*, 147(1), 10-16.

Abubakar, A. R., & Haque, M. (2020). Preparation of medicinal plants: Basic extraction and fractionation procedures for experimental purposes. *Journal of Pharmacy and Bio-Allied Sciences*, 12(1), 1-9.

Adeyemi, O. S., & Akanji, M. A. (2012). Psidium guajava leaf extract: effects on rat serum homeostasis and tissue morphology. *Comparative Clinical Pathology*, 21(1), 401-407.

Adjatin, A., Djengue, H. W., Ekpelikpeze, O., Bonougbo, Z., Adomako, J., Asogba, F., Dansi, A., & Gbenou, J. (2019). Phytochemical screening and cytotoxicity of juices and bark extracts of sugarcane (*Saccharum officinarum* Linn) in Benin. *International Journal of Biosciences*, 14(5), 95-105.

Ajala, E. O., Ajala, M. A., Ayinla, I. K., Sonusi, A. D., & Fanodun, S. E. (2020). Nano-synthesis of solid acid catalysts from waste-iron-filling for biodiesel production using high free fatty acid waste cooking oil. *Scientific Reports*, 10(1), 132-156.

Alka, P., Prakash, J., Madhu, C., Uma, C., & Daman, S. (2020). Screening of natural compounds that targets glutamate racemase of *Mycobacterium tuberculosis* reveals the anti-tubercular potential of flavonoids. *Scientific Reports*, 1(10), 949-955.

Allué-Guardia, A., García, J. I., & Torrelles, J. B. (2021). Evolution of drug-resistant *Mycobacterium tuberculosis* strains and their adaptation to the human lung environment. *Frontiers in Microbiology*, 12(1), 137-156.

Antony, B., Benny, M., Kuruvilla, B. T., Gupta, N. K., & Jacob, S. (2022). Acute and sub chronic toxicity studies with herbal pain-relieving formula (Rhuleave-K™) in rats. *Regulatory Toxicology and Pharmacology*, 133(1), 105-214.

Aro, A. O., Dzoyem, J. P., Goddard, A., Fonteh, P., Kayoka-Kabongo, P. N., & McGaw, L. J. (2019). In vitro Anti-mycobacterial, Apoptosis-Inducing Potential, and Immunomodulatory Activity of Some Rubiaceae Species. *Frontiers in Pharmacology*, 10(185), 1-13.

Array, E. J., Tonfack, D. F., Kingne, F., Kinge, E. E., & Womeni, H. M. (2019). Effect of different extraction solvents on the phenolic content and antioxidant activity of turmeric *(Curcuma longa). Food Research*, 1(1), 86 – 90.

Arya, V. (2018). A review on anti-tubercular plants. *International Journal of Pharmacological Technology and Research*, 3(1), 872-880.

Ashraf, M. A., Rasheed, R., Hussain, I., Iqbal, M., Farooq, M. U., Saleem, M. H., & Ali, S. (2022). Taurine modulates dynamics of oxidative defense, secondary metabolism, and nutrient relation to mitigate boron and chromium toxicity in *Triticum aestivum* L. plants. *Environmental Science and Pollution Research*, 29(30), 45527-45548.

Assam, J. P. A., Tcham, M. F. Y., Moni, N. E. D. F., Betote, D. P. H., Fossi, T. C., & Penlap, B. V. (2020). Phytochemical screening, Antimycobacterial activity of three medicinal Cameroonians plants and Acute toxicity of hydroethanolic extract of *Vitellaria paradoxa*. *Journal of Drug Delivery and Therapeutics*, 10(1), 96-104.

Ayati, Z., Ramezani, M., Amiri, M. S., Moghadam, A. T., Rahimi, H., Abdollahzade, A., & Emami, S. A. (2019). Ethnobotany, phytochemistry and traditional uses of Curcuma spp. and pharmacological profile of two important species (*C. longa* and *C. zedoaria*): a review. *Current Pharmaceutical Design*, 25(8), 871-935.

Azadi, D., Motallebirad, T., Ghaffari, K., & Shojaei, H. (2018). Mycobacteriosis and Tuberculosis: laboratory diagnosis. *The Open Microbiology Journal*, 12(1), 41-58.

Azizi, M., Fazeli, F., Mohammadi, M., & Khaneghah, A. M. (2021). Incorporation of essential oils in Iranian traditional animal oil: an assessment of physicochemical and sensory assessment. *Italian Journal of Food Science*, 33(SP1), 69-77.

Babayi, H., Oladosun, P. O., Olatunji, K. T., Aboyeji, D. O., Amadi, E. D., & Lawal, F. (2022). In vitro anti-tubercular activity of *Syzygium aromaticum* extract against *Mycobacteria* species. *Journal of Science, Technology, Mathematics and Education (JOSTMED)*, 18(2), 35-44.

Bahar, M., Ashebr, A., Teka, F., Adugna, N., & Solomon, A. (2018). In-vitro antibacterial activity of selected medicinal plants in traditional treatment of skin and wound infections in eastern Ethiopia. *BioMed Research International*, 11(1), 186-240. Doi: 10.1155/2018/1862401.

Bai, X., Rebecca, E., Oberley, B., Alida, R. O., Williamh, K., Michael, W., Gong, Z., Jennifer, R. H., & Edward, D. C. (2016). Curcumin enhances human macrophage control of *Mycobacterium Tuberculosis* infection. *Respirology*, 21(1), 951–957.

Banaee, M., Gholamhosseini, A., Sureda, A., Soltanian, S., Fereidouni, M. S., & Ibrahim, A. T. A. (2021). Effects of microplastic exposure on the blood biochemical parameters in the pond turtle (*Emys orbicularis*). *Environmental Science and Pollution Research*, 28(1), 9221-9234.

Barberis, I., Bragazzi, N. L., Galluzzo, L., & Martini, M. (2017). The history of tuberculosis: from the first historical records to the isolation of Koch's bacillus. *Journal of Preventive Medicine and Hygiene*, 58(1), E9-E12.

Barry, C. E. (2019). The spectrum of latent tuberculosis: rethinking the biology and intervention strategies. *National Revised Microbiology*, 7(1), 845–855.

Barua, N., & Buragohain, A. K. (2021). Therapeutic potential of curcumin as an antimycobacterial agent. *Biomolecules*, 11(9), 1278-1289.

Bates, I., Fenton, C., & Gruber, J. (2019). Vulnerability to malaria, tuberculosis, and HIV/AIDS infection and disease. Part 1: determinants operating at individual and household level. *Lancet Infectious Diseases*, 4(1), 267–277.

Bhat, P. V., Vinod, V., Priyanka, A. N., & Kamath, A. (2019). Maternal serum lipid levels, oxidative stress and antioxidant activity in pre-eclampsia patients from Southwest India. *Pregnancy Hypertension*, 15(1), 130-133.

Bhunu, B., Mautsa, R., & Mukanganyama, S. (2017). Inhibition of biofilm formation in Mycobacterium smegmatis by Parinari curatellifolia leaf extracts. *BMC Complementary and Alternative Medicine*, 17(1), 1-10.

Cadmus, K. J., Mete, A., Harris, M., Anderson, D., Davison, S., Sato, Y., & Pabilonia, K. L. (2019). Causes of mortality in backyard poultry in eight states in the United States. *Journal of Veterinary Diagnostic Investigation*, 31(3), 318-326.

Cantera, J. L., White, H., Diaz, M. H., Beall, S. G., Winchell, J. M., Lillis, L., & Boyle, D. S. (2019). Assessment of eight nucleic acid amplification technologies for potential use to detect infectious agents in low-resource settings. *PLoS One*, 14(4), 345-367.

Caws, M., Thwaites, G., Dunstan, S., Hawn, T. R., Thi Ngoc Lan, N., Thuong, N. T. T. & Farrar, J. (2018). The influence of host and bacterial genotype on the development of disseminated disease with *Mycobacterium tuberculosis*. *PLoS Pathogens*, 4(3), e100-134.

Chanda, S., & Ramachandra, T. V. (2019). Phytochemical and pharmacological importance of turmeric (*Curcuma longa*): A review. *Research & Reviews: A Journal of Pharmacology*, 9(1), 16-23.

Chitnis, A. S., Davis, J. L., Schecter, G. F., Barry, P. M., & Flood, J. M. (2015). Review of nucleic acid amplification tests and clinical prediction rules for diagnosis of tuberculosis in acute care facilities. *Infection Control & Hospital Epidemiology*, 36(10), 1215-1225.

Chopra, H., Mohanta, Y. K., Rauta, P. R., Ahmed, R., Mahanta, S., Mishra, P. K., & Dhama, K. (2023). An Insight into Advances in Developing Nanotechnology Based Therapeutics, Drug Delivery, Diagnostics and Vaccines: Multidimensional Applications in Tuberculosis Disease Management. *Pharmaceuticals*, 16(4), 581.

Christopher, V. S., Roy, A., & Rajeshkumar, S. (2018). Turmeric Oil Mediated Green Synthesis of Silver Nanoparticles and Their Antioxidant Activity. *Journal of Evolution of Medical and Dental Sciences*, 10(8), 37-45.

Dannenberg, A. M. (2019). Immune mechanisms in the pathogenesis of pulmonary tuberculosis. *Revised Infectious Diseases*, 11(1), S369–S378.

Das, A., Adhikari, S., Deka, D., Baildya, N., Sahare, P., Banerjee, A. & Pathak, S. (2023). An Updated Review on the Role of Nanoformulated Phytochemicals in Colorectal Cancer. *Medicinal*, 59(4), 685-701.

De Jong, W. H., Van Der Ven, L. T., Sleijffers, A., Park, M. V., Jansen, E. H., Van Loveren, H., & Vandebriel, R. J. (2013). Systemic and immunotoxicity of silver nanoparticles in an intravenous 28 days repeated dose toxicity study in rats. *Biomaterials*, 34(33), 8333-8343.

Debjit-Bhowmik, C., Kumar, K. S., Chandira, M., & Jayakar, B. (2009). Turmeric: a herbal and traditional medicine. *Archives of Applied Science Research*, 1(2), 86-108.

Dejene, D. B. (2021). Comprehensive Review on Turmeric (*Curcuma Longa* l.) as Medicinal Plant and its Nutraceutical Quality to Human. *Cancer Therapy & Oncology International Journal*, 18(3), 9-16.

Dembetembe, T. T., Rademan, S., Twilley, D., Banda, G. W., Masinga, L., Lall, N., & Kritzinger, Q. (2023). Antimicrobial and cytotoxic effects of medicinal plants traditionally used for the treatment of sexually transmitted diseases. *South African Journal of Botany*, 154(1), 300-308.

Devi, K.R., Lee, L.J.,Yan,L.T.,Syafinaz,A.N.,Rosnah, I., & Chin, V.K. (2021).Occupational exposure and challenges in tackling *M. bovis*at human–animal interface.*International Archives of Occupational and Environmental Health*, 1(94), 1147–1171

Dillon, S. L., Shapter, F. M., Robert, H. J., Cordeiro, G., Izquierdo, L., & Lee, S. L. (2019). Domestication to crop improvement: genetic resources for Sorghum and Saccharum (Andropogoneae). *Annual Botany*, 5(1), 975–989.

Donfack, V. D., Roque, S., Trigo, G., Fokou, P. T., Tchokouaha, L. Y., Tsabang, N., & Boyom, F. F. (2014). Antimycobacterial activity of selected medicinal plants extracts from Cameroon. *International Journal of Biological and Chemical Sciences*, 8(1), 273-288.

Edwards, D., & Kirkpatrick, C. H. (2018). The immunology of mycobacterial diseases. *Amplified Revised Respiratory Diseases,* 134:1062–1071.

Ehiobu, J. M., Idamokoro, M. E., & Afolayan, A. J. (2021). Phytochemical content and antioxidant potential of leaf extracts of Citrus limon (L.) Osbeck collected in the Eastern Cape Province, South Africa. *South African Journal of Botany*, 141(1), 480-486.

Ejidike, I. P., & Clayton, H. S. (2022). Green synthesis of silver nanoparticles mediated by *Daucus carota* L.: antiradical, antimicrobial potentials, in vitro cytotoxicity against brain glioblastoma cells. *Green Chemistry Letters and Reviews*, 15(2), 298-311.

Ekundayo, E., Kalu, U., & Enya, E. (2020). In-vitro inhibitory activity of extracts of some medicinal plants against *Mycobacterium smegmatis*. *Nigeria Journal of Medicine*, 34(1), 5044-5052.

El Khéchine, A., & Drancourt, M. (2011). Diagnosis of Pulmonary Tuberculosis in a Microbiological Laboratory. *Medecine et Maladies Infectieuses*, 41(10), 509-517.

Enas, E. A., Varkey, B., & Gupta, R. (2020). Expanding statin use for prevention of ASCVD in Indians: Reasoned and simplified proposals. *Indian Heart Journal*, 72(2), 65-69.

Esmail, H., Barry, C. E., Young, D. B., & Wilkinson, R. J. (2019). The ongoing challenge of latent tuberculosis. *Philosophy of Transitional Research and Sociology, B*369(1), 04-37.

Ezeonu, I. M., Ugwu, K. O. & Agbo, M. C. (2021). Prevalence of Tuberculosis, Drug-resistant Tuberculosis and HIV/TB co-infection in Enugu, Nigeria. *African Journal of Infectious Diseases*, 15(2), 24-30.

Ferdous, Z., & Nemmar, A. (2020). Health impact of silver nanoparticles: a review of the biodistribution and toxicity following various routes of exposure. *International Journal of Molecular Sciences*, 21(7), 23-75.

Ferrar, M. B., Wallace, H. M., Brooks, P., Yule, C. M., Tahmasbian, I., Dunn, P. K., & Hosseini, B. S. (2021). A Performance Evaluation of Vis/NIR Hyperspectral Imaging to Predict Curcumin Concentration in Fresh Turmeric Rhizomes. *Remote Sensing*, 13(1), 1807-1823.

Fried, N. M. (2019). Radiometric surface temperature measurements during dye assisted laser skin closure: in vitro and in vivo results. *Lasers in Surgery and Medicine*, 25(1), 291-303.

Gahtori, R., Tripathi, A. H., Kumari, A., Negi, N., Paliwal, A., Tripathi, P., & Upadhyay, S. K. (2023). Anticancer plant-derivatives: deciphering their oncopreventive and therapeutic potential in molecular terms. *Future Journal of Pharmaceutical Sciences*, 9(1), 14-25.

Gemechu, A., Giday, M., Worku, A., & Ameni, G. (2013). In vitro anti-mycobacterial activity of selected medicinal plants against *Mycobacterium tuberculosis* and *Mycobacterium bovis* strains. *BMC Complementary and Alternative Medicine*, 13(1), 1-6.

Giri, N. C. (2022). Protein and Peptide Drug Delivery. *Smart Drug Delivery*, 12(1), 39-44.

Global Tuberculosis Report (2020). Geneva: World Health Organization. Retrieved from: http:// www.who.int/tb/publications/global_ report/en/.

Gurunathan, S., Wu, C., & Freidag, B. (2020). DNA vaccines: a key for inducing long-term cellular immunity. *Current Opinion in Immunology*. 12(1), 442-447. http://dx.doi.org/10.1016/S0952-7915(00)00118-7

Hadi, S. A. (2022). *Epidemiology, Evolution, and Diagnostics of Tuberculosis in Humans and Animals.* Doctoral Dissertation, Submitted to Michigan State University. Michigan: Michigan State University Press.

Hedley, M., Curley, J., & Urban, R. (2020). Microspheres containing plasmid encoded antigens elicits cytotoxic T-cell responses. *Nature Medicine*, 4(1), 365-368.

Horsburgh, J. (2018). Tuberculosis without tubercles. *Tuberculosis as Lung Diseases,* 77(1), 197–198.

Ibrahim, Y. O., Busari, M. B., Yisa, M. A., Abubakar, A. N., Madaki, F. M., & Yusuf, R. S. (2022). Assessment of toxicity and anti-trypanosomal activities of toad venom in rat models. *Comparative Clinical Pathology*, 31(3), 417-425.

Izebe, K. S., Ibrahim, K., Onaolapo, J. A., Oladosu, P., Ya'aba, Y., Njoku, M., Shehu, M. B., Ezeunala, M., & Ibrahim, Y. K. (2020). Evaluation of In-VitroAnti-Tuberculosis Activity of Tetrapleura tetraptera Crude and Fractions on Multidrug Resistant *Mycobacterium tuberculosis*. *Journal of Tuberculosis Research*, 8(1), 165-176.

Jagielski, T., Minias, A., van Ingen, J., Rastogi, N., Brzostek, A., Żaczek, A., & Dziadek, J. (2016). Methodological and clinical aspects of the molecular epidemiology of *Mycobacterium tuberculosis* and other mycobacteria. *Clinical Microbiology Reviews*, 29(2), 239-290.

Jagielski, T., Van Ingen, J., Rastogi, N., Dziadek, J., Mazur, P. K., & Bielecki, J. (2014). Current methods in the molecular typing of *Mycobacterium tuberculosis* and other mycobacteria. *BioMed Research International*, 1(1), 645-802. Doi: 10.1155/2014/645802.

Kahaliw, W., Aseffa, A., Abebe, M., Teferi, M., & Engidawork, E. (2017). Evaluation of the antimycobacterial activity of crude extracts and solvent fractions of selected Ethiopian medicinal plants. *BMC Complementary and Alternative Medicine*, 17(1), 1-9.

Kasta, G. (2020). Antimicrobial activity of ethanol extract of rhizome turmeric (*Curcuma longa* L.) for growth of *Escherichia coli*, *Staphylococcus aureus* and *Candida albicans*. *Asian Journal of Pharmaceutical Research and Development*, *8*(3), 5-8.

Khadka, S., Hashmi, F. K., & Usman, M. (2020). Preventing COVID-19 in low- and middle-income countries. *Drugs Therapy Perspectives*, 36(1), 250–252. https://doi.org/10.1007/s40267-020-00728-8

Khan, S., Shujah, S., Nishan, U., Afridi, S., Asad, M., Shah, A. U. H. A., & Khan, M. (2023). Nannorrhops ritchiana Leaf-Based Biomolecular Extract-Mediated Silver Nanoparticles as a Platform for Mercury (II) Sensing, Antimicrobial Activity, and DNA Interaction. *Arabian Journal for Science and Engineering*, 1(1), 1-12.

Kitimu, S. R., Kirira, P., Sokei, J., Ochwangi, D., Mwitari, P., & Maina, N. (2022). Biogenic synthesis of silver nanoparticles using Azadirachta indica methanolic bark extract and their anti-proliferative activities against DU-145 human prostate cancer cells. *African Journal of Biotechnology*, 21(2), 64-72.

Konappa, N., Udayashankar, A. C., Dhamodaran, N., Krishnamurthy, S., Jagannath, S., Uzma, F., & Jogaiah, S. (2021). Ameliorated antibacterial and antioxidant properties

by *Trichoderma harzianum* mediated green synthesis of silver nanoparticles. *Biomolecules,* 11(4), 535.

Kozińska, M., Augustynowicz-Kopeć, E., Gamian, A., Chudzik, A., Paściak, M., & Zdziarski, P. (2023). Cutaneous and Pulmonary Tuberculosis—Diagnostic and Therapeutic Difficulties in a Patient with Autoimmunity. *Pathogens*, 12(2), 331-342.

Kumar, P., Mandal, G. P., Paul, A., Munsi, S., & Samanta, I. (2022). Substitution of antibiotic growth promoter with locally available plant derivatives: in-vitro study. *Indian Journal of Animal Health*, 10(2), 855-867.

Kwaghe, A. V., Umeokonkwo, C. D., & Aworh, M. K. (2020). Evaluation of the National Tuberculosis Surveillance and Response Systems, 2018 to 2019: National Tuberculosis, Leprosy and Buruli Ulcer Control Programme, Abuja, Nigeria. *The Pan African Medical Journal*, 35(1), 1-11.

Lee, M., Lee, J., & Carroll, M. W. (2019). Linezolid for treatment of chronic extensively drug-resistant tuberculosis. *North England Journal of Medicine*, 367(1), 1508-1518.

Lorke, D. (1983). A new approach to practical acute toxicity testing. *Archives of Toxicology*, 54(1), 275-287.

Maiolini, M., Gause, S., Taylor, J., Steakin, T., Shipp, G., Lamichhane, P., & Deshmukh, R. R. (2020). The war against tuberculosis: a review of natural compounds and their derivatives. *Molecules*, 25(13), 3011-3023.

Maiti, S., Parua, S., Nandi, D. K., Mondal, K. C., & Samanta, S. (2019). Hepatotoxic effect of Rifampicin as an Anti-Tuberculosis drug on male Albino rat. *Journal of Drug Delivery and Therapeutics*, 9(3), 26-32.

Majid, S. 1., Pawel, P., Francesco E., José M., & Álvarez-S. (2020) Green Synthesis of Silver Nanoparticles Using *Astragalus tribuloides* Delile. Root Extract: Characterization, Antioxidant, Antibacterial, and Anti-Inflammatory Activities. *Nanomaterials*, 10(1), 2383- 2294.

Mangwani, N., Singh, P. K., & Kumar, V. (2020). Medicinal plants: adjunct treatment to tuberculosis chemotherapy to prevent hepatic damage. *Journal of Ayurveda and Integrative Medicine*, 11(4), 522-528.

Marais, B. J., R. P. Gie., & H. S. Schaaf. (2019). "The clinical epidemiology of childhood pulmonary tuberculosis: a critical review of literature from the pre-chemotherapy era," *International Journal of Tuberculosis and Lung Disease,* 8(3), 278– 285.

Marcu, D. T. M., Adam, C. A., Mitu, F., Cumpat, C., & Aursulesie, V. (2023). Cardiovascular involvement in tuberculosis: From pathophysiology to diagnosis and complication. A Narrative Review. *Diagnostics (Basel),* 13(3), 432-447. doi: 10.3390/diagnostics13030432.

Markowitz, N., Hansen, N. I., Wilcosky, T. C., Hopewell, P. C., Glassroth, J., Kvale, P. A., Mangura, B. T., Osmond, D., Wallace, J. M., Rosen., M. J., & Reichman, L. B.

(2018). Tuberculin and anergic testing in HIV-seropositive and HIV-seronegative persons. *Annual International Medicine.* 119(1), 185–193.

Martin, C., LiLow, W., Gupta, A., Cairul Iqbal Mohd Amin, M., Radecka, I. T., Britland, S., & Raj, P. (2015). Strategies for antimicrobial drug delivery to biofilm. *Current Pharmaceutical Design*, 21(1), 43-66.

Masi, G., Bernardi, E., Martini, C., Vassura, I., Skrlep, L., Fabjan, E. Š., & Chiavari, C. (2020). An innovative multi-component fluoropolymer-based coating on outdoor patinated bronze for Cultural Heritage: Durability and reversibility. *Journal of Cultural Heritage*, 45(1), 122-134.

Mazlun, M. H., Siti, F., Sabran, S. F., Mohamed, M., Abubakar, M. F., & Abdullah, Z. (2019). Phenolic Compounds as Promising Drug Candidates in Tuberculosis Therapy. *Molecules*, 1(24), 24-49.

Medrano, J. M., Maiello, P., Rutledge, T., Tomko, J., Rodgers, M. A., Fillmore, D., & Lin, P. L. (2023). Characterizing the Spectrum of Latent *Mycobacterium tuberculosis* in the Cynomolgus Macaque Model: Clinical, Immunologic, and Imaging Features of Evolution. *The Journal of Infectious Diseases*, 227(4), 592-601.

Mekonnen, G. A., Mihret, A. S., Tamiru, M., Hailu, E., Olani, A., Aliy, A., Sombo, M., Lakew, M., Gumi, B., Ameni, G., Wood, J. L. N., & Berg, S. (2020). Genotype Diversity of *Mycobacterium bovis* and Pathology of Bovine Tuberculosis in Selected Emerging. Dairy Regions of Ethiopia. *Frontiers in Veterinary Science*, 7(55), 39-40.

Mendiratta-Lala, M., Aslam, A., Maturen, K. E., Westerhoff, M., Maurino, C., Parikh, N. D., & Owen, D. (2022). LI-RADS treatment response algorithm: performance and diagnostic accuracy with radiologic-pathologic explant correlation in patients with SBRT-treated hepatocellular carcinoma. *International Journal of Radiation Oncology, Biology and Physics*, 112(3), 704-714.

Moges, A., & Goud, V. V. (2022). Optimization, characterization, and evaluation of antioxidant and antibacterial activities of silver nanoparticles synthesized from *Hippophae salicifolia D. Don. Inorganic Chemistry Communications,* 146(1), 086-110.

Mohammed, A., Wudil, A. M., Alhassan, A. J., Muhammad, I. U., Idi, A., & Abdulmumin, Y. (2016). Acute and subchronic toxicity studies of aqueous, methanolic and n-Hexane root extracts of *Curcuma longa* L. on albino rats. *British Journal of Pharmaceutical Research*, 14(02), 1-8.

Mueller-Harvey, I. (2019). Tannins: their nature and biological significance. In: Secondary plants products. In J. C. Caygill and I. Mueller-Harvey (Eds.), *Antinutritional and beneficial actions in animal feeding* (pp. 17-70). Nottingham: Nottingham *University Press* (UK).

Muhammad, F. M., & Fathuddin, R. (2021). The Screening for the Antitrypanosomal Potentials of the Extracts of *Curcuma longa L*. *Acta Scientific Microbiology*, 4(2), 76–81.

Namdeo, A. G., Varghese, R., Kapase, Y., & Kumbhar, P. (2023). Integrative Medicine in the Treatment of COVID-19: An Indian Perspective. *Current Traditional Medicine*, 9(1), 44-83.

Nampoothiri, S. V., Suresh, K. B., Esakkidurai, T., & Pitchumani, K. (2018). Green synthesis of silver nanoparticles using a characterized polyphenol rich fraction from *Terminalia bellirica* and the evaluation of its cytotoxicity in normal and cancer cells. *Journal of Biologically Active Products from Nature*, 8(6), 352-363.

Natarajan, A., Beena, P. M., Devnikar, A. V., & Mali, S. (2020). A systemic review on tuberculosis. *Indian Journal of Tuberculosis*, 67(3), 295-311.

National Committee for Clinical Laboratory Standards (NCCLS) (1995). *How to Define, Determine, and Utilize Reference Intervals in the Clinical Laboratory*, Approved Guideline. Villanova, PA: NCCLS Publication.

National Institute for Pharmaceutical Research and Development (NIPRD) (2020). *Methodology for the Determination of Anti-Tubercular Activity of Natural Products.* Idu, Abuja: NIPRD.

Ngadino, S., Koerniasari, E., & Sudjarwo, S. A. (2018). Evaluation of antimycobacterial activity of Curcuma xanthorrhiza ethanolic extract against *Mycobacterium tuberculosis* H37Rv in vitro. *Veterinary World*, 11(3), 37-49.

Nghilokwa, E., Sokei, J., Mwitari, P., & Maina, N. (2020). Sub-acute and chronic toxicity of silver nanoparticles synthesized by *Azadirachta indica* extract. *African Journal of Biotechnology*, 19(6), 320-331.

Nguta, J. M., Appiah-Opong, R., Nyarko, A. K., Yeboah-Manu, D., Addo, P. G., Otchere, I., & Kissi-Twum, A. (2016). Antimycobacterial and cytotoxic activity of selected medicinal plant extracts. *Journal of Ethnopharmacology*, 182(1), 10-15.

Nosrati, H., Hamzepoor, M., Sohrabi, M., Saidijam, M., Assari, M. J., Shabab, N., & Alizadeh, Z. (2021). The potential renal toxicity of silver nanoparticles after repeated oral exposure and its underlying mechanisms. *BMC Nephrology*, 22(1), 228.

Nyambuya, T., Mautsa, R., & Mukanganyama, S. (2017). Alkaloid extracts from *Combretum zeyheri* inhibit the growth of *Mycobacterium smegmatis*. *BMC Complementary and Alternative Medicine*, 17(1), 1-11.

Ofori, M., Danquah, C. A., Ossei, P. P. S., Rahamani, G., Nugbemado, I. N., Doe, P., & Ninkyi, T. K. (2022). Antitubercular activities of *Crinum asiaticum* bulb extract using aeroso-linduced *Mycobacterium smegmatis* in mice model. *Journal of Applied Pharmaceutical Science*, 12(5), 156-164.

Ogbaini-Emovon, E. (2009). Current trends in the laboratory diagnosis of tuberculosis. *Benin Journal of Postgraduate Medicine*, 11(1), 79-90.

Oghenejobo, M., Bethel, O. U., Opajobi, O. A., & Uzoegbu, U. (2017). Antibacterial evaluation, phytochemical screening and ascorbic acid assay of turmeric (*Curcuma longa*). *MOJ Bioequivalence Availability*, 4(2), 063-081.

Okonkwo, J. C., Umegwuagu, J. I., Okonkwo, I. F., & Onunkwo, D. N. (2019). Effect of sun dried, dehulled and boiled kidney beans on hematological and serum biochemistry of broiler chickens. *International Journal of Environment, Agriculture and Biotechnology*, 4(3), 22-31.

Olatunji, K. T., Aliyu, A., Ya'aba1, Y., Mohammed, B. S., & Oladosu, P. (2021). Phytochemical Analysis and Anti-Tuberculosis Activity of Extracts of *Detarium senegalense* Bark and Root. *Journal of Advances in Microbiology*, 21(1), 44-45

Olugbodi, J. O., David, O., Oketa, E. N., Lawal, B., Okoli, B. J., & Mtunzi, F. (2020). Silver nanoparticles stimulates spermatogenesis impairments and hematological alterations in testis and epididymis of male rats. *Molecules*, 25(5), 1063-1076.

Ong, M. S., Deng, S., Halim, C. E., Cai, W., Tan, T. Z., Huang, R. Y. J., & Yap, C. T. (2020). Cytoskeletal proteins in cancer and intracellular stress: *A Therapeutic Perspective*, 12(1), 238.

Pandit, A., Sachdeva, T., & Bafna, P. (2012). Drug-induced hepatotoxicity: a review. *Journal of Applied Pharmaceutical Science*, 1(1), 233-243.

Parte, A. C. (2018). List of Prokaryotic names with Standing in Nomenclature bacterio.net), 20 years on. *International Journal System of Evolution Microbiology*, 68(1), 1825–1829.

Paul, R., Kavinarmatha, K., & Parthiban, S. (2023). Tantalum doped titanium dioxide nanoparticles for efficient photocatalytic degradation of dyes. *Journal of Molecular Structure*, 1277(1), 134869-134888.

Periayah, M. H., Halim, A. S., & Saad, A. Z. M. (2017). Mechanism action of platelets and crucial blood coagulation pathways in hemostasis. *International Journal of Hematology-Oncology and Stem Cell Research*, 11(4), 319.

Poro, K. E., Hoekou, Y., Pissang, P., Kpabi, I., Kosi, M., Dagnra, A.Y., Tchacondo, T., & Komlan, B. (2021). In vitro Antimycobacterial Activity of Selected Medicinal Plants against *Mycobacterium tuberculosis*. *International Journal of Current Microbiology and Applied Sciences,* 10(02), 31-46.

Radhika, R., Gayathi, C., Kartik, M., & Mukesh, D. (2020). Inhibitory activity of traditional plants against *Mycobacterium smegmatis* and their action on filamenting temperature sensitive mutant Z (FTSZ) – A cell division protein. *PLOS ONE*, 1(1), 1-21.

Raj, S., Trivedi, R., & Soni, V. (2022). Biogenic Synthesis of Silver Nanoparticles, Characterization and Their applications—A Review. *Surfaces*, 5(1), 67–90.

Rajendran, P., Bharathidasan, R., & Sureka, I. (2017). Phytochemical Screening GC-MS and FTIR Analysis of Sugarcane Juice. *International Journal of Pharmaceutical Research and Health Sciences*, 6(1), 1962-1967.

Rathore, S. S., Murthy, H. S., Mamun, M. A. A., Nasren, S., Rakesh, K., Kumar, B. T. N., & Khandagale, A. S. (2021). Nano-selenium supplementation to ameliorate nutrition physiology, immune response, antioxidant system and disease resistance against *Aeromonas hydrophila* in monosex Nile tilapia (*Oreochromis niloticus*). *Biological Trace Element Research*, 199(1), 3073-3088.

Ravindran, P. N., Nirmal Babu, K., & Sivaraman, K. (2018). *Turmeric. The golden spice of life*. Turmeric. The Genus Curcuma. Boca Raton, FL, USA: CRC Press.

Riley, R. (2019). Airborne infection. *American Journal of Medicine,* 57(1), 466–475.

Ryder, B. M. (2021). *Early innate immunity against mycobacterial infection.* Doctoral Dissertation Submitted to University of Otago. Otago: University of Otago Press.

Safitri, C. N. H., Ritmaleni, C., Rintiswati, N., Sardjiman., & Takushi, K. (2018). Evaluation of benzylidene-acetone analogues of curcumin as antituberculosis. *Asian Journal of Pharmaceutical and Clinical Research,* 11(4), 226-230.

Sakarde, A., John, J., Ahirwar, A. K., & Hardas, V. (2022). Serum Lipid Profile Parameters as Markers of Oxidative Stress in Preeclampsia: A Case-control Study. *Natural Journal of Laboratory and Medicine,* 11(1), B025-029.

Samreen, F., Anjna, K., & Prakash, V. D. (2021). Advances in adjunct therapy against tuberculosis. *Deciphering the Emerging Role of Phytochemicals Medical Commication,* 2(4), 494-513.

Sanusi, S. B., Bakar, M. F. A., Mohamed, M., Sabran, S. F., Norazlimi, N. A., & Isha, A. (2018). Anitimycobacterial activity and potential mechanism of action of *Campnosperma auriculatum* shoot extract. In AIP Conference Proceedings, 2016(1), 020-129.

Sanyaolu, A., Schwartz, J., Roberts, K., Evora, J., Dhother, K., Scurto, F., & Patel, S. (2019). Tuberculosis: A review of current trends. *Epidemiology International Journal*, 3(1), 1-13.

Sayantani, C., & Ramachandra, T. V. (2021). Phytochemical and Pharmacological Importance of Turmeric (*Curcuma longa*). *A Journal of Pharmacology,* 9(1), 1299-2349.

Scully, R. E., Mark, E. J., McNeeley, W. F., & Ebeling, S. H. (2019). Case records of the Massachusetts General Hospital: Case 29. *North England Journal Medicine,* 339(1), 831–838.

Sharifi-Rad, M., Anil Kumar, N. V., Zucca, P., Varoni, E. M., Dini, L., Panzarini, E., & Sharifi-Rad, J. (2020). Lifestyle, oxidative stress, and antioxidants: back and forth in the pathophysiology of chronic diseases. *Frontiers in Physiology*, 11(1), 694-708.

Shittu, O. K. (2015). Effect of Methanol Extract of *Telfairia occcidentalis* on Haematological Parameters in Wister Rats. *Asian Pacific Journal of Tropical Disease*, 5(8), 654-657.

Shittu, O. K., Ihebunna, O., & Gara, T. Y. (2022). Removal of contaminant in electroplating wastewater and its toxic effect using biosynthesized silver nanoparticles. *SN Applied Sciences*, 4(10), 266-281.

Shittu, O. K., Oluyomi, O. I., & Gara, T. Y. (2021). Safety assessment of bio-synthesized iodine-doped silver nanoparticle wound ointment in experimental rats. *Clinical Phytoscience*, 7(1), 1-8.

Singh, V., Cardoso, N., & Huszár, S. (2023). Chemotherapy for Drug-Susceptible Tuberculosis. In Tuberculosis: *Integrated Studies for a Complex Disease*, 10(4), 229-255.

Sivakumar, A., & Jayaraman, G. (2011). Anti-tuberculosis activity of commonly used medicinal plants of south India. *Journal of Medicinal Plants Research*, 5(31), 52-63.

Smith, D., & Wiengeshaus, E. (2018). What animal models can teach us about the pathogenesis of tuberculosis in humans. *Revised Infectious Diseases*, 11(1), S385-S393.

Soolingen van, D., Hoogenboezem, T., De Haas, P. E. W., Hermans, P. W. M., Koedam, M. A., Teppema, K. S., Brennan, P. J., Besra, G. S., Portaels, F., Top, J., Schouls, L. M., & A. van Embden, J. D. (2019). A novel pathogenic taxon of the *Mycobacterium tuberculosis* complex, Canetti: characterization of an exceptional isolate from Africa. *International Journal of Systemic Bacteriology*, 47(1), 1236–1245.

Srisrimal, D. A., Mohandoss, D. K. D., Srisrimal, A., Darshakumar, R. D., Prabhu, S., Tamarakar, S., & Murkunde, Y. (2023). Silver Nanoparticles: Evaluation of In Vivo Toxicity in Rats. *BioNano Science*, 13(1), 176-185.

Sudjarwo, S. A., Eraiko, K., & Sudjarwo, G. W. (2019). The potency of chitosan-*Pinus merkusii* extract nanoparticle as the antioxidant and anti-caspase 3 on lead acetate-induced nephrotoxicity in rat. *Journal of Advanced Pharmaceutical Technology & Research*, 10(1), 27-40.

Sulaiman, A. F., Akanji, M. A., Oloyede, O. B., Sulaiman, A. A., Olatunde, A., Joel, E. B. & Adeyemi, O. S. (2015). Oral Exposure to Silver/Gold Nanoparticles: Status of RatLipid Profile, Serum Metabolites and Tissue Morphology. *Journal of Medical Science*, 15(2), 71-79.

Swetha, V., Lavanya, S., Saleena, G., Push Palaksmi, E., Samsrajal. J., & Annadurai, G. (2020). Synthesis and Characterization of Silver Nanoparticles from Ashyranthus Aspera extract for Antimicrobial Activity Studies. *Journal of Applied Science and Environmental Management*, 24(7). 1161-1167.

Temu, T. M., Polyak, S. J., Wanjalla, C. N., Mandela, N. A., Dabee, S., Mogaka, J. N, & Zifodya, J. S. (2023). Latent tuberculosis is associated with heightened levels of pro- and anti-inflammatory cytokines among Kenyan men and women living with HIV on long-term antiretroviral therapy. *Acquired Immune Deficiency Syndrome*, 10(1), 1097-10108.

Tietz, N. W. (1987). *Fundamentals of Clinical Chemistry* (3rd ed.). Philadelphia, PA: W.B. Saunders.

Tufan, E., Sivas, G. G., Gökmen, B. G., Karaoğlu, S. Y., Dursun, E., Ak, E. Ç., & Tunali-Akbay, T. (2023). Whey Protein Concentrate Ameliorates the Methotrexate-Induced Liver and Kidney Damage. *British Journal of Nutrition*, 1(1), 1-21.

Uchenna, E. F., Adaeze, O. A., & Steve, A. C. (2015). Phytochemical and antimicrobial properties of the aqueous ethanolic extract of *Saccharum officinarum* (sugarcane) bark. *Journal of Agricultural Science*, 7(10), 291-303.

Venkatesh, R., & Kalaivani, K. (2017). Effect of *Solanum villosum* (mill.) extract and its silver nanoparticles on hematopoietic system of diethyl nitrosamine-induced hepatocellular carcinoma in rats. *Innovare Journal Health Science*, 5(1), 13-16.

Weissberg, D., Böni, J., Rampini, S. K., Kufner, V., Zaheri, M., Schreiber, P. W., & Wolfensberger, A. (2020). Does respiratory co-infection facilitate dispersal of SARS-CoV-2? Investigation of a super-spreading event in an open-space office. *Antimicrobial Resistance & Infection Control*, 9(1), 1-8.

Wen, H., Dan, M., Yang, Y., Lyu, J., Shao, A., Cheng, X., & Xu, L. (2017). Acute toxicity and genotoxicity of silver nanoparticle in rats. *PloS One*, 12(9), e0185554.

World Health Organization (WHO) (2020). Tuberculosis Fact Sheet. Retrieved from: https://www.who.int/newsroom/fact sheets/detail/tuberculosis.

World Health Organization (WHO) (2022). *Addressing Poverty in TB Control. Options for National TB Control Programs.* Geneva: World Health Organization.

World Health Organization (WHO) (2023). *Global Tuberculosis Report 2022*. Washington, DC: WHO Global TB Programme.

Xie, Y. L., Cronin, W. A., Proschan, M., Oatis, R., Cohn, S., Curry, S. R., & Dorman, S. E. (2018). Transmission of Mycobacterium tuberculosis from patients who are nucleic acid amplification test negative. *Clinical Infectious Diseases*, 67(11), 1653-1659.

Xu, L., Yi-Yi, W., Huang, J., Chun-Yuan, C., Zhen-Xing, W., & Xie, H. (2020). Silver nanoparticles: Synthesis, medical applications and biosafety. *Theranostics*, 10(20), 89-96.

Yu, C., Tang, J., Liu, X., Ren, X., Zhen, M., & Wang, L. (2019). Green biosynthesis of silver nanoparticles using *Eriobotrya japonica* (Thunb.) leaf extract for reductive catalysis. *Materials*, 12(1), 189-199.

Zahro, A. N., Sumarni, W., & Kurniawan, C. (2023). The Tradition of Making Lontong Tuyuhan in Rembang Regency as a Science Learning Resource. *Journal Penelitian Pendidikan IPA*, 9(1), 207-215.

Zaitsev, S. Y., Bogolyubova, N. V., Zhang, X., & Brenig, B. (2020). Biochemical parameters, dynamic tensiometry and circulating nucleic acids for cattle blood analysis: A review. *Peer Journal*, 8(1), e8997.

Zignol, M., van Gemert, W., & Falzon, D. (2020). Surveillance of anti-tuberculosis drug resistance in the world: an updated analysis, 2017-2019. *Bulletin of World Health Organization*, 90(1), 111D-119D.